NASA CR-54154
CAL UB-1989-E-4

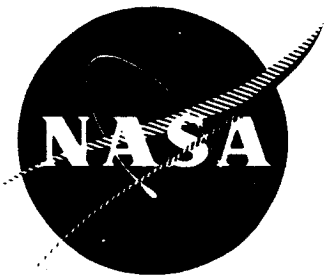

LASIG II
PULSED LASER ION GENERATOR STUDY

by
R.E. Biss and A.S. Gilmour, Jr.

Prepared for

NATIONAL AERONAUTICS AND SPACE ADMINISTRATION

CONTRACT NAS 3-5919

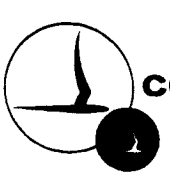

CORNELL AERONAUTICAL LABORATORY, INC.
OF CORNELL UNIVERSITY, BUFFALO 21, N. Y.

NOTICE

This report was prepared as an account of Government sponsored work. Neither the United States, nor the National Aeronautics and Space Administration (NASA), nor any person acting on behalf of NASA:

A) Makes any warranty or representation, expressed or implied, with respect to the accuracy, completeness or usefulness of the information contained in this report, or that the use of any information, apparatus, method, or process disclosed in this report may not infringe privately owned rights; or

B) Assumes any liabilities with respect to the use of, or for damages resulting from the use of any information, apparatus, method or process disclosed in this report.

As used above, "person acting on behalf of NASA" includes any employee or contractor of NASA, or employee of such contractor, to the extent that such employee or contractor of NASA, or employee of such contractor prepares, disseminates, or provides access to, any information pursuant to his employment or contract with NASA, or his employment with such contractor.

NASA CR-54154
CAL UB-1989-E-4

FINAL REPORT

LASIG II
PULSED LASER ION GENERATOR STUDY

by
R.E. Biss and A.S. Gilmour, Jr.

Prepared For
NATIONAL AERONAUTICS AND SPACE ADMINISTRATION

October 5, 1965

CONTRACT NAS 3-5919

Technical Management
NASA Lewis Research Center
Cleveland, Ohio
Spacecraft Technology Division
Raymond R. Nicholls

PULSED LASER ION GENERATION STUDY

by

R. E. Biss and A. S. Gilmour, Jr.

ABSTRACT

Thirteen materials were illuminated in vacuum with the focused output of a pulsed ruby laser. Illumination of materials such as chromium, columbium, tantalum, thorium, tungsten and zirconium resulted in the emission of ion currents of 3 to 4 amperes. Thrusts from this laser-induced emission have been measured at over 4 millipounds. An average ion energy of 40 electron volts, with a specific impulse of 660 seconds has been obtained. Measurements were made on the density and energy distribution of the emitted ions.

AUTHOR

TABLE OF CONTENTS

TABLE OF CONTENTS Continued

TABLE OF CONTENTS Continued

LIST OF ILLUSTRATIONS

LIST OF ILLUSTRATIONS Continued

LIST OF ILLUSTRATIONS Continued

PULSED LASER ION GENERATION STUDY

By

R. E. Biss, and A. S. Gilmour, Jr.

Cornell Aeronautical Laboratory, Inc.

1.0 SUMMARY

The purpose of the research discussed in this report is to determine detailed electrical and mechanical parameters of the laser-excited emission process. In particular the phenomena of this emission process were investigated with a view to application to pulsed ion thrustors.

The project effort was divided into several phases. Several emitter materials were evaluated with respect to properties of their ion yield; the effects of emitter geometry and dimensions on ion output were investigated; the relationship between power density near the focal point of the laser beam and ion yield was studied in detail; angular distribution of emission density and energy was measured; the types of particles emitted were studied; and impulse measurements on the various materials were made.

The emitter evaluation work on thirteen materials (aluminum, chronium, columbium, copper, hafnium, iron, lead, molybdenum, rhenium, tantalum, thorium, tungsten and zirconium) indicated that there would be no dearth of materials yielding high ion output. One of the primary factors affecting ion output is the absorption of laser light by the material. The use of a material is limited by its susceptibility to damage from the power density of the laser beam. It was found that the emitter geometry had a negligible effect on the ion output, while the optical geometry, i.e., dimension of focal spot, cone angle of the focused light, and location of focal spot, had a considerable effect on output. For example, the output ion yield could be increased several orders of magnitude with optimum adjustments of focusing parameters.

During the experiments two ruby laser rods were used. These two rods, while physically similar in appearance, possessed significant differences in their distribution of power density across their emitted laser beams. One ruby had essentially a uniform power-density distribution, whereas the other ruby had preferred moding characteristics resulting in areas of very intense power density (non-uniform distribution) when integrated over the entire pulse time.* In addition, the ruby with the non-uniform power-density distribution had a lower divergence than the ruby with the uniform power density distribution. These variations in the laser output led to significant differences in the maximum achievable laser power density when the beams were focused. As a result, significant differences were observed in the measured ion yield when the focal points of the laser beams were near the emitter surface.

An output ion charge between 1500 and 2000 microcoulombs per unit pulse from tungsten was measured with the non-uniform power density laser. This charge level, along with the average measured ion energy of 15ev, would indicate an impulse of 4 micropounds-seconds per pulse, and a thrust during the pulse of 14 millipounds. This intense ion emission was obtained using the non-uniform power density laser which also led to the presence of neutral particles. These neutral particles are undesirable because they are wasteful of propellant and are incapable of being electrically accelerated.

Using the uniform power density laser, ion yields of 200 to 500 microcoulombs per unit pulse were measured with higher emitted ion velocities than those obtained with the nonuniform-power-density laser. Thrusts of 4 millipounds over a pulse length of 1300 microseconds have been obtained at an average laser output power during the pulse time of 1.7 kilowatts using thorium as a target. No neutral particles were measured when using this ruby.

---

* The moding of the laser may change with time. The power density characteristics noted were obtained by taking a time integrated photograph of a single laser pulse.

Detailed tests were performed on four of the original thirteen materials, rhenium, tantalum, thorium and tungsten, to determine their feasibility for use in a Laser-Generated-Ion Thrustor. These tests were designed to investigate in detail the mechanical forces, ion output, charge to mass ratios of emitted ions, the presence of neutral particles in the resulting plasma, angular distribution of emission density and velocity, power density and specific impulse.

The above properties of the laser induced emission were measured or calculated from the results obtained with several special experimental configurations. In addition, thrust measurements were made using a pendulum with an electromagnetic pickup of the motion due to the laser induced impulse.

A hemispherical collector equipped with Faraday cages was used to measure ion density at selected elevation angles. Three of the cages also had insulated shield electrodes to permit measurement of ion energy. The angular density distribution from the various emitters was found to be approximately cosinusoidal. Variations in the level of incident laser power did not significantly change the angular ion distribution. The angular distribution could be radically modified, however, by the application of a magnetic field coaxial with the incident laser beam. It was found that the application of a 1400 gauss magnetic field will increase the laser generated thrust by at least 50% (and this estimate may be conservative since the ion density coaxial with the laser beam, could not be measured). Thrust in the presence of this external magnetic field was not measured due to the difficulty of mounting the pendulum near the electromagnet.

Energy measurements made with the energy probes on the hemispherical collector showed that the energy of the emitted ions of all four materials selected for detailed tests was greater than 200 electron volts, and in fact, ions were detected with 600 volts of retarding potential. Using the energy measuring assemblies in the hemispherical collector it was found impossible to eliminate either electrons or ions with a retarding potential

of -600 or +600 volts on the shield electrode which had a hole with a 0.005 inch diameter.

A quadrupole mass spectrometer was then used to monitor the emitted particles. This allowed for the sorting of the ionized particles, a search for neutral particles and measurement of ion energy. Energy measurements in the mass spectrometer, where electrons could be denied access to the collector by retarding and focusing potentials on the quadrupole rods, showed singly charged ions having energies greater than 200 volts for the four materials tests. The measuring equipment was not sufficiently sensitive to warrant further investigation of the ion energy profile.

Doubly charged atomic ions were found to be present in the spectrometer measurements on the emission outputs of rhenium and tantalum. The number of doubly charged ions was approximately 20 percent of the number of singly charged ions at an elevation angle of 30° when the uniform power density laser was used. Using the non-uniform power density laser, only about 3 percent of the ions were doubly charged atomic ions at this same elevation angle. Some neutral particles were found with tungsten when the non-uniform power-density laser was used. With the ruby laser having a uniform power density, no neutral particles were found during measurements on any of the four materials. Comparing weight loss measurement to measured emitted charge, when the uniform power density laser was used, 80 percent of the weight loss could be accounted for, the remainder being lost to the charge measuring circuit through the aperture required for the transmission of the laser beam.

2.0 INTRODUCTION

The research conducted during this program and discussed in this report investigated in detail the electrical and mechanical properties of laser induced emission. These properties were investigated in order to ascertain the applicability of this emission mechanism for use in a pulsed ion thrustor. The average initial emission velocity of the laser-generated ions was 3 to 6 kilometers per second and produced thrusts of about ten millipounds.

Prior to this contract the application of laser-induced-ion-generation to a pulsed thrustor had not been considered. The interaction between intense coherent light, as produced by a laser, and a metallic surface is in fact an extremely new field. In 1962-63, CAL personnel at Cornell University [1, 2] engaged in studies and research on the electrical effects obtained by laser-surface interaction. This work was continued and expanded at CAL.[3] In this study the quantity, energy, and electrical characteristics (ionization) of laser-excited emission from metal surfaces in high vacuum were measured and associated mechanisms analyzed. Most of the work in this CAL project was carried out with tungsten because the experiments at Cornell University suggested that tungsten would be an excellent selection.

Other work going on in this area was the interaction of a laser beam with a variety of metal surfaces in air at atmospheric pressure.[4] This study, carried out by CAL Physicists, was motivated largely by a recognized need to improve material forming and manufacturing technology for "space age" components and devices.

In examining the possible application of lasers to simulation of hypervelocity particle impact on a surface, scientists at CAL performed a rigorous and detailed analysis of mechanical phenomena occurring both within and on the surface of a solid when the surface is exposed to an energy impulse.[5] A well established end result of laser-surface interaction is the deposition of sizable energy (heat) impulses, so these analytical results pertain directly to the comprehensive theory of laser-surface interaction.

Effects in atmosphere and in high vacuum have been demonstrated to be quite different (except for the initial energy (light) absorbing mechanism). The work on this present program was carried out in a high vacuum environment since any application of this electric thrustor would of necessity require operation in a vacuum.

It has been observed that the amount of light energy absorbed by different materials varies considerably. For example, in his laser machining experiments, Williams[6] found that enough light energy was absorbed from eight, four-joule pulses from a ruby laser to remove about 10^{-3} in^3 of iron, nickel and tungsten. He was unable, however, to remove more than 3×10^{-4} in^3 of copper with twenty, four-joule pulses which indicates that the reflectivity of molten copper is considerably above those for Fe, W, and Ni.

In initial investigations into the interactions of a light wave with a surface, some workers[1, 7] simply used the classical electromagnetic wave-surface interaction to qualitatively describe some of the heating phenomena observed experimentally. Of course, this approach neglected the lattice structure of the material and imperfections in it. The light beam from the laser was considered as a plane electromagnetic wave normally incident on a metallic surface, and the metal was considered to be perfectly homogeneous. The reflection and absorption characteristics at the interface were calculated by solving Maxwell's equations and the classical exponential absorption of the radiation at the surface was obtained.

The most complete analytical work accomplished before the start of this program on the surface and internal temperatures of materials after they have absorbed the laser light energy is that of Ready.[7] He used the classical heat equation, and obtained computer solutions subject to some justifiable assumptions for the temperature of the irradiated material as function of time, distance, and power input. Unfortunately, Ready's results reported thus far do not extend to temperatures at which interesting electron and ion emission occur for application to a pulsed ion thrustor. Other laser surface interaction work[8, 9] was also at low incident laser power densities.

During the course of this program[10, 11, 12, 13] a few papers have been published concerning laser surface interaction. These papers consider low power density illumination of the surface and hence usually only electron emission, or low ion emission. The high ion emission levels obtained at CAL have been reported in two papers.[14, 15]

The equipment used at CAL during the program was unique and specialized. The investigations were all designed to arrive at specialized data to allow detailed design of a lab model thrustor. The desired data included energy and density distributions of the emitted charge, laser induced impulse or thrust and analysis of the species of emitted particles.

The initial portion of the program included evaluation of thirteen possible emitter materials and the effect of emitter geometry on the ion generation. In addition, it was found necessary to investigate the effect of laser optics on the levels of ion and neutral yield.

3.0 GENERAL TEST APPARATUS

A photograph of the experimental apparatus used for this program is shown in Figure 1. The laser was built at CAL and uses a 6 inch long by 1/4 inch diameter ruby crystal operating at 6943 Å, with a total internal reflecting chisel tip on one end and a flat uncoated transmitting plane on the other end. The ruby crystal was located along one focal line of an elliptical reflector and an EG&G FX-45 linear flash tube was located along the other focal line of the cavity. Outputs up to about 10 joules were available from this laser at inputs up to 2000 joules. The reflector cavity was flushed continuously with dry nitrogen cooled through a heat exchanger immersed in liquid nitrogen. Cooling was necessary so that the laser could be fired at high energy levels and at reasonable repetition rates without drifting of the laser output level.

Light from the pulsed ruby laser was collimated by passing it through a telescope and then it was focused on the end of the emitter. Aiming and focusing of the laser light at a desired emitter was facilitated by the CAL-owned three-axis precision positioner. With this device the entire laser-optics assembly was left undisturbed, consequently optical alignment was maintained as the output spot was moved to predetermined locations. A photocell and amplifier detected a small portion of the laser light (scattered from the focusing lens) and provided a signal for the oscilloscopes proportional to the instantaneous amplitude of the laser light. The emitter mounting fixtures and the collector assemblies were electrically isolated from ground in the experiments so that emitted and collected currents could be measured independently. Viewing resistors were appropriately located so that the wave forms of the current through the collectors or the emitters could be observed. Dual beam oscilloscopes were used to observe simultaneously the wave forms of any of the following: the laser light, the emitter current, or the collector current.

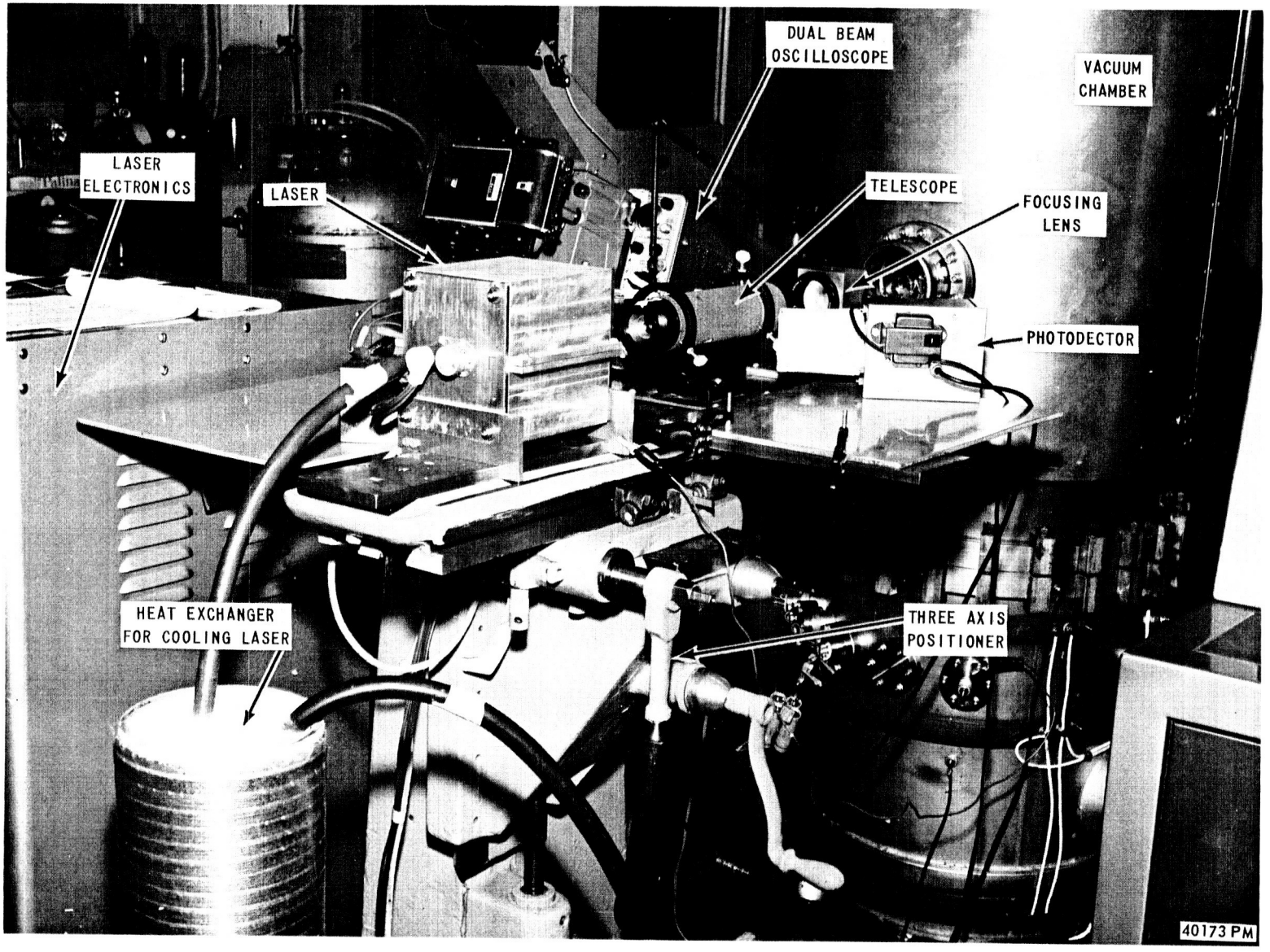

Figure 1 EXPERIMENTAL SETUP FOR STUDY OF LASER STIMULATED EMISSION

The telescope used to collimate the laser light also broadened the beam width for added convenience in aligning and focusing the light spot on the emitter. To prevent destruction of the telescope eye piece by the very intense laser light (a problem experienced in previous experiments) the eye piece optics were converted from a cemented to an air-spaced design. The telescope magnification was one of the experimental variables and will be discussed in Section 6. The magnified, collimated laser energy was focused onto the target situated in vacuum with a focusing lens located external to the vacuum system. This allowed for variation in the laser power density at the emitter surface by adjusting the position of the focusing lens. A 7-inch projector lens, which was selected for enhancing flatness of field and good resolution at the expense of color correction, was used for this purpose.

All the experiments were performed with the emitter material in a vacuum. Except for special tests, the vacuum station was a Varian VI-16B Ultra High Vacuum System with a stainless steel vacuum chamber 18 inches in diameter and 36 inches high. The operating vacuum for all the experiments was typically in the 10^{-9} to 10^{-10} Torr region. It has been found, however, that there is no measurable change in ion generation with background pressures up to 10^{-4} Torr.

3.1 Ruby Laser Characteristics

Two ruby laser rods were used during this program. Due to variations in the impurity distribution in the crystals and small physical variations, these two rods exhibited significant differences in their emission characteristics. The main and most important difference noted was the distribution of the power density output from the two lasers when integrated over the entire pulse time.

The output of a ruby laser is composed of a large number of coherent filamentary oscillations. The distribution of the impurity materials in the ruby determine the position and frequency of these filamentary oscillations and thus the density profile of the emitted power. The two rubies used in the experiments had large differences in the distribution of their outputs.

The first ruby used, Ruby #1, had essentially a uniform power density across the emitted laser beam averaged over the entire pulse time. A photograph of the averaged laser output is shown in Figure 2. It can be seen that the laser power density changes slowly across the edge of the beam but over 60% of the area has a uniform distribution.

Ruby #2, however, had two regions of high power density, the density of one region being higher than the other. An integrated laser output from Ruby #2 is shown on Figure 3. The major portion of the laser beam has significantly lower output power than the high intensity regions. This concentration of laser power of Ruby #2 compared to Ruby #1 lead to significant differences in the ion yields attainable with the two ruby rods.

Although the above difference between the rubies was the most important, two other differences existed. These were:

1) The laser beam formed by the non-uniform power density ruby was less divergent than that formed by the uniform power density ruby. This lower divergence, 5 milliradians as compared to 10

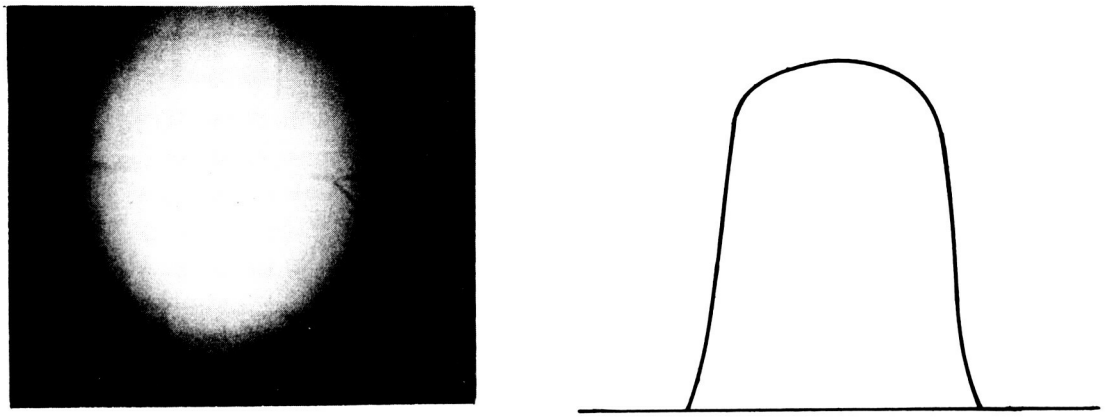

Figure 2 PHOTOGRAPH OF LASER OUTPUT RUBY NUMBER 1
UNIFORM POWER DENSITY LASER

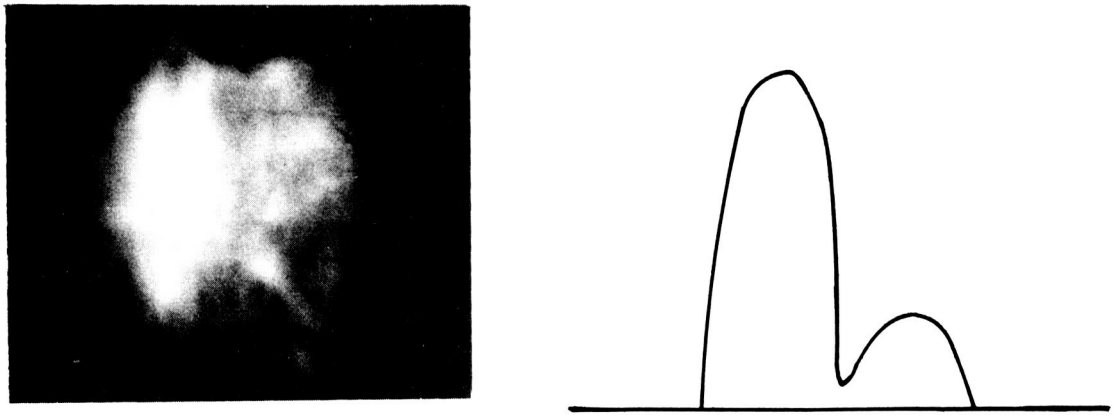

Figure 3 PHOTOGRAPH OF LASER OUTPUT RUBY NUMBER 2
NONUNIFORM POWER DENSITY LASER

milliradians, allowed for a smaller focal point.

2) The efficiency of the flash tube - laser combination was slightly higher for the non-uniform power density ruby.

All these differences tended to produce a higher power density at the focal point of the beam from the non-uniform power-density ruby than that from the uniform power density ruby. The high laser power densities achieved produced higher ion emission when focused near the emitter surface. However, the extremely high power densities tended to cause high yields of neutral efflux, an undesirable trait in an electric thrustor application.

3.2 Power Supply Considerations

The flash tube-laser combinations used in the experimental configuration were operated within certain limits of power supply voltages. The lower limit of the operating voltage depended on having sufficient energy emitted by the flash lamp to pump enough electrons in the rubies to sufficiently high energy levels to overcome inherent losses in the devices and to produce lasing. The upper voltage limit was established by the desire to have a significant flash tube lifetime. (The lifetime of a flash tube decreases as it is operated at higher voltages.) The power supply used at CAL, which is essentially bank of capacitors with a coupled trigger circuit to initiate the capacitor discharge, operated between 2000 and 2500 volts.

The energy level attained from the laser could be changed by modifying the number of charged capacitors in the circuit. There was provision for the connection of 4, 7, 10 or 19, 35 microfarad capacitors. The length of the laser pulse attained with these capacitor banks in the circuit was approximately 265, 480, 705, and 1300 microseconds, respectively. As the number of capacitors in the circuit increased,the peak output power of the laser at any fixed voltage increased slightly, probably due to more efficient pumping in the ruby after the initial losses were overcome. Thus, the variations in the power supply allowed for flash-lamp and, therefore, laser output changes over a very wide range of energies and a narrower range of peak powers.

4.0 EMITTER MATERIAL EVALUATION

The first phase of the program was an evaluation study of thirteen emitter materials. From these materials, four were to be selected for further tests. The selection criteria included factors such as ion output per unit laser input, maximum ion output obtainable per square centimeter of emitter surface, ionization efficiency, velocity of emitted particles, atomic mass, computed and measured impulse and factors relating to the physical handling properties of the materials. No single material tested was best in all respects.

4.1 Description of Experiment and Apparatus

The experimental apparatus used to measure the quantity and energy of the emitted ions from a selected group of thirteen materials is shown in the block diagram of Figure 4. The experiment was arranged to permit testing of various materials under similar conditions. Nine emitter materials could be mounted and evacuated at one time.

Photographs of the experimental emitter and anode assembly are shown in Figure 5. The assembly is also shown mounted in the port of the vacuum chamber. The emitters (except for the chromium sample) were all .020 diameter wires approximately 3/16" long. They were mounted in a stainless steel plate with copper blocks between the emitters. The samples were clamped in a precision multi-section vise. The construction allowed for easy assembly and removal of any or all the emitters without contaminating or abrading the emitter samples. The emitter samples were chemically degreased and cleaned prior to assembly and then were vacuum degassed during bakeout of the vacuum chamber.

The nine anodes, in order to provide nearly identical collecting surfaces for all the emitters, were stainless steel cylinders heliarc welded together and mounted over the emitter support plate. The anode and emitters were electrically insulated; however, the spacing between the emitter support

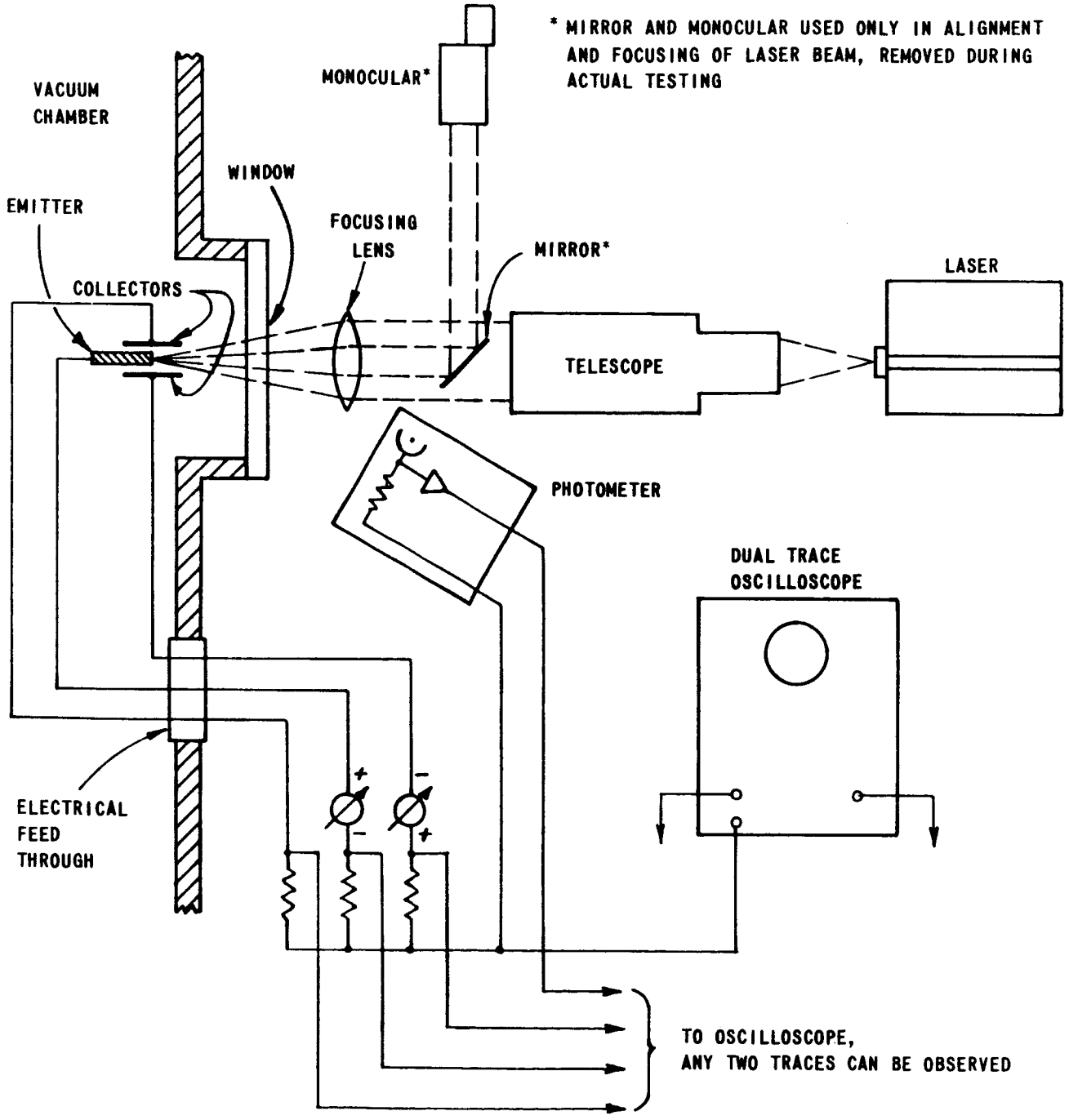

Figure 4 BLOCK DIAGRAM - APPARATUS FOR LASER-SURFACE INTERACTION EXPERIMENTS

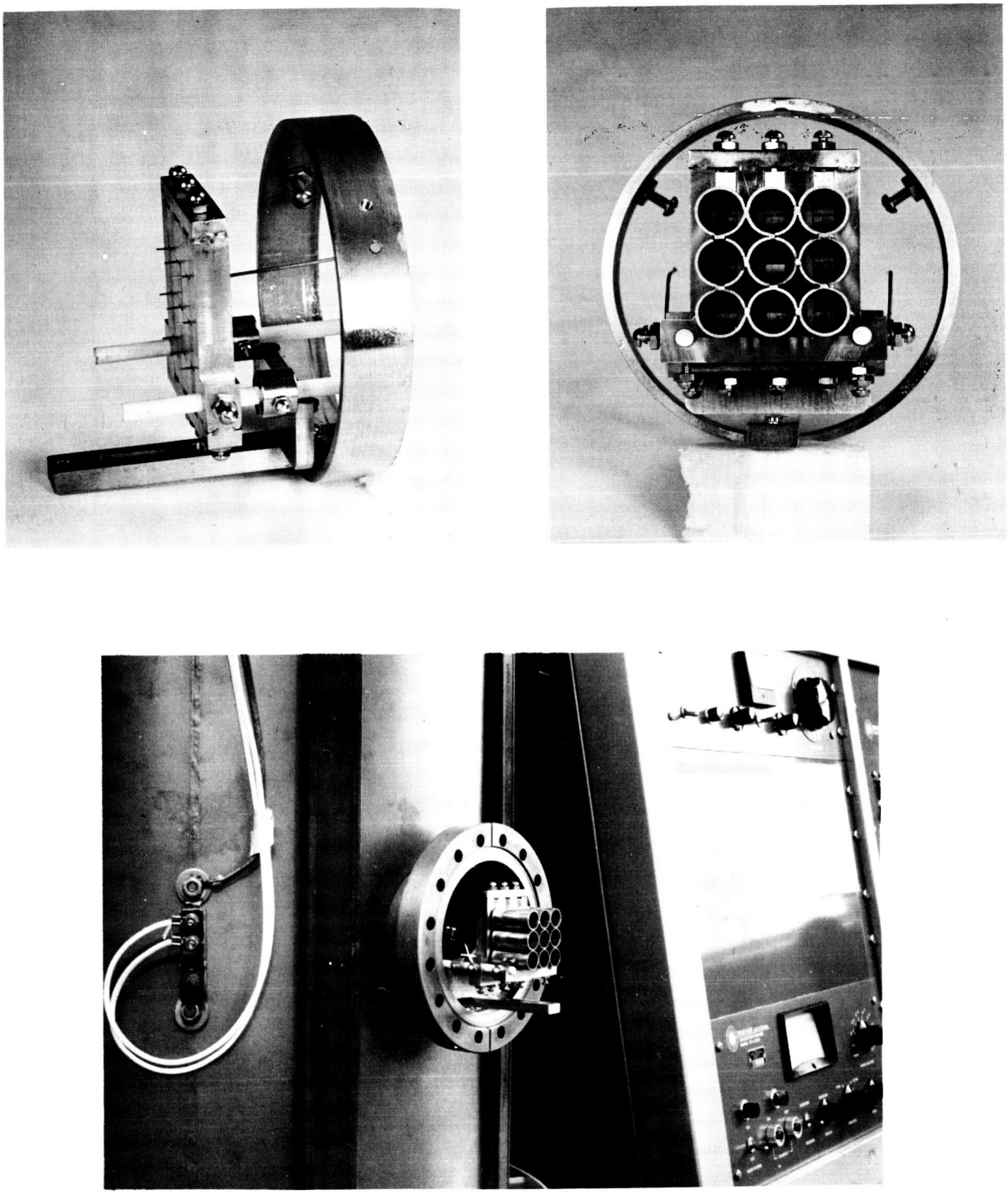

3496

Figure 5

EMITTER MATERIAL EVALUATION APPARATUS

plate and anode assembly was small enough (.055 inches) to prevent any migration of material from one emitter to another. The anode cylinders were 1/2 inch in outside diameter with a .032 inch wall, and were 1-1/8 inches long. It was felt that this diameter and length would permit collection of most of the emitted plasma when a reasonable accelerating voltage was applied to the anode.

Eight different materials (tungsten was repeated for control purposes) were installed in the first experiment. The materials tested were tungsten, tantalum, zirconium, columbium, rhenium, molybdenum, aluminum and copper. The second experiment tested chronium, columbium, hafnium, iron, lead, rhenium, thorium, tungsten and zirconium. Four materials were included in both experiments partly to serve as a control and partly to obtain additional information on their performance. In the first experiment Ruby #1 was used (the uniform power density laser), while in the second experiment Ruby #2 was used.

During the first experiment it was found that, due to the geometry of the emitted plasma plume, not all the emitted particles were being collected. Those not collected formed thin films of material on the vacuum window in front of the experimental assembly. Figure 6 shows a photograph of the deposits. The films interfered with further experimentation on some of the materials; however, sufficient information had been obtained so that a comparison between the various materials could be made. The collector geometry was then modified slightly for the second experiment to try to minimize the amount of uncollected material.

4.2 Test Conditions

The emitter-material evaluation experiments were performed under two different test conditions. The results are discussed separately and then a comparison of all the materials will be made in Section 4.3 by normalizing the results from both tests. The main difference in the two test conditions

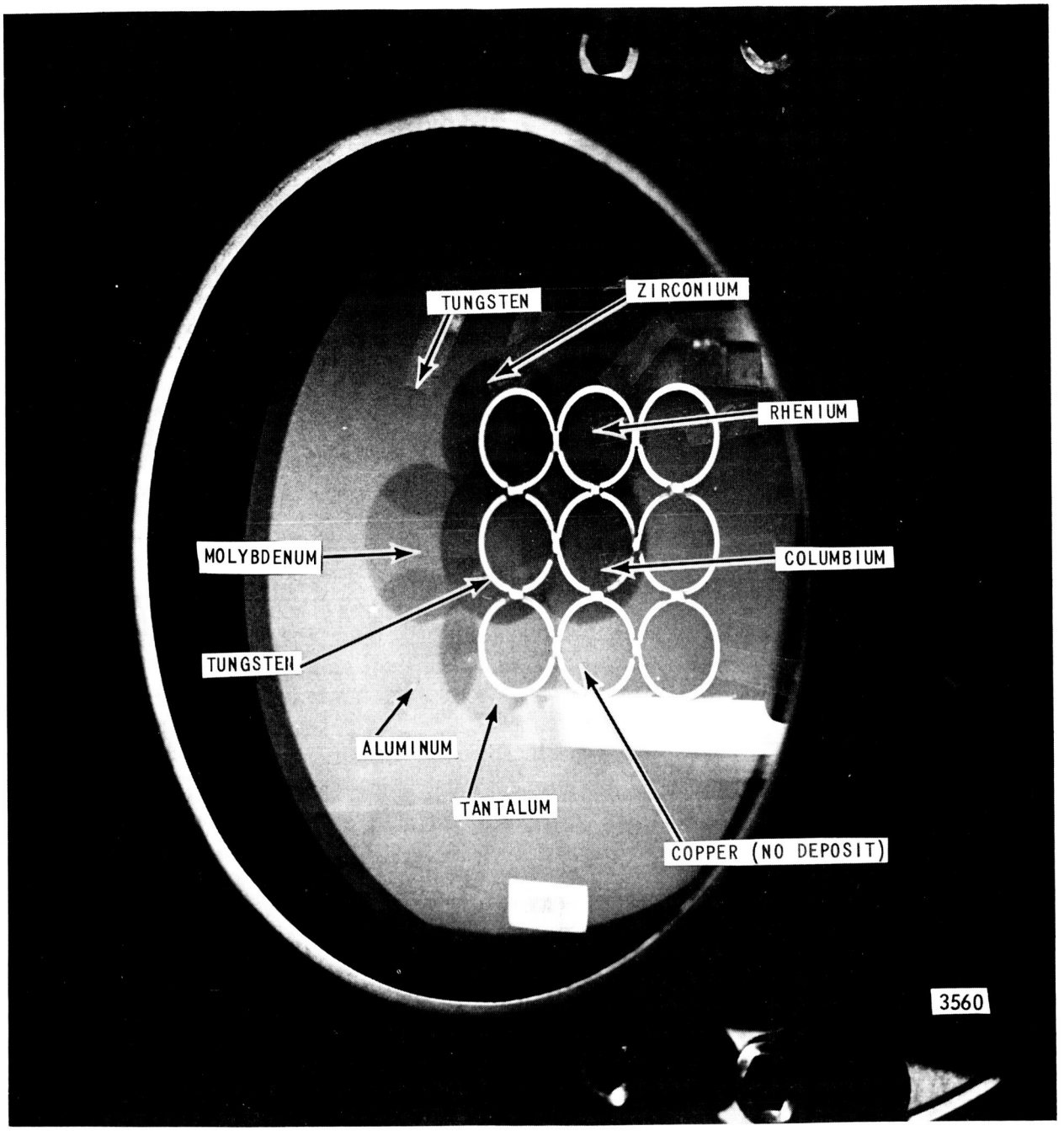

Figure 6 EMITTER MATERIAL DEPOSITED ON CHAMBER WINDOW

was the use of the two rubies described in Section 3.1, which had different moding characteristics. The dependence of ion yield on moding and laser optics will be discussed in Section 6, where several tungsten targets were tested with the two rubies and two different sets of focusing optics.

The first material evaluation experiment was conducted using a 35 mm lens, a fixed focus position, and Ruby #1, (the uniform power density ruby). The second experiment used a new 35 mm lens, a fixed focus position, and Ruby #2 (the non-uniform power density ruby). (The reason for using a new 35 mm lens in the second experiment was that the original eye piece developed a small bubble on the axis in one of the lens elements.) The focus was set at a position which maximized the ion current generated.

The variables in the test conditions thus included:

1. The efficiency of the flash tube - laser combination.
2. The moding and divergence of the laser rod.
3. The position of the laser beam focal point with respect to the emitter surface.
4. Telescope magnification.
5. Total laser energy incident on the emitter.

During these material evaluation experiments, measurements were made of the emitted ion charge and velocity. The parameters of interest for a propulsion application are the emitted mass, total impulse and energy required for each emitted ion. The results of the emitter evaluation tests (discussed in Section 4.3) will be expressed in terms of these parameters.

The emitted mass due to singly ionized atoms is given by

$$m_i = \frac{n_i M}{eN} \qquad (1)$$

The total impulse, I_t , of the ion emission is calculated using

$$I_t = m_i u_i \qquad (2)$$

and the energy, E , of each emitted ion is computed using

$$E = \frac{1}{2} \frac{e m_i u_i^2}{n_i} + V_1 \quad (ev) \qquad (3)$$

4.3 Test Results

A. Material Experiment Using the Uniform Power Density Laser

The initial material evaluation experiment was performed with Ruby #1 on eight materials mounted in the diode structure described in Section 4.1. These materials were tungsten (2 pieces), tantalum, zirconium, columbium, rhenium, molybdenum, aluminum and copper.

The experimental configuration used was such that a fair amount of emitted charge escaped the anode assembly and condensed on the vacuum window. The thin films on the window did not seem to affect the measurements too severely except in the case of the center tungsten sample where large changes in the collected charge did occur. The films on the window shown in Figure 6, are indications of either material evaporation or ion emission and provide a qualitative check on the relative emission amplitude of the various materials.

Shown in Figure 7 is a plot of collected charge versus laser energy for the materials tested in the initial experiment. The discontinuities in the curves in Figure 7 at 1.9 and 3.2 joules of laser energy are caused by the changes in laser output pulse length (changes in the number of charged capacitors in the power supply). Figure 8 shows representative oscillograms for all 8 materials. Copper and aluminum are not plotted in Figure 7 since the level of charge emitted was only 10 nanocoulombs for aluminum and 0.6

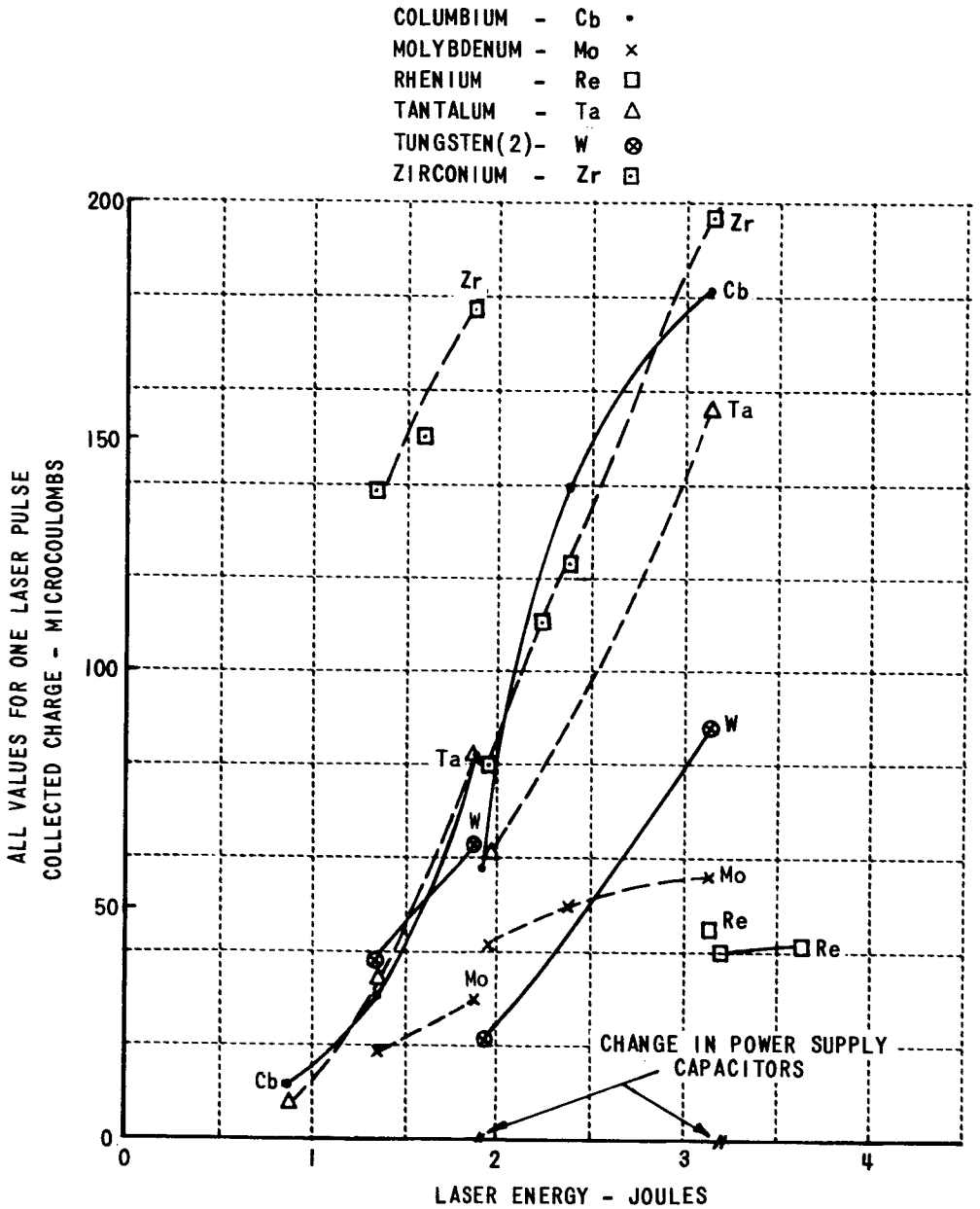

Figure 7 ION OUTPUT AS FUNCTION OF LASER ENERGY
RUBY NO. 1

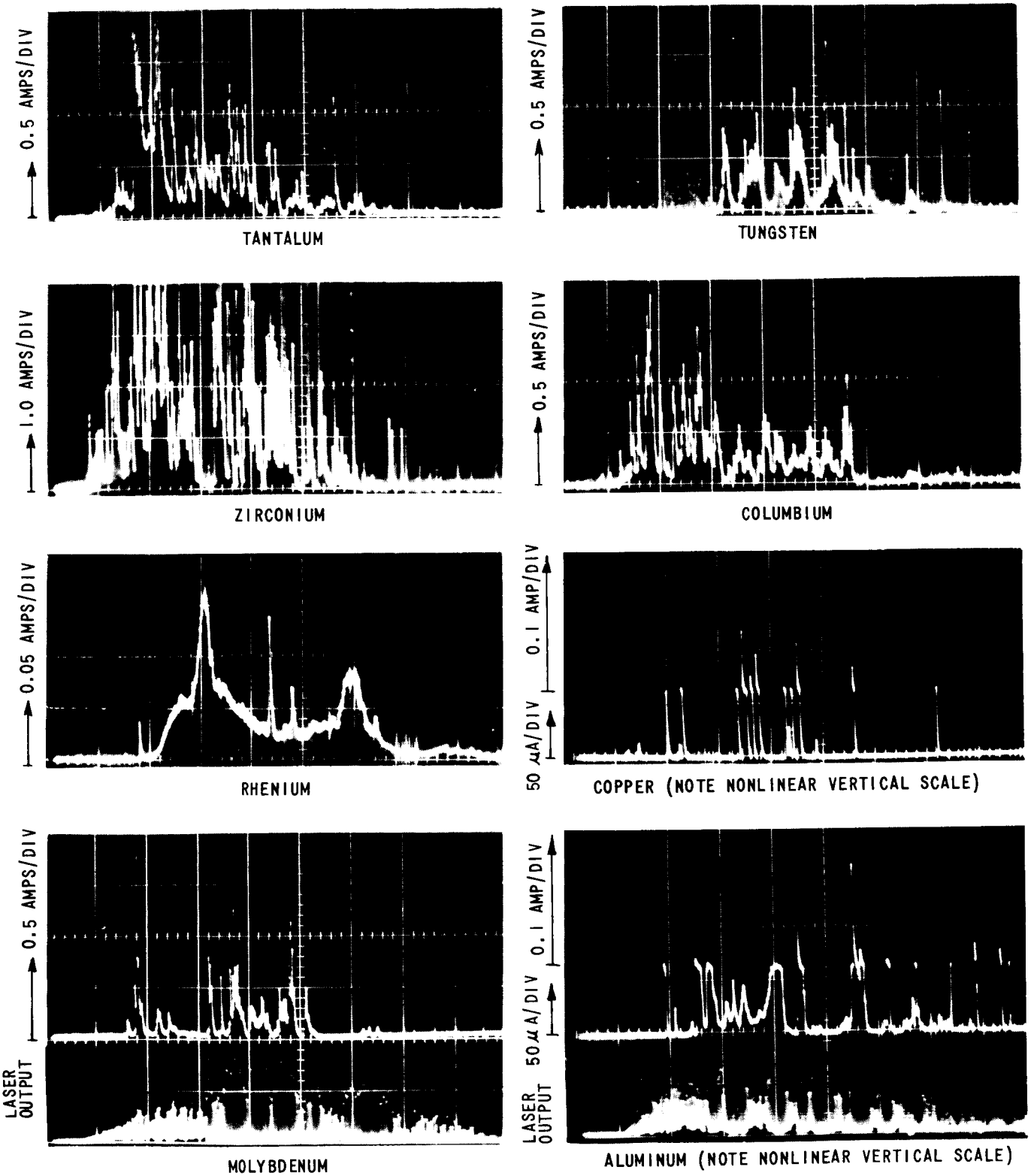

All data taken with approx. 3.3 joules input to emitter. Time base in all traces = 100 μsec/div.

Figure 8 REPRESENTATIVE ION CURRENT OSCILLOGRAMS

nanocoulombs for copper when the laser energy was 3.3 joules and the power was 4.7 kilowatts. Figure 6 shows that the film deposited on the window was negligible for copper and quite thin in the case of aluminum.

It should be noted that the current (or vertical) scales for copper and aluminum on Figure 8 are non-linear. The major portion of the collected current for both of these materials is less than 70 μa. There are, however, spikes of current up to 0.2 amps. In order to show these two ranges of ion current on a single oscillogram the measuring circuit contained two resistors in parallel. The large-value resistor was used for measuring the low level current. The low-value resistor was in series with a back-biased diode so that current was conducted only when the voltage drop across the resistor exceeded the bias voltage on the diode. This low-value resistor would then effectively carry the entire circuit current. Thus, in the two figures, the lower 1.2 divisions display the voltage drop and thus the current through the large value resistor, with a current scale of 50 μa/div. The upper portion (above 1.2 divisions) of the oscillograms display the voltage drop or current through the low value resistor, with a current scale of 0.1 amps/div.

Two materials, rhenium and molybdenum, showed low ion charge collected and an abnormally slow increase in collected charge with increasing laser output. It would almost appear that the emitted particles from these two materials formed a plume much smaller than the plumes of the other materials tested or else formed a plume which decreased in size with increasing laser energy.

Three other materials, tantalum, columbium and zirconium, showed rapid increases in positive ion collection for increasing laser energy although the behavior of zirconium was not consistent. There was a distinct change in the characteristics of the collected current when the duration, peak power, and wave shape of the laser burst was modified by adding capacitors to the flash-lamp storage bank.

The results for tungsten showed some inconsistencies between the two pieces tested. The lower output results are plotted on the curve of Figure 7. The central tungsten piece showed an initial emitter charge approximately three times larger than that plotted. However, each succeeding laser shot showed significantly lower output, leveling off at approximately 100 microcoulombs at 3.3 joules which is very near the value plotted. This result may have been precipitated by either insufficient preparation or degassing of the wire at low laser energies.

All of the values of the collected charge for the various materials were low since not all the emitted current was collected and the input laser power was partially reflected by the thin film on the vacuum window. However, a relative comparison of the total impulse, emitted charge and ion energy was made for the various materials, and is shown in Figure 9.

The transit time of the ions between the emitter and the collector was measured during the experiment. The average velocity of the emitted ions lies between 3 and 9 km/sec., the large collector area did not permit a more accurate determination. The impulse and ion energy on Figure 9 were calculated from an ion velocity determined using the average collector-emitter separation. In contrast to data taken later in the program this averaged velocity did not show a ($v \propto \sqrt{M}$) relationship for the materials tested, which might infer a difference in the shape of the various emission plumes.

B. Material Experiment Using the Non-uniform Power Density Laser

The second material evaluation experiment used a slightly modified assembly in which an electrically insulated cover plate was mounted over the collector cylinders. The plate had nine 1/4 inch diameter holes centered over the emitters. The arrangement did not interfere with the transmission of laser light to the emitters, but made it possible to capture approximately two thirds of the material, either charged or uncharged that appeared to

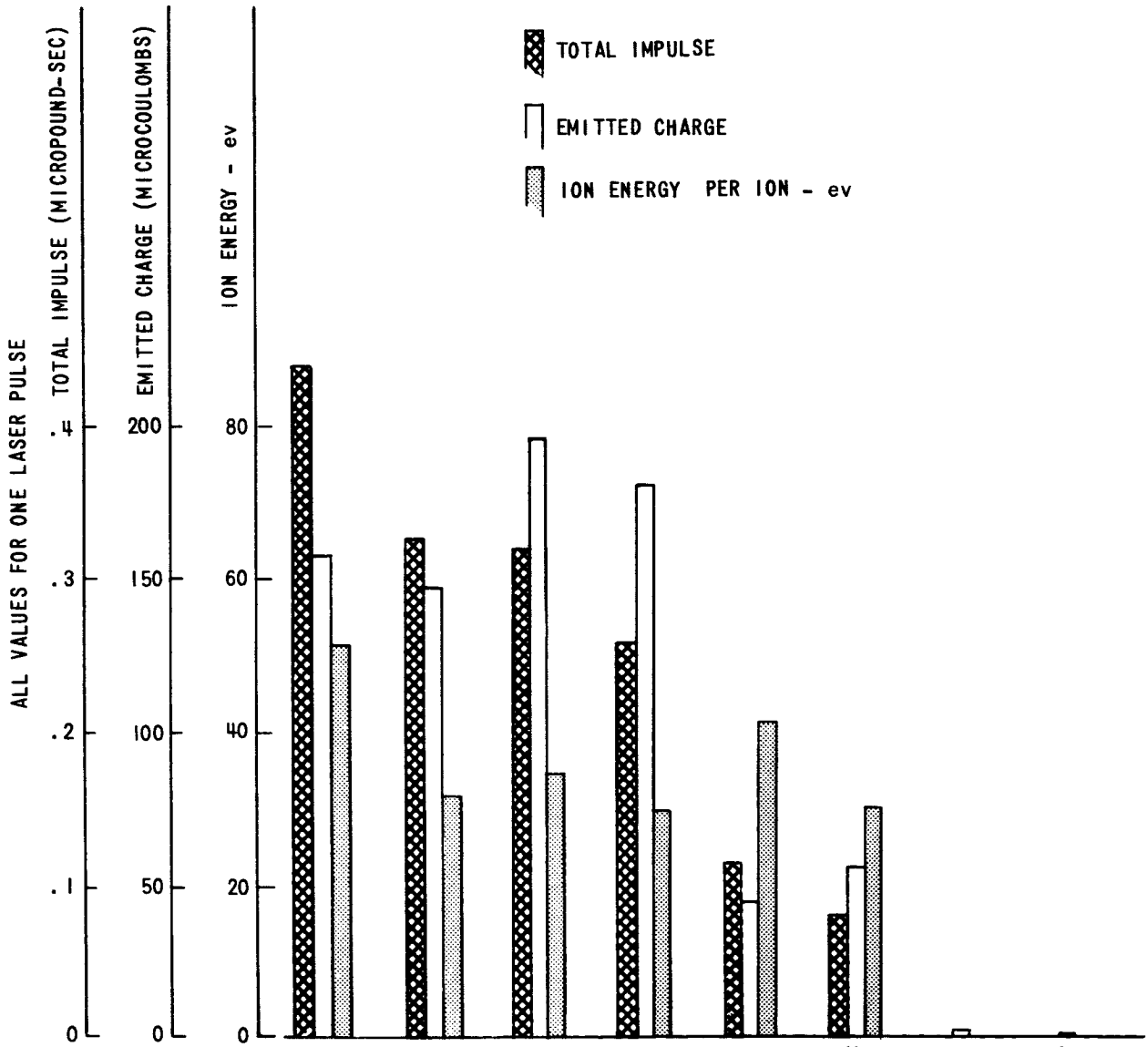

Figure 9 EMITTER COMPARISON BAR GRAPH

escape from the collector assembly in previous tests. A comparison of the charge collected on the cylinders and on the cover plate permitted a partial understanding of the form of emission, i.e., plume configuration and ion velocities. The data obtained with this configuration indicated that the charge was emitted with a cosinusoidal distribution.

The materials tested during this second experiment were chromium, columbium, hafnium, iron, lead, rhenium, thorium, tungsten and zirconium. This test was performed using ruby #2 and a replacement eye piece in the telescope. As noted in Section 3.1, the output of ruby #2 had about one half the beam divergence of that of ruby #1, and also had a moding characteristic producing intense hot spots in the beam. This arrangement gave the highest SPOD* value obtained during the program and resulted in the highest ion yield per joule input. This intense laser power density, however, also caused neutral material to be ejected from the emitter.

Four materials (columbium, rhenium, tungsten and zirconium) were retested partly to serve as controls, and partly to obtain data on performance of these four materials at a high SPOD value. The results of the second group of experiments are plotted in Figure 10. The laser input level used in the series of comparison runs graphed in Figure 10 was adjusted to yield outputs in the range of about 100 microcoulombs, which was the same as the output range experienced in evaluating the first series of emitters. Note that this output level was obtained with 1.0 joule laser output power using the high SPOD value whereas 3.3 joules was required to obtain comparable levels in the first series of runs using the lower SPOD value. The impulse and ion energy values were calculated using the ion velocity determined by the transit time measurements to the collector cover plate. These measurements were reasonably accurate because the distance to the cover plate from the emitter varied only 2 percent. These calculated values

---

* SPOD value is an abbreviation for Focal Spot Power Density.

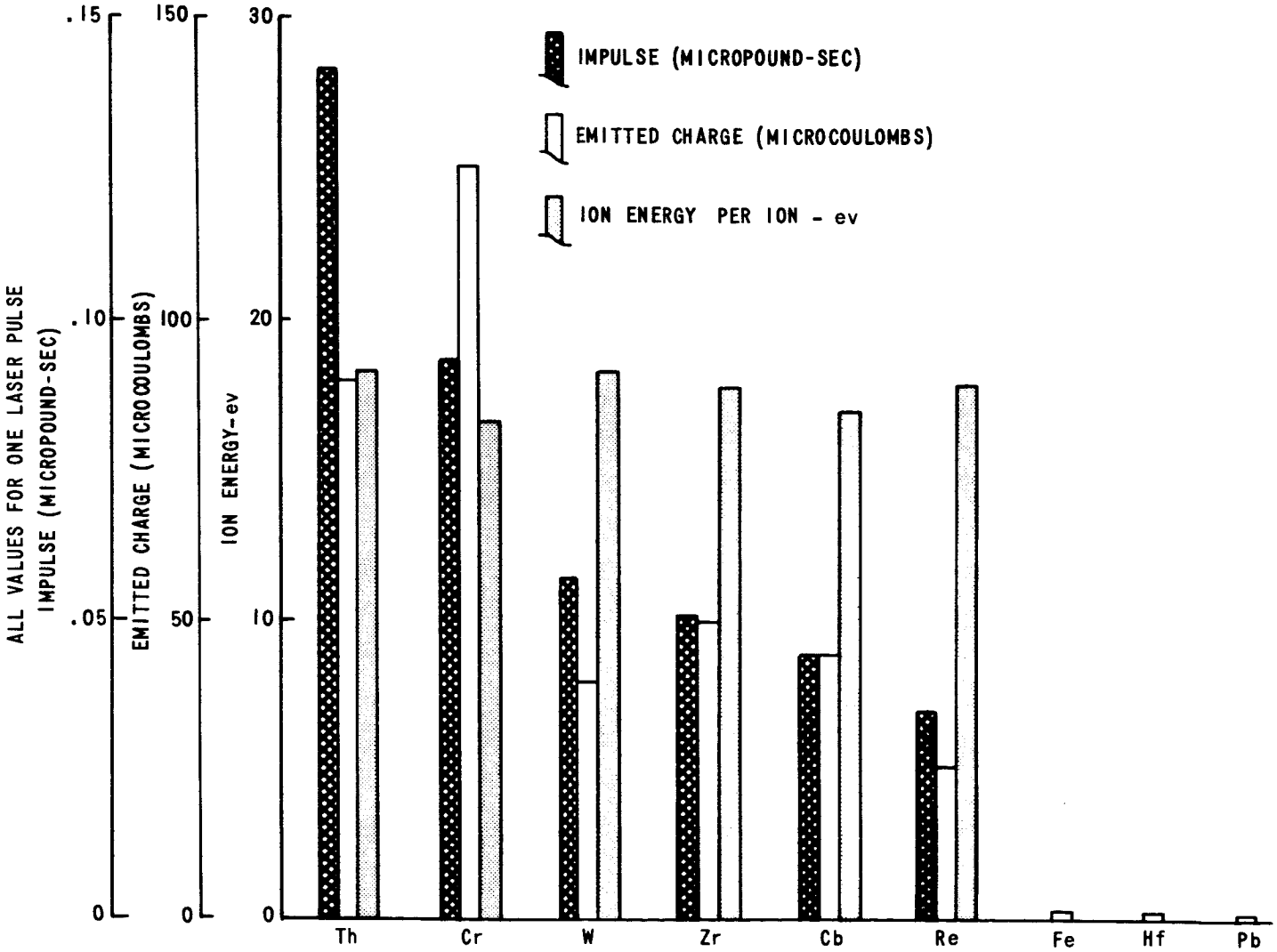

Figure 10 TOTAL IMPULSE, COLLECTED CHARGE AND ION ENERGY AT 1.0 JOULE LASER ENERGY RUBY NO. 2

of velocity agreed reasonably well with those calculated using the average emitter-to-collector distance and the emitter-to-collector transmit time. The velocities calculated show a ($v \alpha \sqrt{M}$) relationship between the various materials.

Two of the materials, thorium and zirconium, were operated up to a high level of input energy in conjunction with the high SPOD value. The other materials in the test were not tested at the higher levels because of: 1) the presence of a metallic film on the vacuum window, 2) low ion current yield in the original test, or 3) extreme damage to the specimen. The ion outputs for thorium and zirconium at a high input level (3.3 joules) combined with a high SPOD value are graphed in Figure 11. For thorium the output increased over 20 times as the input was raised 3.3 times (with no change in optics). For zirconium, the output increased nearly 30 times as the input was raised 3.3 times (with no change in optics). For zirconium, the yield at 3.3 joules at the high SPOD value was about 10 times the yield with 3.3 joules and low SPOD value. The values for zirconium when tested at a low SPOD value with Ruby #1 are also included on Figure 11 for comparison. While the emitted charge and impulse are significantly lower, the ion energy is higher due to the higher ion velocity attained when Ruby #1 was used.

C. Relative Results

Using the results from the materials common to both experiments a comparison is made in Figure 12 of all materials on the basis of ion output and mechanical impulse, the two parameters of particular significance. The data presented was found by determining the laser levels where the repeated materials had the same collected charge in the two experiments and then using the measured values for the other materials at these laser levels. Aluminum, copper and lead are not shown in the chart of Figure 12 since they had essentially zero output both in emitted charge and impulse. (Lead subsequently showed a high level of ion output and impulse during the pendulum experiments, see Section 7.) Referring to the comparison data in

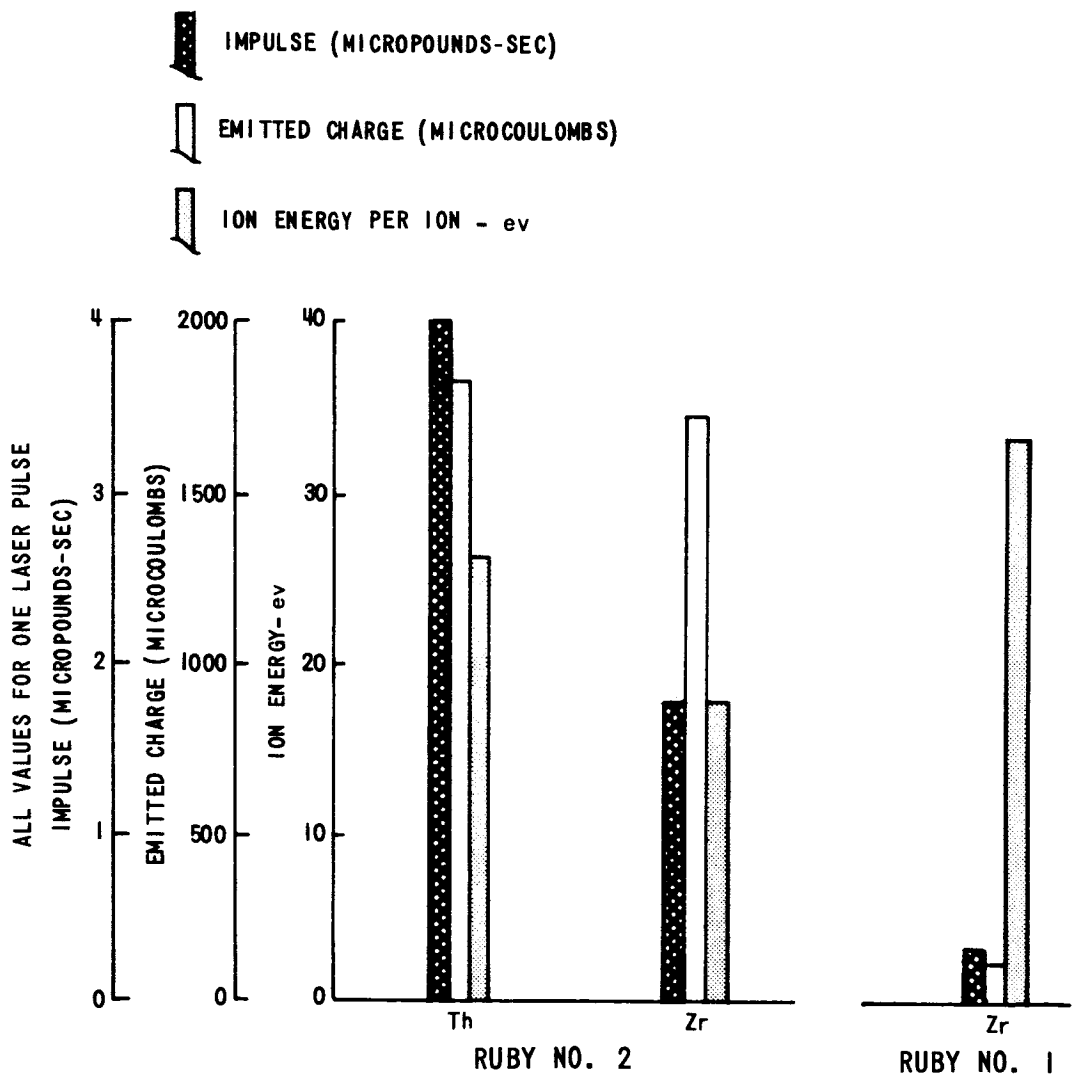

Figure 11 TOTAL IMPULSE, COLLECTED CHARGE AND ION ENERGY AT 3.3 JOULES LASER ENERGY

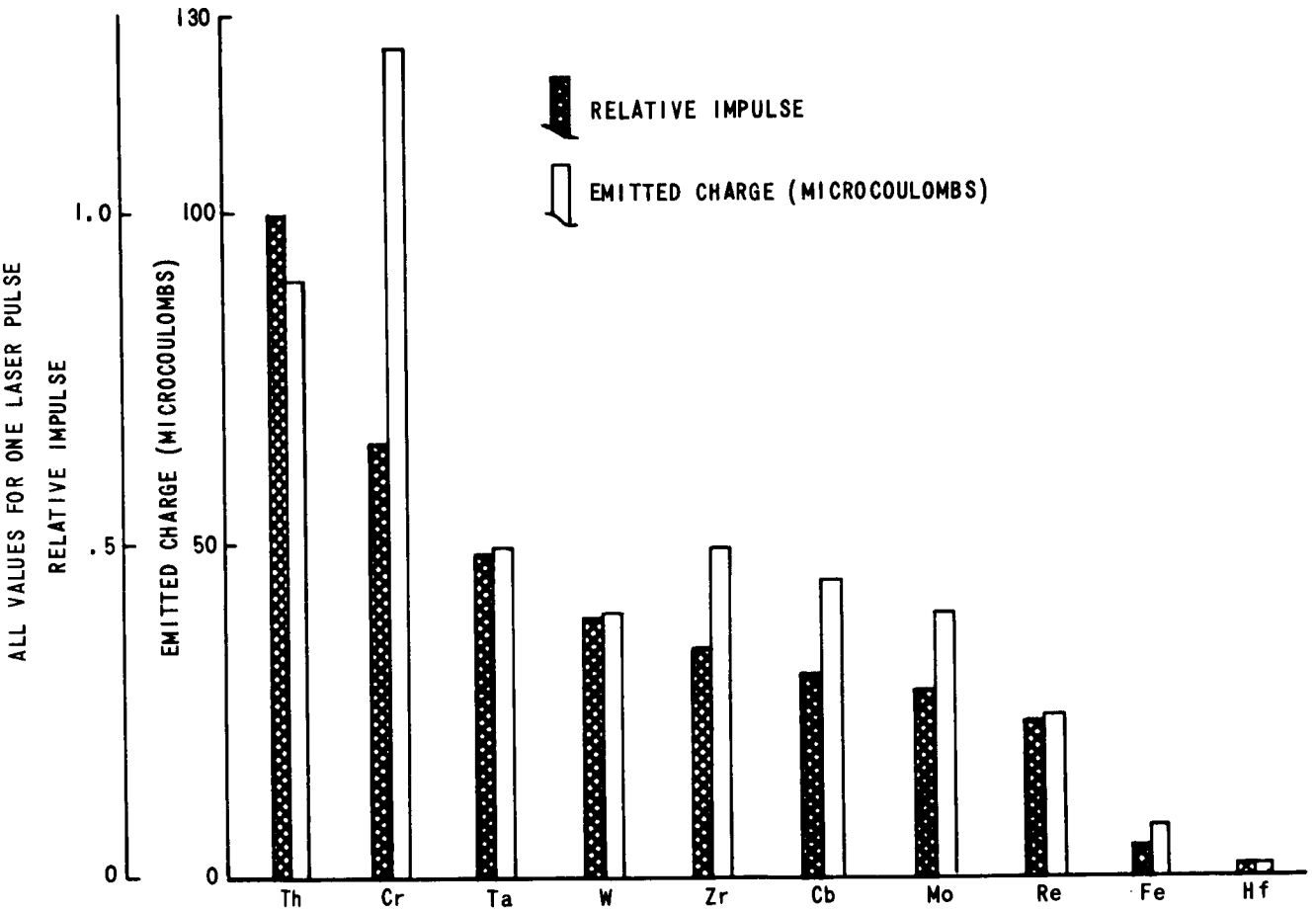

Figure 12 COMPARISON DATA FOR ALL EMITTER MATERIALS HAVING SIGNIFICANT OUTPUTS

the chart: chromium produced the highest emitted charge; it was particularly good in giving sizable output at low laser input levels; it suffered considerable surface damage even at relatively low input levels; and it proved incapable of being pushed to high ion yields. Thorium gave respectable charge output per joule, performed well when pushed to very high outputs, has a high atomic weight, but is toxic, flammable and physically hard to handle. Tantalum and tungsten appeared to behave in similar fashion. The latter emitter samples were consumed in a controllable fashion, i.e., the ends of the wires did not split or develop deep holes; are easily and safely handled, and chemically stable. Tungsten has performed well, although not with perfect consistency, at combined high input levels and high SPOD values. Tantalum has not been tested at combined high input levels and high SPOD values. The remaining materials had progressively lower (although not much lower) yields and share many properties such as high susceptibility to surface damage and material loss significantly beyond that expected if all emitted material had been ionized. Experiments with various SPOD values were performed on tungsten emitters and are discussed in Section 6.

4.4 Material Selection

Four materials were to be selected for extensive tests of their electrical characteristics which were pertinent to an electric thrustor application. The selection of these materials was based on the results of the emitter evaluation tests described in Section 4.3; and the impulse measurements discussed in Section 7. The factors considered were the ion yield per joule of transmitted laser energy, measured and calculated impulse and calculated ion energy at a fixed laser energy and rate of ion yield increase with change in laser energy. In addition, the physical damage inflicted to the material, especially as a function of laser power density, the availability and the ease of handling the materials were also considered in the selection.

The materials selected for further tests were chromium, lead, thorium and tungsten. There was a possibility of a high percentage of neutral emission with chromium and lead. Chromium was damaged by the intense

laser power density of Ruby #2, however its high charge emission and measured impulse suggested it should be investigated further. Lead, with its very low melting and boiling points and damage by Ruby #2, was also suspected of high neutral emission but it was also worthy of further investigation. Two other materials, rhenium and tantalum, were selected as possible alternates in case chromium and lead had to be discarded. In fact, during the tests to measure the emitted species of particles using a quadrupole mass spectrometer, lead and chromium did have large neutral yields and further tests on these materials were not performed. Table I gives a brief exposition of the measured or calculated results and the physical properties of the six materials discussed in this section. Section 4.5 discusses one possible explanation of the variation in laser induced damage to the various materials based on their physical properties.

4.5 Relation of Damage to Physical Properties of the Materials

The emission of positive ions from metallic surfaces as a result of laser illumination requires average power densities from a focused laser of the order of 10^6 watts per cm^2. In many cases this extremely high power density bombardment of surfaces causes severe physical damage. The material damage or neutral emission due to laser illumination appears to be directly proportional to material boiling point times its thermal conductivity divided by (1 - reflectivity at 6943 Å). Shown in Figure 13 are

(1) Boiling Point x Thermal Conductivity

and (2) Boiling Point x Thermal Conductivity ÷ (1 - Reflectivity at 6943 Å)

for the various materials.

Both copper and aluminum, because of their high thermal conductivity and high reflectivity at 6943 Å, should incur only minimum changes in surface condition as a result of laser beam illumination. This was, in fact, true and in the case of copper no surface change was noted during the material evaluation tests until 5 KW of laser power were directed toward the surface

Table I

	Thorium	Chromium	Tungsten	Lead	Rhenium	Tantalum
Impulse	Good	Good	Fair	Good	Good	Fair
Collected Charge (Impulse Test)	Good	Good	Very good	Good	Fair	Fair
Emitted Charge (Material Evaluation Test)	Good	Very good	Fair	Poor	Fair	Good
Material Damage	Fair	Poor	Good	Very poor	Good	Fair
Availability	Poor	Fair	Good	Good	Good	Good
Size Availability	Poor	Poor	Good	Good	Good	Good
Ease of Handling	Poor	Fair	Good	Poor	Good	Good
Melting Point	Low	Medium	Very high	Very low	Very high	Very high
Boiling Point	Medium	Low	Very high	Low	Very high	Very high
Atomic Weight	Very high	Low	High	High	High	High

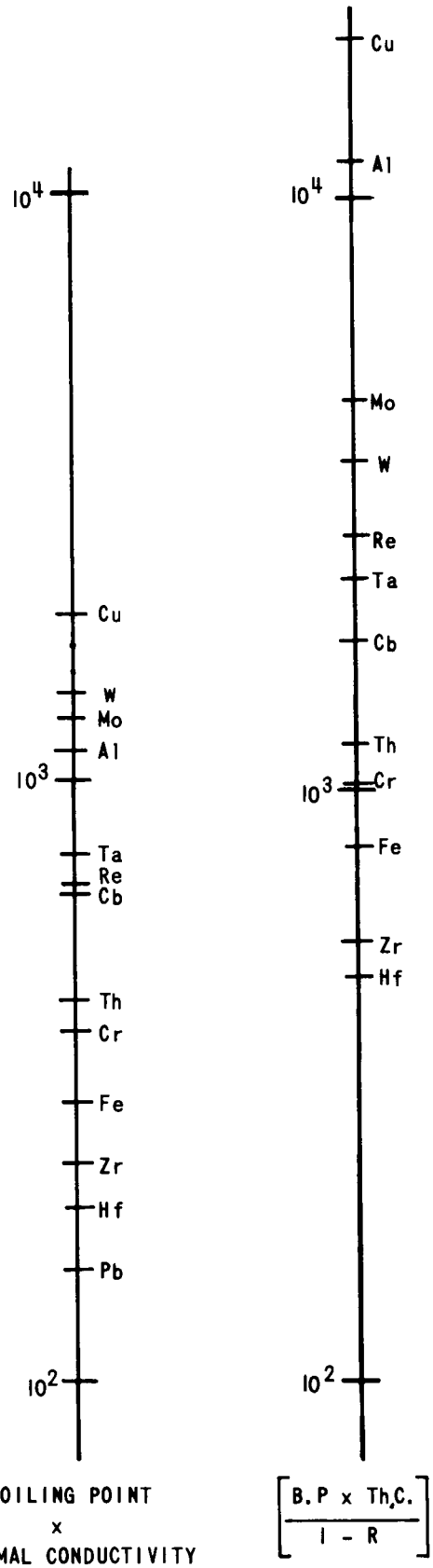

Figure 13 THERMAL CHARACTERISTICS OF VARIOUS EMITTER MATERIALS (IN CAL/CM^2/CM/SEC)

and even then visible material changes were minimal. Materials with low values of thermal conductivity times boiling point divided by (1 - Reflectivity) such as hafnium and zirconium showed a high degree of surface damage. Lead is not plotted due to the lack of spectral reflectance data. However, both the boiling point and the thermal conductivity of lead are quite low and a high degree of damage might be expected.

5.0 GEOMETRY STUDY

Previous measurements [1] of laser generated electron emission showed the emitter geometry to be one of the parameters effecting the electron yield. The possibility thus existed that laser-generated ion emission might also be a function of emitter geometry. For this reason, apparatus was assembled to investigate the effect of this parameter on ion emission.

In the tests performed during this program the dependence of ion yield on emitter configuration was found to be minor. This apparent discrepancy between the electron and the ion emission results probably relates to the laser power density used for emission. The power density required for ion emission was at least an order of magnitude higher than that required for electron emission.

5.1 Geometry Test Configuration

The experimental test configuration shown in Figure 14 was constructed to permit examination of the effects of emitter geometry on emission. The tungsten targets included wires of 0.020, 0.060 and 0.250 inches diameter and a 0.020 inch thick plate.

Since the material test experiment had caused some trouble with metal deposition on the chamber window in the emitter evaluation tests, the open end of the anode for the geometry test was shielded with a wire mesh, as shown in Figure 14b. The tungsten mesh, 140 by 140 wires per inch, with .0013 diameter wires, did not completely eliminate the deposition of a film on the vacuum window although it greatly decreased the rate of growth of the film.

Unfortunately, the wire mesh directly in the path of the laser beam interfered with the experiment in that it attenuated the laser light. In addition, very peculiar oscillograms of what was thought to be ion current were

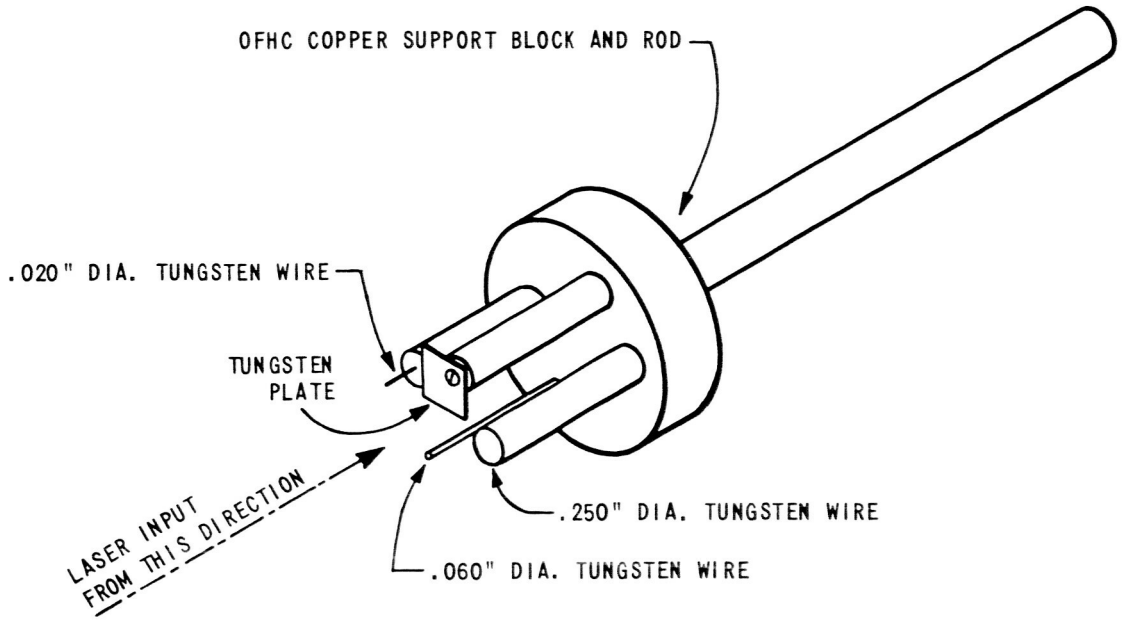

Figure 14a EMITTER CONFIGURATION FOR STUDIES OF GEOMETRY EFFECT

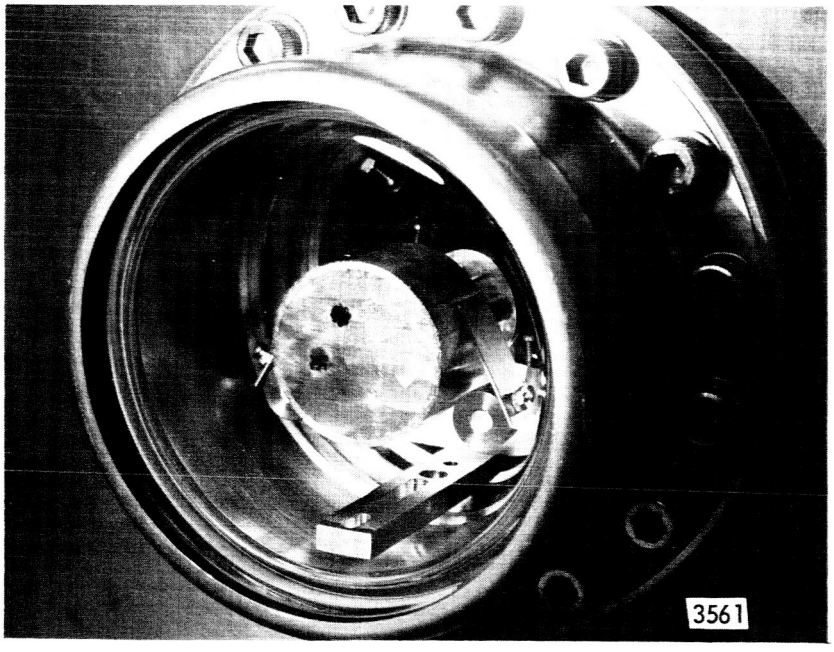

Figure 14b COMPLETE ELECTRODE ASSEMBLY FOR STUDIES OF GEOMETRY EFFECT

obtained. A selection of oscillograms showing this "ion" current appears in Figure 15. The laser burst is shown at the bottom of each oscillogram and the "ion" current "collected" by the screen is shown at top. Note that the "ion" current extends for milliseconds after the cessation of the laser pulse.

A brief experiment was performed to show that the electron emission from the screen was the cause of the anomalous ion current. The beam from the laser was moved so that it still passed through the screen (as it did when attempts were being made to obtain ion current from a tungsten emitter) but so that it did not illuminate the emitter. This configuration is shown in Figure 16. The laser was pulsed at 5 minute intervals and the data shown in Figure 15 was obtained. This data shows conclusively that the anomalous ion current was, in fact, electron current from the screen. Current was emitted from the screen long after the laser burst stopped because of the long thermal time constant of the screen. The wild oscillation on the current traces probably resulted from plasma oscillations which in turn resulted from the interaction of the electron current released from the screen with the gas desorbed from the heated screen. Support for this plasma-oscillation theory is evidenced by the decrease in the amplitude of the oscillations in succeeding laser shots after the t=0 shot. (The screen was outgassed to some extent with each laser shot so that less gas was available on succeeding shots for interaction with the emitted electrons.) Figure 17 shows the fine detail of the oscillation and shows that the frequency of the oscillation was about 150 Kc/s. This frequency is typical of ion-plasma oscillation frequencies. The emission interference problem was eliminated with the laser by melting small (1/4 inch diameter) holes through the mesh over the various targets. The formation of a window film in the path of the laser light occurred as in the emitter evaluation experiments but did not severely interfere with the transmission of the laser energy during tests.

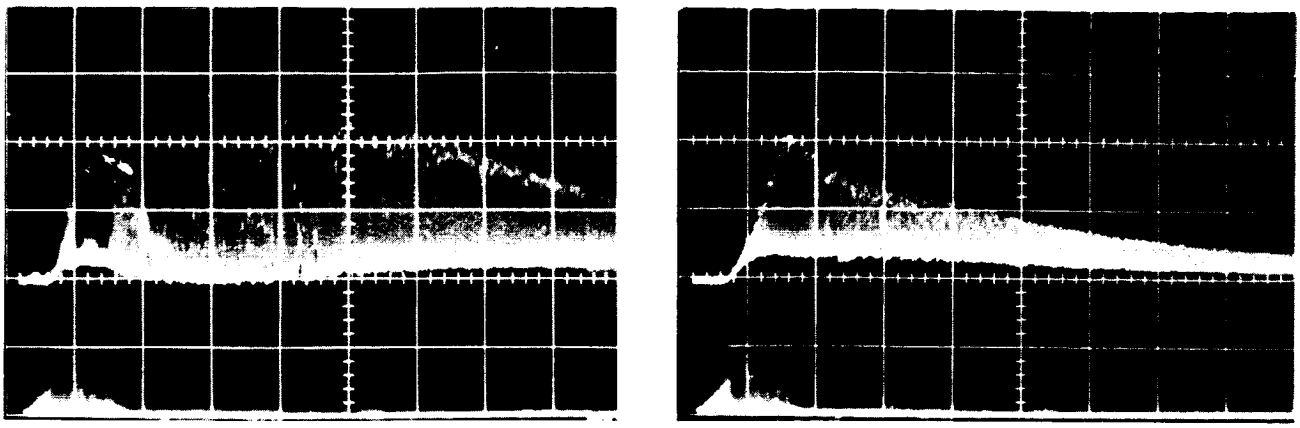

t = 0

t = 5 min

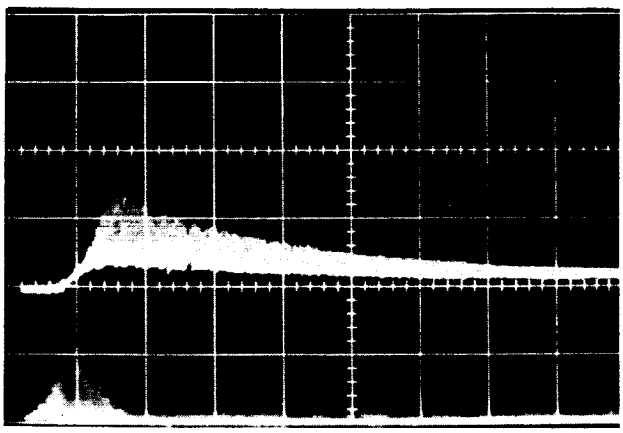

t = 10 min

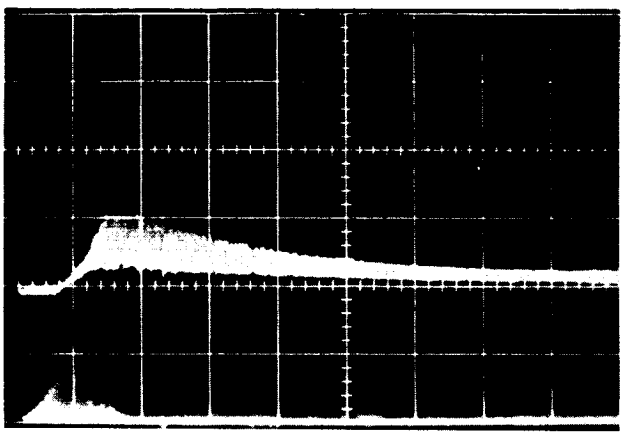

t = 15 min

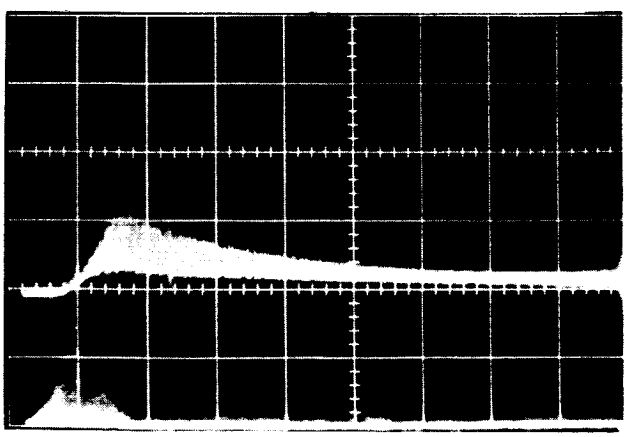

t = 20 min

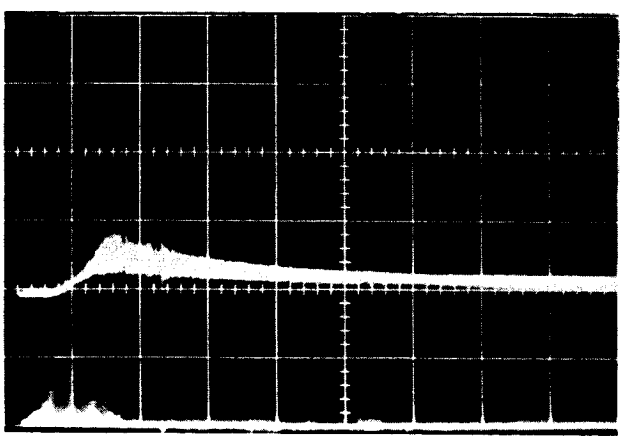

t = 25 min

Figure 15 OSCILLOGRAMS SHOWING ANOMALOUS ION CURRENT (TOP TRACE) FOR LASER SHOTS (BOTTOM TRACE) TIMED 5 MINUTES APART. THE TIME SCALE IS 500 μS/DIV, AND THE CURRENT IS 2 MA/DIV, IN ALL TRACES

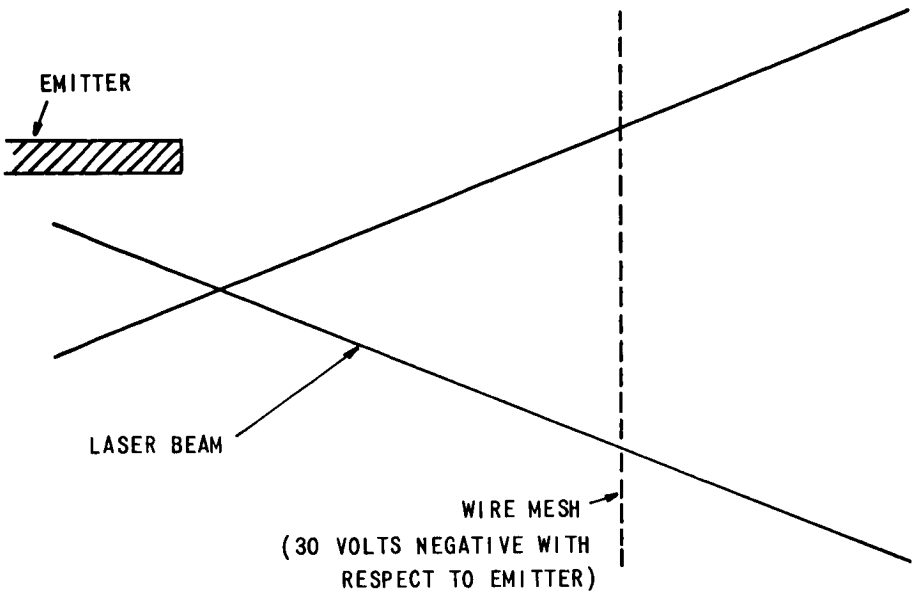

Figure 16 CONFIGURATION USED TO TEST FOR EMISSION FROM WIRE MESH

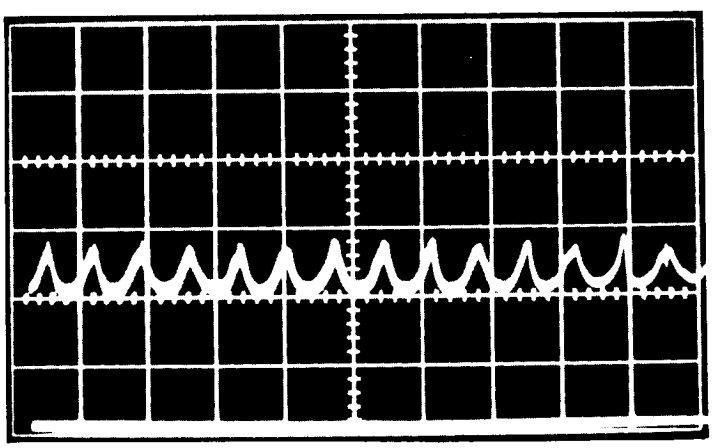

Figure 17 EXPANDED TRACE (10 μ SEC/DIV) SHOWING NATURE OF OSCILLATIONS IN OSCILLOGRAMS OF FIGURE 15

5.2 Emitter Geometry Results

No significant variation of emission properties with emitter geometry was found with the representative emitter forms tested. The emitter geometries noted were illuminated at various power densities at various locations, i.e., near the edges and near the center. They were also illuminated with the laser focal spot at various distances from the illuminated surface. Figure 18 indicates how insensitive the emitted ion current was to focus position. The main difference found between the emitters was the degree of irreparable damage caused to the 0.020 inch thick tungsten plate with Ruby #2. Ruby #2 had a tendency to drill holes in many materials and a thin plate did cause experimental difficulties as noted in Section 7.

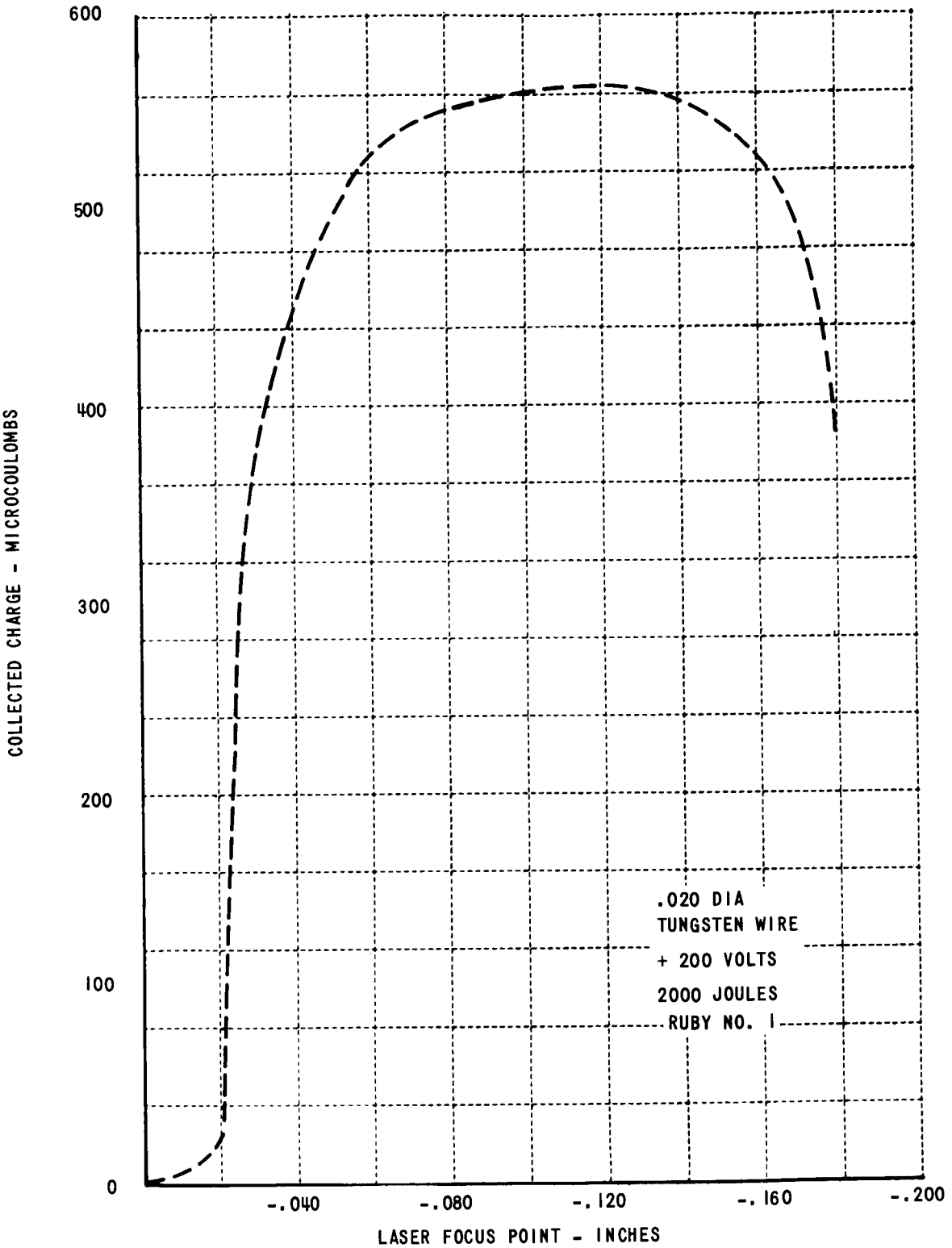

Figure 18 VARIATION IN COLLECTED CHARGE VS LASER FOCUS POSITION

6.0 EFFECTS OF OPTICAL PARAMETERS

During a study of the effects of emitter geometry on ion generation a flash tube used to pump the laser failed mechanically and damaged the ruby. The damage to the ruby appeared at that time to be serious enough to warrant replacement, although later tests established that the ruby essentially operated with its previous properties. Ion output with the replacement ruby was substantially higher than that obtained with the first ruby, as shown in Figure 19. The characteristics (noted in Section 3.1) of the ruby giving higher output were examined with the following results. The replacement ruby (referred to in this report as ruby #2) had a slightly higher efficiency than ruby #1 in terms of energy out with respect to energy input to flash lamp, its output beam had about one half the overall divergence of the beam produced by ruby #1, the moding of ruby #2 concentrated the output in two narrow pencils of light so that combined with the reduced overall divergence the power density at the point of focus when using ruby #2 was about 30 times greater than the level obtained with ruby #1.

6.1 Test Configuration and Results

Most of the tests made on optical parameters were performed using the nine-emitter test assembly fitted with tungsten emitters cut from the same lot of material and subjected to as nearly identical preparation and cleaning as possible. A few tests described later in this section were made with a larger single-collector cylindrical assembly (used originally in LASIG I). This test assembly allowed visual observation of the emitter during an actual emission episode and enabled testing for possible effects of collector geometry on ion yields.

Emission data were taken using equipment and techniques identical to those used for the emitter evaluation tests, but with a four-level variation in optical parameters as shown in the following table.

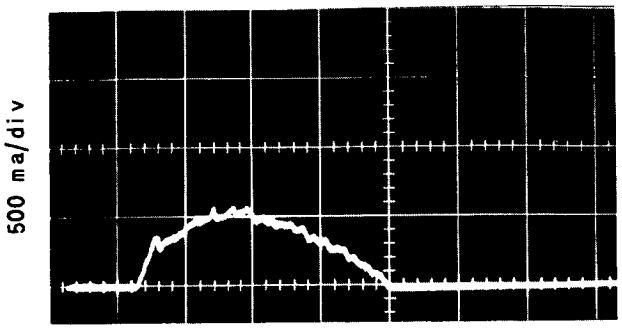

7.5 JOULES INPUT
270 μ COULOMBS OUTPUT
FOCAL DISTANCE 0.160"

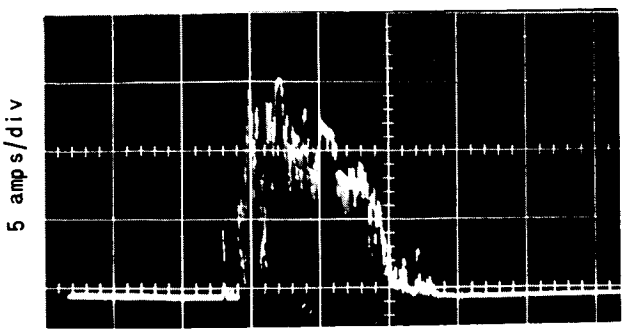

1.0 JOULES INPUT
2160 μ COULOMBS OUTPUT
FOCAL DISTANCE 0.135"

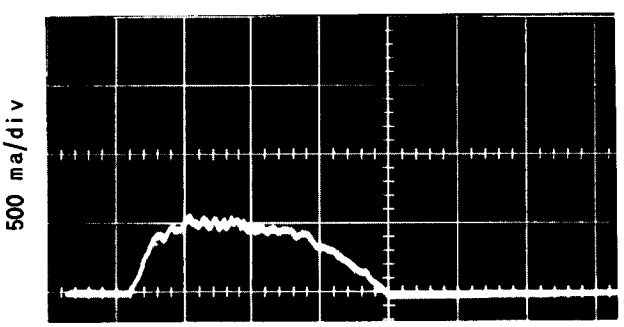

7.5 JOULES INPUT
305 μ COULOMBS OUTPUT
FOCAL DISTANCE 0.135"

RUBY #1

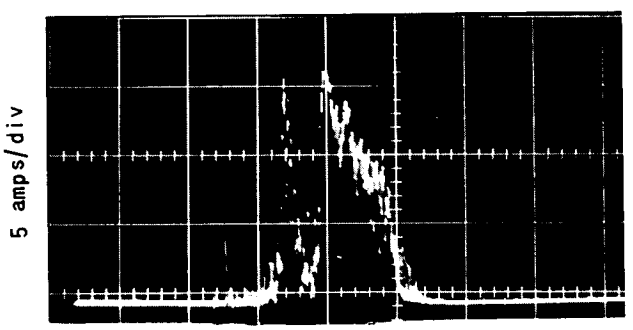

1.0 JOULES INPUT
1580 μ COULOMBS OUTPUT
FOCAL DISTANCE 0.135"

RUBY #2

Figure 19 ION CURRENTS OBSERVED WITH DIFFERENT RUBIES
(SAME 1/4" DIAMETER TUNGSTEN ROD USED FOR ALL TESTS)

Optical Configuration	Ruby	Telescope Eyepiece Focal Length (Millimeters)	Overall Image Diameter (Inches)	Mode-Spot Image Diameter (Inches)
1	1	50	20.5×10^{-3}	no spots
2	1	35	14.5×10^{-3}	no spots
3	2	50	10.4×10^{-3}	2 spots 3.4×10^{-3}
4	2	35	7.3×10^{-3}	2 spots 2.4×10^{-3}

The test results are shown in Figure 20. In all cases, the output increases as the image size is decreased, i.e., as spot power density is increased. As power level is increased beyond a threshold point determined by the specific optical configuration, the output current increases very sharply but not necessarily to a level that indicates runaway breakdown. There was no evidence of permanent changes in the emitter after these high output episodes and reducing the laser level retraces the points on the lower part of the curve with no hysteresis. If input power is increased sufficiently a runaway arc finally does occur. During this arc, current is controlled by the external circuit and no longer bears a functional relationship to laser level. Spot power densities with optical configurations #3 and #4 are so high that total laser input could not be utilized beyond 550 and 700 joules respectively, runaway arcs occurring as power was increased beyond these levels. Optical configuration #2 allowed power increases beyond the threshold condition, e.g., at 1500 joules laser input energy, with subsequent increases in output and with no evidence of runaway arcs. In fact, the spot power density with configuration #2 was not high enough to produce runaway arcs at any power level available in the experiment. With optical configuration #1 power density conditions required even for the rapid threshold increase in output current could not be achieved.

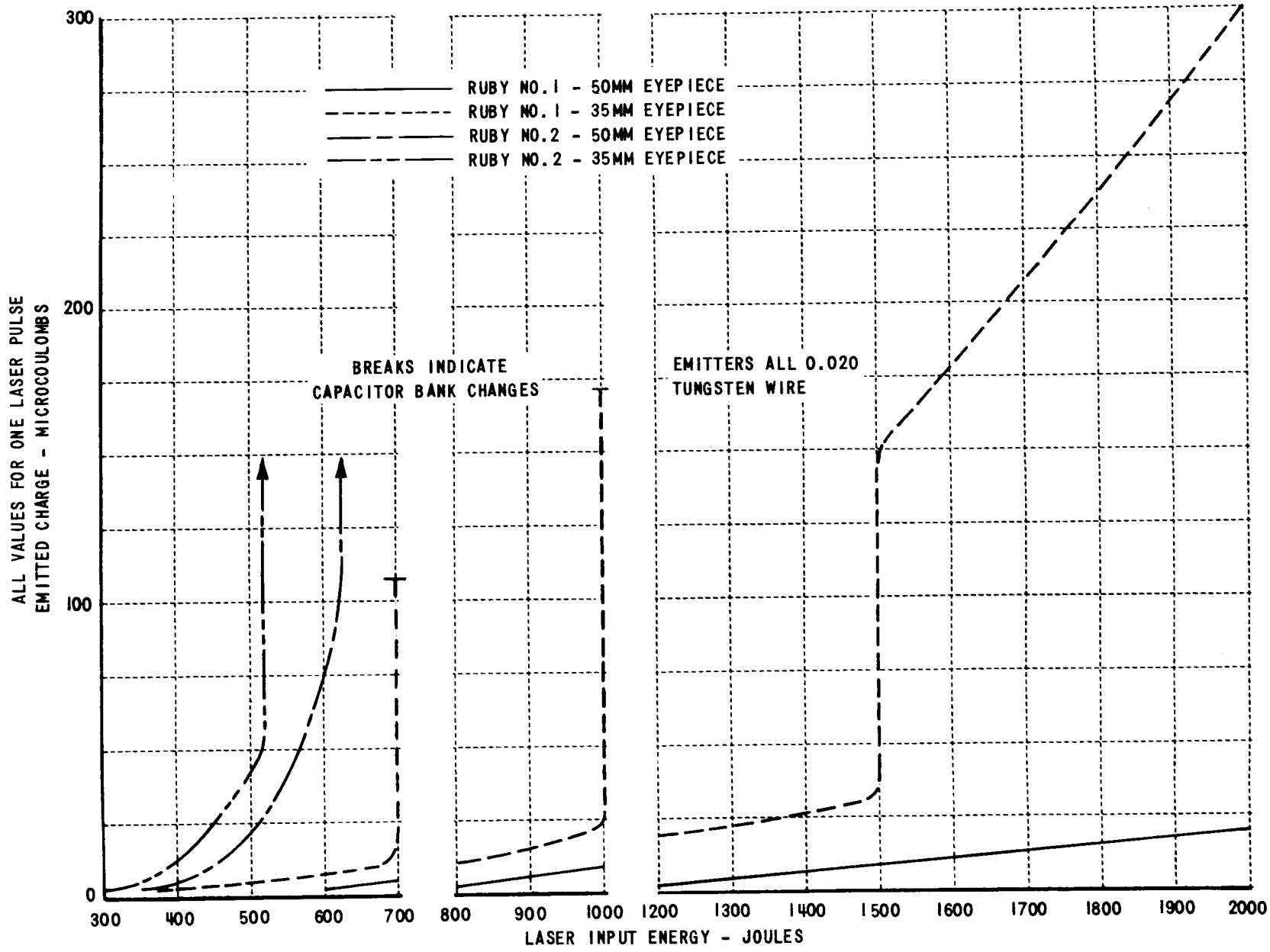

Figure 20 ION EMISSION AS FUNCTION OF FOCUSING PARAMETERS AND LASER ENERGY

During these tests it was observed that extremely intense blue-white light was produced in the vicinity of the emitter during an emission episode. The possibility was considered that this light was intense enough and of a short enough wavelength to stimulate photoelectrons from the stainless steel collector structure. The photo-emitted current, if it existed, could not be distinguished from ion current in the measurements that were being taken. Accordingly, a brief series of data were taken (with modified apparatus) of the time history of light produced during an emission process and current flowing between the laser illuminated object and the stainless steel collector. Sample results from these tests are shown in Figure 21. The overall wave shape correspondence verifies that the emitted light is related to the ion emission process and the time delay between the light pattern and the ion current pattern indicates that ion emission truly was being measured. Had the emission been photo-emission from the stainless steel collector cylinder, there would have been negligible time delay between the two traces.

In order to investigate emitter conditions associated with the threshold step in ion output a test fixture having a large radius open-ended cylinder collector was installed. Photographs were taken of the emitter during emission episodes at various input levels. A filter having 90 db attenuation at ruby laser light wavelengths (6943 Å) was used so that the photographs would show only the light generated by the emission process. The photographs of the light emitted by the heated emitter and plasma together with associated ion emission traces are shown in Figures 22 and 23. A below-threshold emission episode is shown in the upper photographs of Figure 22. A small, highly concentrated light spot occurred right over the surface of the emitter and ion output followed typically spiked patterns indicating possible large variations in ion velocity. When the laser power was increased the light spot over the emitter grew and intense streamers developed. The accompanying current trace shows the extremely spiked output evolving into something resembling an anode vacuum-arc as described in the literature.[16]

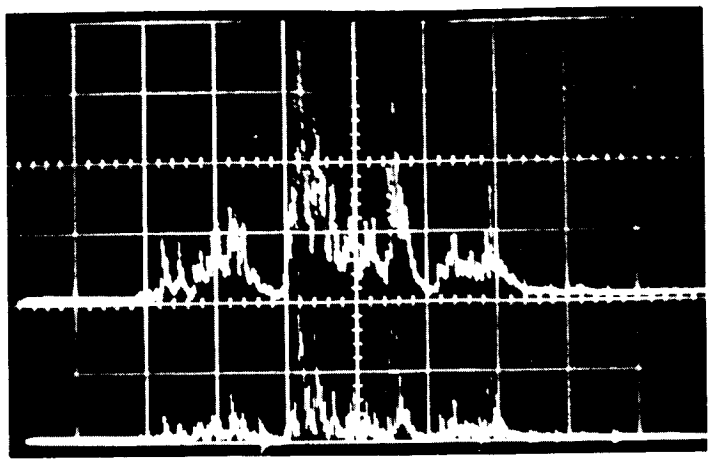

50 us/div

TYPICAL TRACE SHOWING ENTIRE EMISSION PULSE

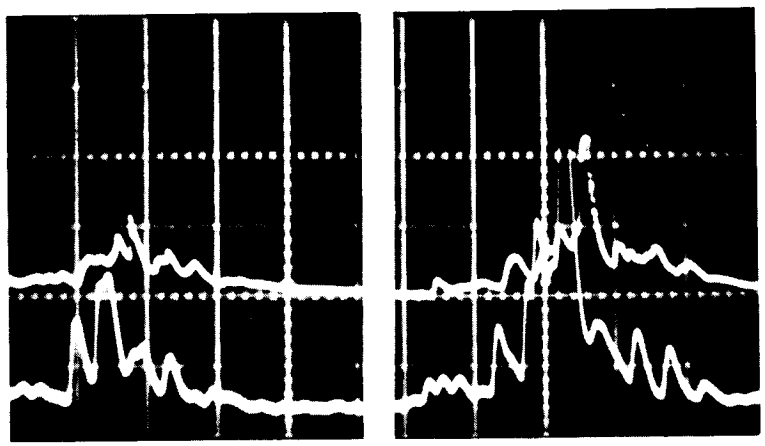

5 us/div 5 us/div

TYPICAL TRACES WITH EXPANDED TIME BASE TO SHOW TIME DELAY

*REFLECTED LASER LIGHT ATTENUATED APPROX. 90db,
NOT OBSERVABLE IN PHOTODETECTOR OUTPUT.

Figure 21 ION CURRENT AND LIGHT EMITTED BY LASER EXCITED EMITTER (RUBY #2)

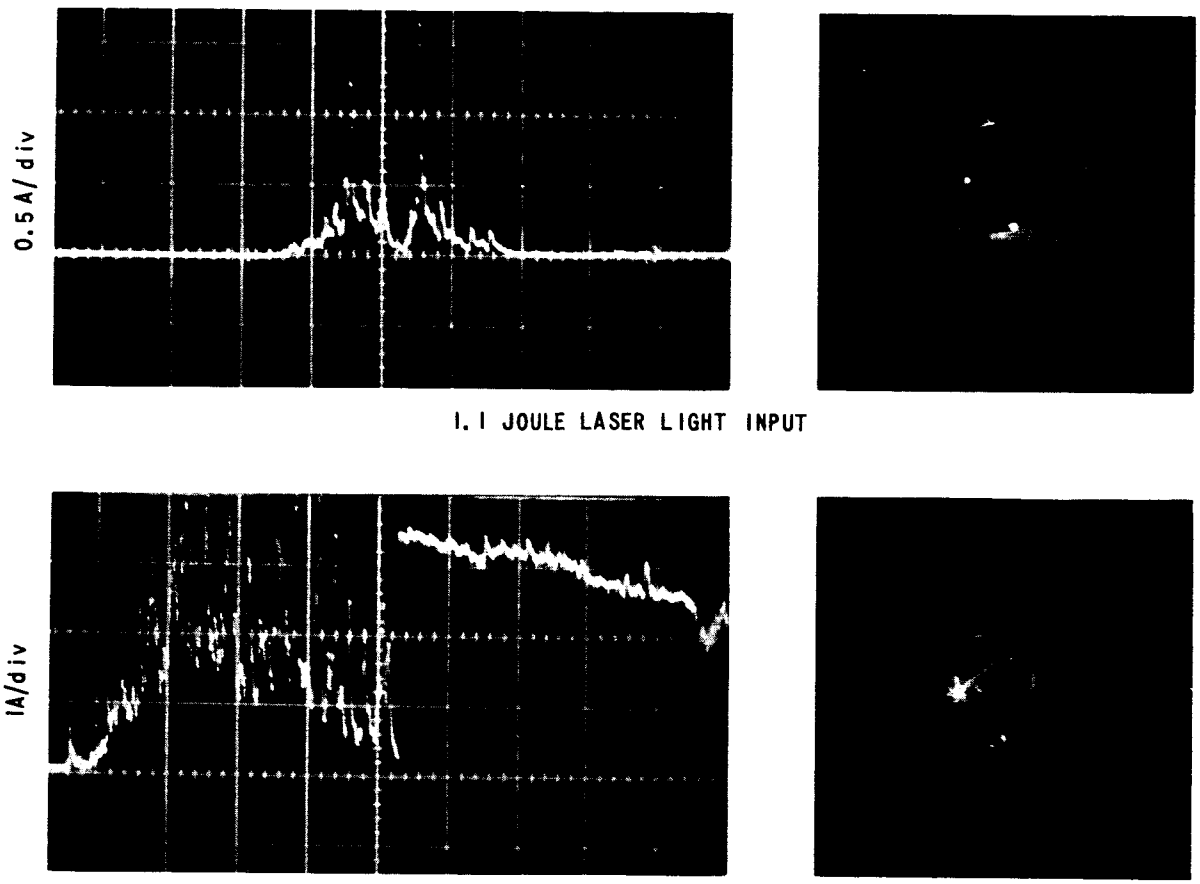

Figure 22 EMITTED CURRENT AND LIGHT USING LOW DIVERGENCE RUBY (RUBY #2)

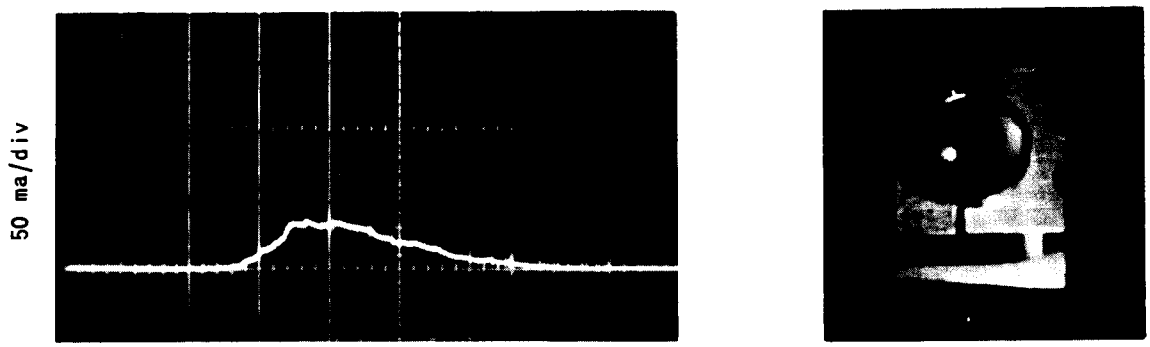

3.5 JOULES LASER LIGHT INPUT

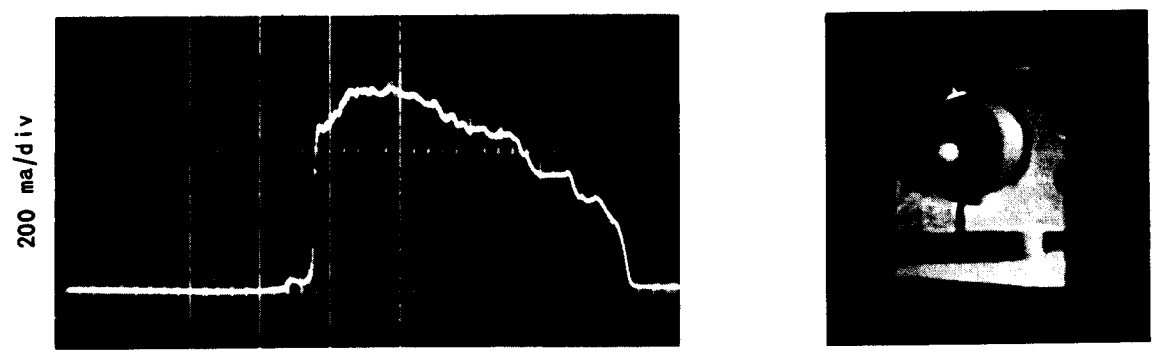

5.5 JOULES LASER LIGHT INPUT

EMITTER - 0.020" TUNGSTEN WIRE

EMITTER PHOTOGRAPH TAKEN THROUGH
FILTER ATTENUATING LASER LIGHT
(6943A°) BY 90 DB

Figure 23 EMITTED ION CURRENT AND LIGHT USING HIGH DIVERGENCE RUBY (RUBY #1)

Formation of plasma streamers occurred at the same laser power levels whether or not there was voltage between the emitter and collector, so the threshold jump in ion output was not caused by a conventional arc mechanism. It appeared that when the power density of the laser beam at the focus point was above a threshold level, achievable with high SPOD value configurations, very high velocity particles were generated that produced distinct streams of ionized plasma between emitter and collector. Thus, while the laser light persisted, conditions like those occurring during a vacuum arc were produced. Since the mechanism that produced the dense ionized plasma streams was caused by an external source, the laser, the discharge normally was not self-sustaining and current levels were much lower than those of a free-running vacuum arc.

Illumination of the emitter with a configuration having a much lower spot power density resulted in a different character of ion emission and a different type of light spot near the emitter as shown in Figure 23. Ion output levels were considerably lower than those shown in Figure 22 and the trace was smooth, suggesting a relatively monoenergetic emission process. The plasma produced during the emission process at these low SPOD values showed negligible streamer formation and there was no indication of incipient vacuum-arcs.

The general conclusions that one may draw from the results described in this section are that maximum yield per unit light input will be produced by maximizing the spot power density, that is, by using a ruby and optical configuration that yields the smallest possible image. As shown in Figure 20, maximum output from any given emitter will be obtained at substantially lower SPOD values but at some sacrifice in efficiency in terms of output couloumbs per joule input. In all of these cases, best output was obtained when the optical focus was located between 0.150 to 0.250 inch away from the emitting surface. There is evidence, although the mechanism is not yet understood, that the light beam focus is altered by the plasma. One would expect that the focus would be moved very close to the emitter during most

of the emission episode. Photographs taken from a more advantageous angle show that the light spot, i.e., the location of plasma generation, is in fact just above the emitter surface. Some optical interaction by the plasma cloud is further suggested by the fact that, although the laser power density is quite low at the plane of the emitter because of focusing a full one-quarter inch away, small craters whose size is a direct function of the optical image size are produced in the emitter surface. It should be noted however, that these craters are of the same type and dimension as those reported in the literature for anode vacuum arcs.

7.0 BALLISTIC PENDULUM EXPERIMENT

The selection of four materials for further study, based primarily on previously measured ion yields and calculated impulse, was very difficult. Many materials demonstrated reasonable ion yields, but only two (thorium and chromium) were clearly superior with respect to ion yield, and only thorium showed a superior impulse level. As a result of the difficulty in choosing between the various materials, a relatively simple test apparatus was designed which would permit direct measurement of impulse from the various materials.

The impulse measurements were made using a ballistic pendulum suspended in an evacuated bell jar as is shown in Figure 24. The bell jar was evacuated by a mechanical forepump and an oil diffusion pump to a pressure in the low 10^{-5} torr range. The system was not bakeable and, because of outgassing during laser illumination, the initial impulse readings on the various materials had to be disregarded. Only after the target had been heated by several laser bursts did the impulse readings become repeatable. Several difficulties, which will be described in detail at the end of this section, made the impulse measurements of relative value only.

The supports for the pendulum bob (just barely visible in Figures 24 and 25)were 0.0045 inch diameter stainless-steel wires. Two wires were used to restrict sideways and turning motions of the bob. An annular copper disc mounted coaxially with the pendulum bob was used to collect ions or electrons emitted from the target during laser illumination. The emitter was operated near ground potential, the actual potential being the voltage drop across the stainless-steel wires (which had a resistance of approximately 10 ohms) and the viewing resistor (either 1 ohm or 10 ohms). It was observed that, as a function of potential on the emitter (+140 to -140 volts), no change in the impulse occurred. The entire system would have to be movable, to monitor the change in thrust developed by electrostatic acceleration.

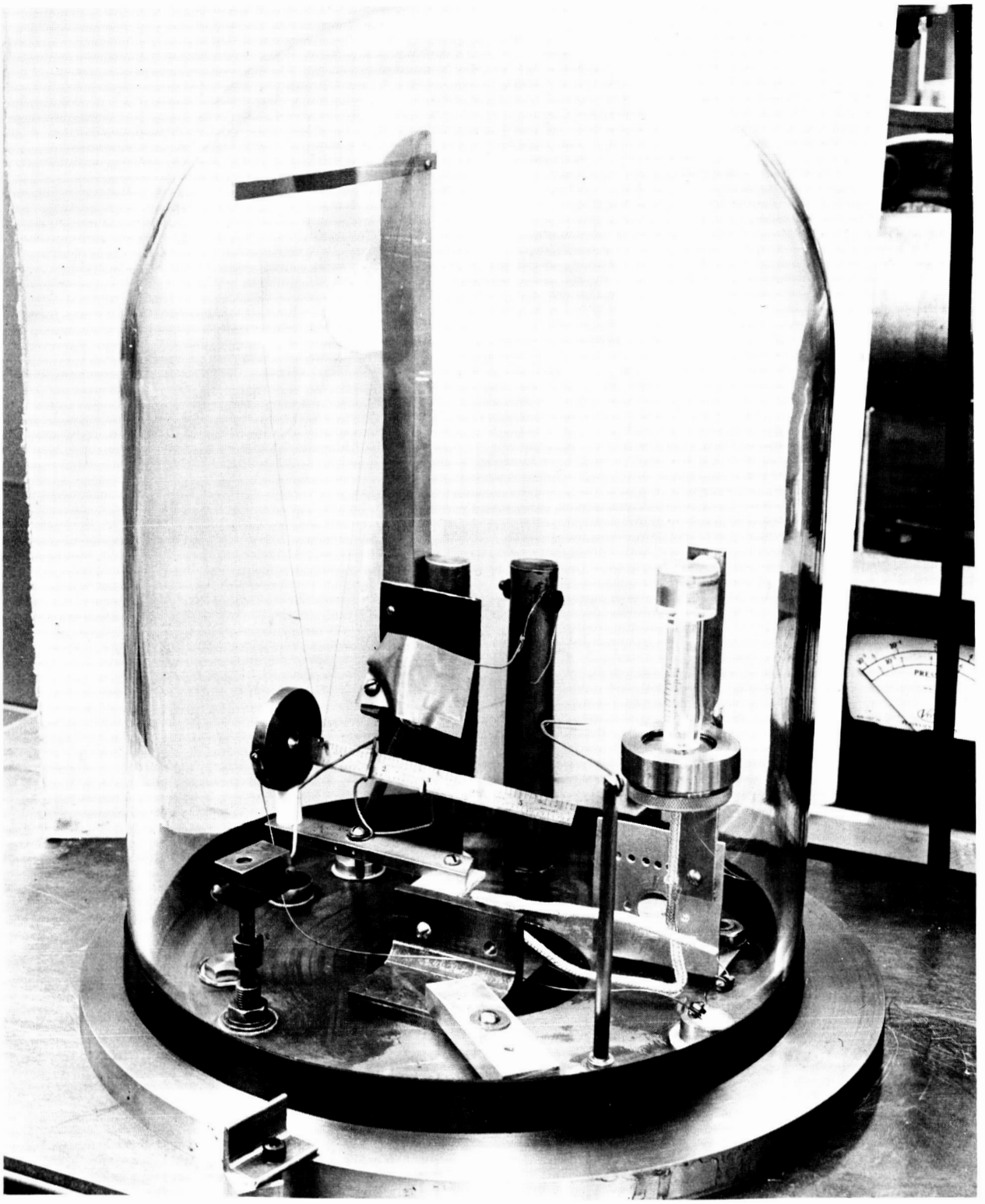

Figure 24 BALLISTIC PENDULUM, BELL-JAR CONFIGURATION

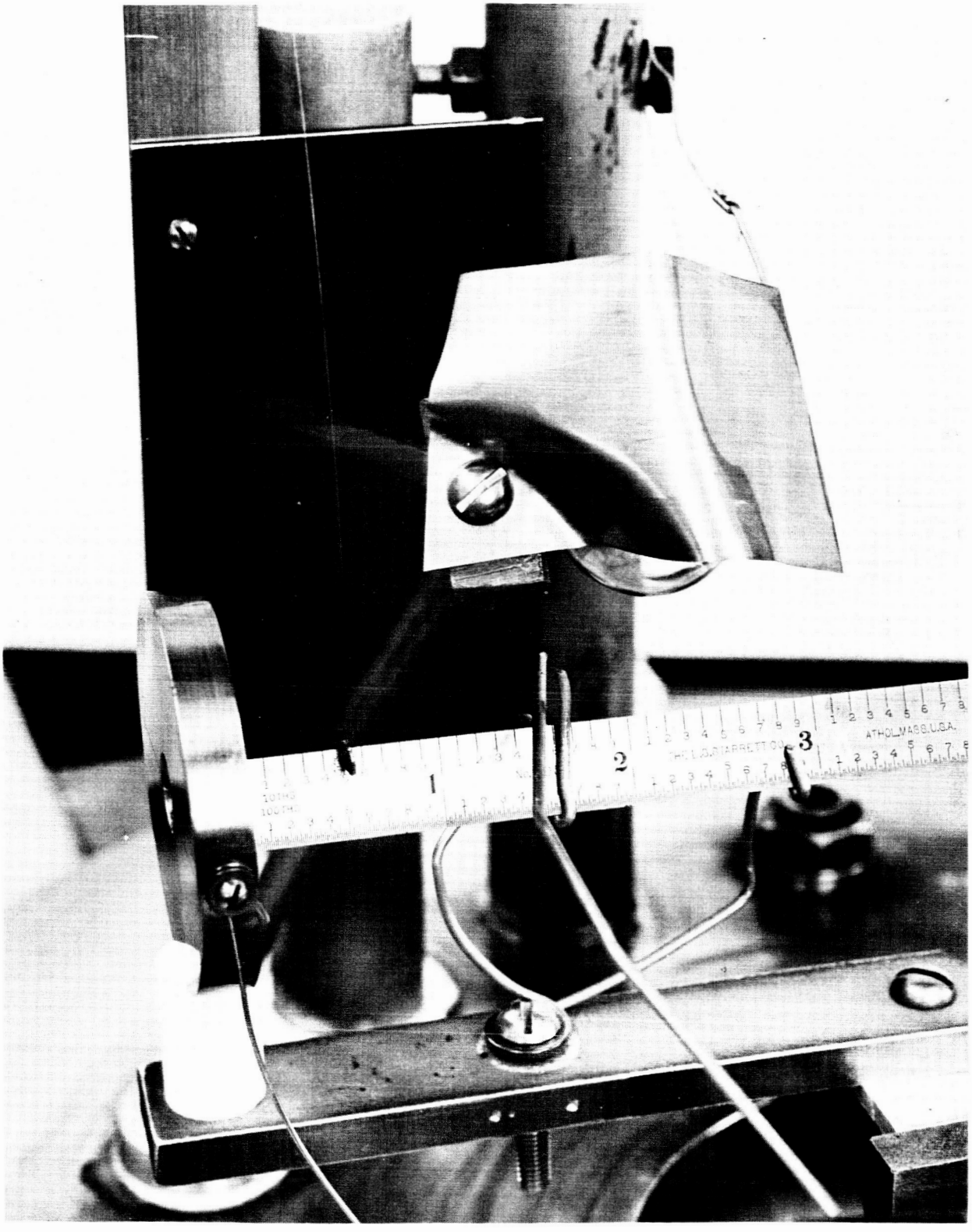

Figure 25 BALLISTIC PENDULUM TEST CONFIGURATION

After being initiated by the laser radiation, the pendulum swing was observed to remain unchanged for periods longer than five minutes and had to be stopped mechanically. This behavior, as well as visual observations of the initial pendulum swing (using goggles designed to reject all light in the region of the laser frequency), indicated that there was no significant loss in the pendulum system.

7.1 Test Conditions

The resultant deflection of the pendulum due to ion emission was measured visually and photographed. To assure that adequate motion of the target (between 0.03 and 0.25 inch) might be obtained, the materials tested had about the same weight as the support wires. This was taken into account in calculating the energy of the particle emission when the target was illuminated with focused laser radiation. On the basis of the pendulum structure shown in Figure 26 and the following assumptions,

1. conservation of momentum,
2. constant force over a time t ,
3. all the wire weight concentrated at its center,
4. the potential energy at the top of the pendulum swing concentrated at the center of the gravity of the suspended system,

and 5. no pendulum losses, e.g., friction, magnetic hysteresis, etc.

the impulse and thrust of the laser induced emission can be calculated as follows.

The force equation

$$F = ma$$

gives

$$Fdt = mdv$$

or

$$Ft = mv$$

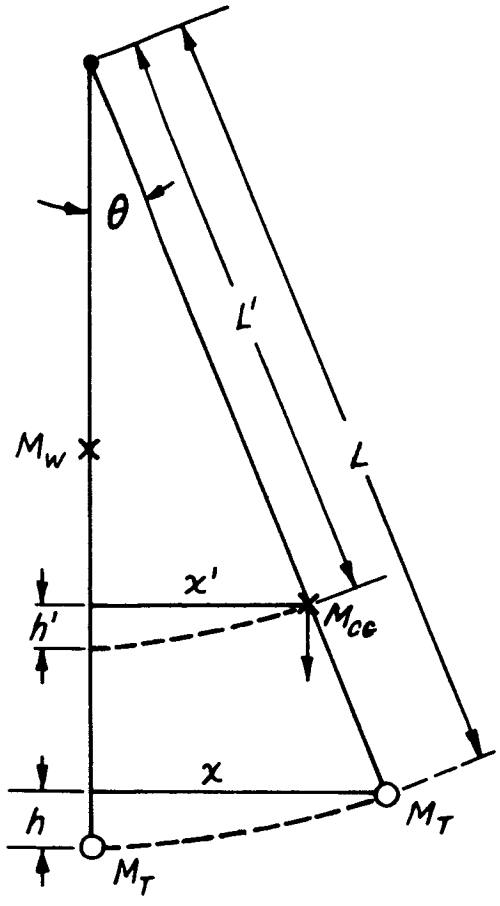

Figure 26 SKETCH OF PENDULUM MOTION

where the constant of integration is zero because of the initial conditions. The target as well as the wire is accelerated; however, the center of gravity of the wire has only half the velocity of the target so that

$$Ft = M_t v_t + M_w v_w$$

can be written as

$$Ft = \left[M_t (L\dot{\theta}) + M_w \left(\frac{L}{2}\dot{\theta}\right)\right]$$

or as

$$Ft = \left[M_t + \frac{M_w}{2}\right] v_t \tag{4}$$

The kinetic energy imparted to the pendulum and wires is:

$$K.E. = \frac{1}{2} \sum_i M_i v_i^2$$

which can be written as

$$K.E. = \frac{1}{2}\left[M_t (L\dot{\theta})^2 + M_w \frac{(L\dot{\theta})^2}{3}\right] \tag{5}$$

or as

$$K.E. = \frac{1}{2}\left[M_t + \frac{M_w}{3}\right] v_t^2$$

Assuming no losses, at the top of the pendulum swing all of the kinetic energy is converted to potential energy which can be expressed as

$$P.E. = (M_{cg}) g h' \tag{6}$$

or as

$$P.E. = (M_t + M_w) g h'$$

Equating the kinetic energy to the potential energy gives

$$v_t^2 = \frac{2(M_t + M_w) g h'}{\left[M_t + \frac{M_w}{3}\right]} \tag{7}$$

From geometrical considerations it can be shown that $h' = h\, L'/L$ and that $(L-h)^2 + x^2 = L^2$ but $h^2 << x^2$ and $h^2 << 2Lh$; therefore, one obtains:

$$h = \frac{x^2}{2L} \left(\frac{L'}{L}\right) \tag{8}$$

However, the distance of the center of gravity of the system from the pivot point can be expressed as:

$$L' = \frac{M_t + \left[\frac{M_w}{2}\right] L}{M_t + M_w} \tag{9}$$

Substituting equations (8) and (9) into equation (7), one obtains:

$$v_t^2 = \frac{\left[M_t + \frac{M_w}{2}\right] g x^2}{\left[M_t + \frac{M_w}{3}\right] L} \tag{10}$$

The impulse imparted to the pendulum system by the material emitted when the target is illuminated with laser radiation is found by combining equations (4) and (10) to obtain

$$F_t = \frac{\left[M_t + \frac{M_w}{2}\right]^{3/2}}{\left[M_t + \frac{M_w}{3}\right]^{1/2}} \cdot \sqrt{\frac{g}{L}} \cdot x \tag{11}$$

Design of the pendulum experiment included the use of ruby #2 together with a 35 millimeter eyepiece in the telescope. The use of ruby #2 with its regions of high power density within the beam and the high degree of focusing used, caused considerable damage to most targets which in general had dimensions of about .060 x .060 x 0.200 inch, and limited the level at which some targets could be illuminated.

7.2 Test Results

The relative impulse and force imparted to the various targets as well as the collected charge is shown in Figures 27 (a) and (b). Both charts are normalized to the same maxima. The maximum collected charge was 335 microcoulombs with tungsten as a target. The two materials which showed much higher relative performance than expected were rhenium and lead. Lead suffered rapid damage, but its force and ion yields at low laser

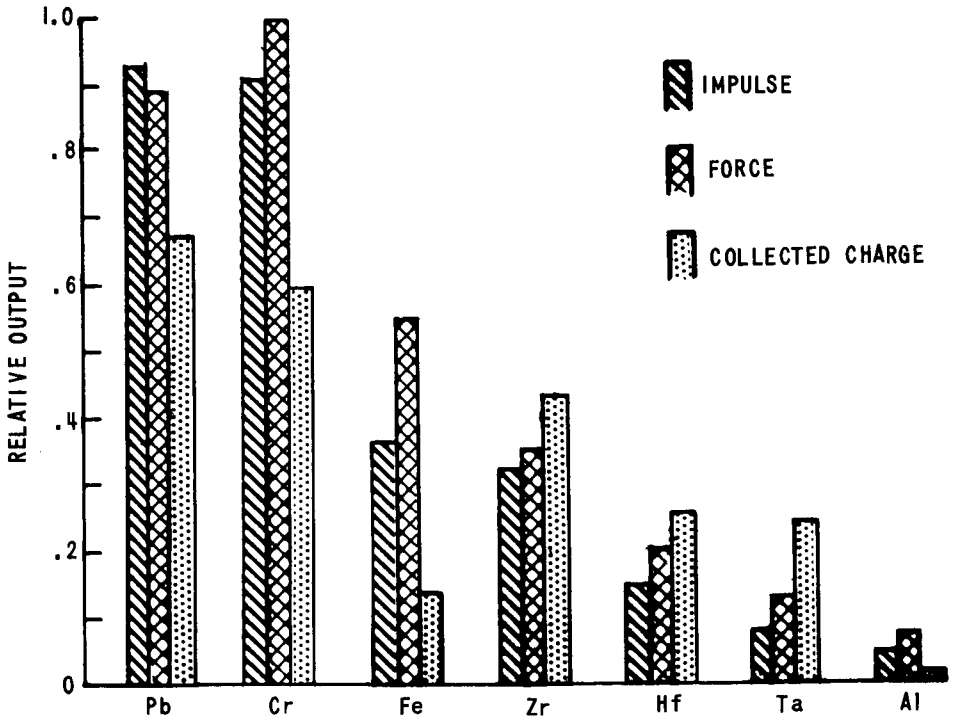

(a) LASER ENERGY LEVEL 1.4 JOULES

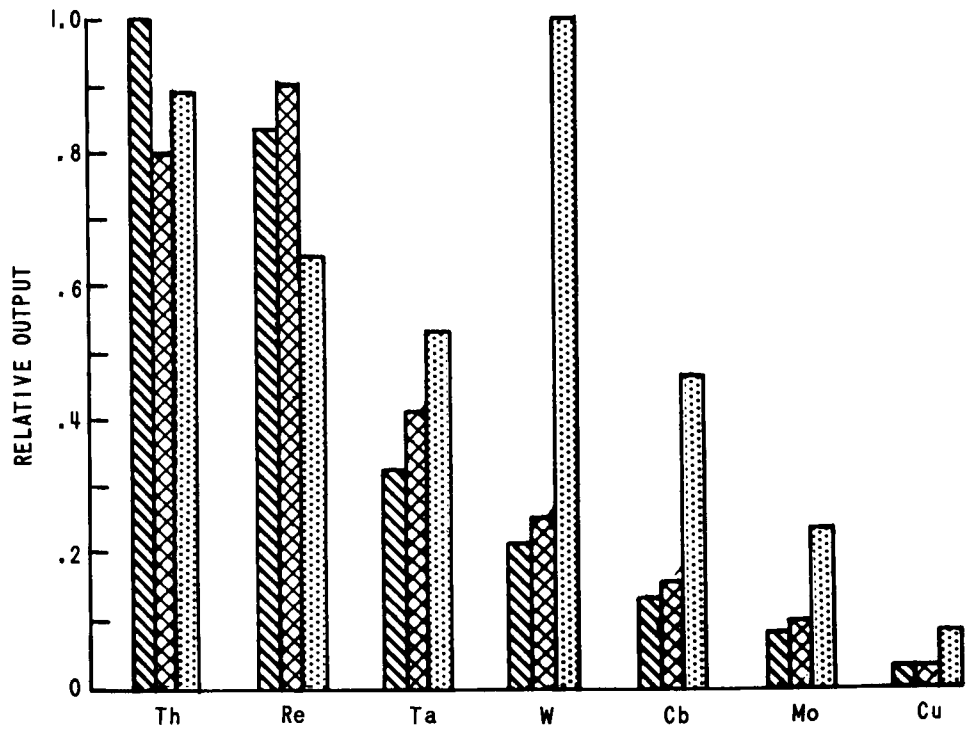

(b) LASER ENERGY LEVEL 3.3 JOULES

Figure 27 RESULTS OF RELATIVE IMPULSE FORCE AND COLLECTED CHARGE MEASUREMENTS (a) AND (b) BOTH NORMALIZED TO SAME VALUE (RUBY NO. 2)

energy levels compared favorably with those found for other materials at a much higher energy level.

The maximum measured thrust was 4.7 millipounds with a chromium target (order of magnitude value). Thorium had the largest impulse approximately 2.0×10^{-3} millipound-seconds. These values are based on calculations using equation (11), which takes into account the finite weight of the mounting wires.

The pendulum approach, while convenient and rapid, could not be accurately calibrated. During the measurements some thrust resulted in precessional motion, some was lost in friction, the pivot possibly damped the larger excursions, and the inaccuracies in determining the center of the mass system came into play. In the attempt to calibrate the system, the same inaccuracies were present. The larger thrusts or pendulum displacements were subject to the largest errors and damping forces so that the materials with the larger measured impulses have relative values that are too low.

The problems involved in this ballistic pendulum setup were caused to a great extent by the need for a light-weight target (approximately 60 mg). The target shape chosen was a flat plate rather than a wire. The ion emission from both the plate and the wire has been shown to be almost identical, and the use of a plate permitted easier attachment of the mounting wires. In addition, the flat plate was less subject to rotation or precession around its mounting point. However, in trying to ascertain the emitted particle velocity other problems became apparent. Several materials suffered rapid damage (including holes through the material), e.g., lead, hafnium, chromium, aluminum, iron, and zirconium. The remaining materials also suffered significant damage but only after undergoing a greater number of laser shots at a higher laser power level. The material sustaining the least damage was tungsten even though this material was irradiated with the laser many more times than were any of the others. The impulse, thrust, and collected charge measurements are, however, a good measure of the relative performance of the various materials.

Later in the program a new pendulum assembly which was accurately calibrated was used to measure the thrust of the four materials selected for extensive tests. This experimental configuration and results are discussed in Section 10.

8.0 ANGULAR DISTRIBUTION OF EMITTED IONS

Data on the axial distribution of velocity and density of laser induced ion emission was required in order to make thrustor performance predictions and to make possible the conceptual design of a thrustor. An eight aperture hemispherical collector was designed and constructed to obtain these data.

8.1 Design of the Eight-Aperture Hemispherical Collector

The collector system for the experimental program to study the axial distribution of velocity and density of emitted particles consisted of a hemispherical collector with eight sampling probe positions. The collector surface was made hemispherical so that all emitted particles had equal path lengths to the collector surface. The emitter was located at the center of the hemispherical collector surface. An opening in the center of the collector structure allowed the laser light to illuminate the emitter. Two views of the experimental test apparatus are shown in Figure 28. Eight probes were inserted at selected angles in the collector surface. The probe positions and their intended functions are shown on Table II.

Table II

AZIMUTH ANGLE (DEGREES)	ELEVATION ANGLE (DEGREES)	PROBE MEASUREMENT CAPABILITY
0	30	QUANTITY AND ENERGY
90	15	QUANTITY
90	30	QUANTITY
90	45	QUANTITY
90	60	QUANTITY
90	75	QUANTITY
180	15	QUANTITY AND ENERGY
270	60	QUANTITY AND ENERGY

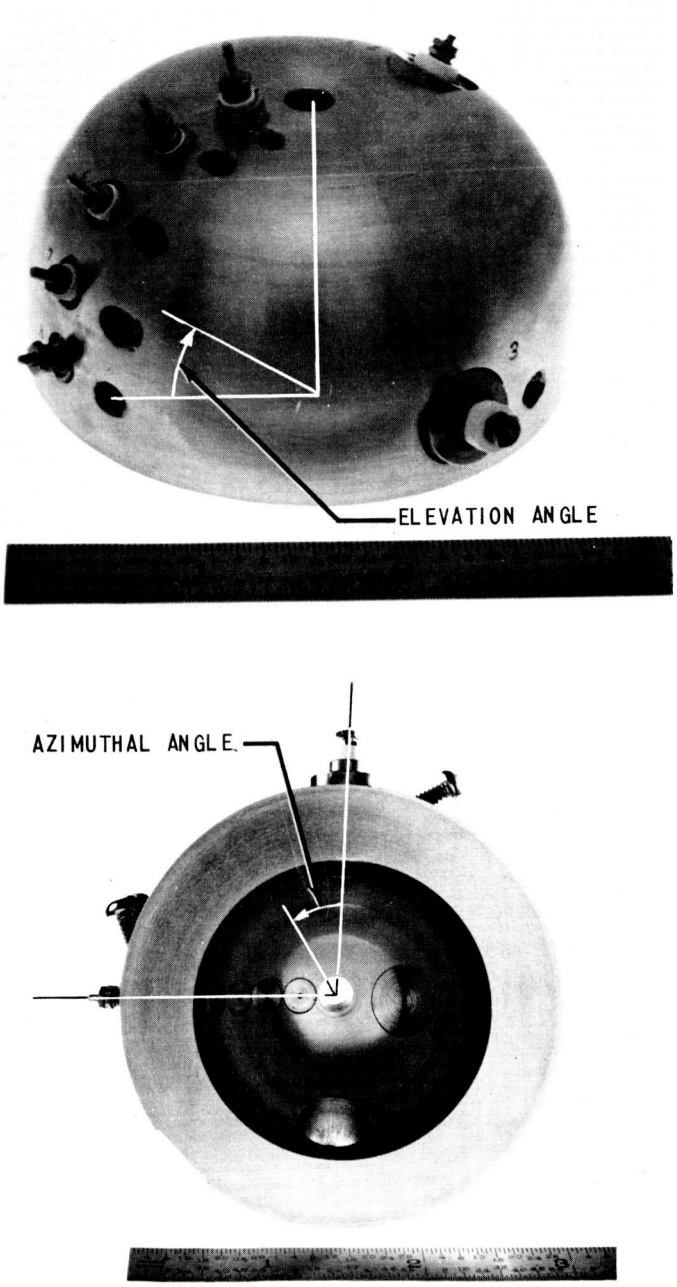

Figure 28 EIGHT-APERTURE HEMISPHERICAL COLLECTOR

The azimuthal angle is the angle around the periphery of the collector, whereas the elevation angle refers to the angle between the collector probe and the plane of the emitter.

Previous evidence and theory suggests axial symmetry of the emitted plasma plume, therefore, to obtain the best possible sample of axial emission parameters with the eight probes available, it was decided to place the five simple probes in one plane, in one 90° sector of the collecting volume. The three multiple-plate probes, the ones that could measure energy as well as quantity, were located so that their azimuthal angles (looking toward the emitter) were 90° apart, thus obtaining some plasma sampling in all quadrants. The "elevation angles" of the multiple plate probes were 15°, 30° and 60°. With the arrangement described, any deviation of the plasma plume from axial symmetry was detected and detailed measurements as a function of elevation angle were achieved.

There were no discontinuities in the inner surface of the hemispherical collector except the 0.030 inch sampling holes. The selected diameter of the sampling holes was small enough to produce negligible effect on the electrical field within the hemisphere yet large enough to pass a reasonable fraction of the total emission for reliable, noise-free measurements. Electrically insulated Faraday cages were located behind each opening. The three cages equipped with an additional shield electrode are shown in Figure 29. With this electrode arrangement, the energy as well as quantity of emitted particles entering each outer shell hole could be measured.

Currents collected by the probe cages were small, typical values ranging from 10^{-5} to 10^{-4} times the emitted current. To obtain noise-free, high-frequency recording of these currents, special care had to be exercised in wiring the electrical connections inside the bell jar. In previous experiments where low current measurements were involved, it was found that even a very short length of exposed wire inside the vacuum chamber would collect enough charge from the plasma generated during the laser excitation of the emitter to mask the true collected current. To prevent undesired

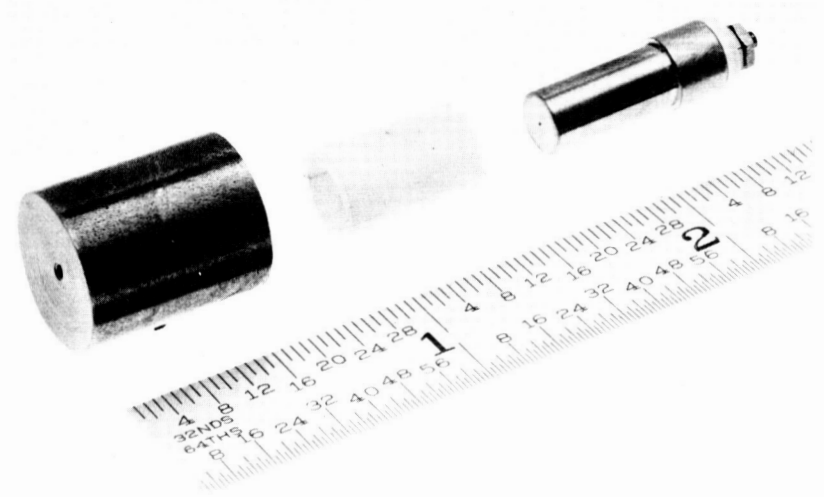

EXPLODED VIEW

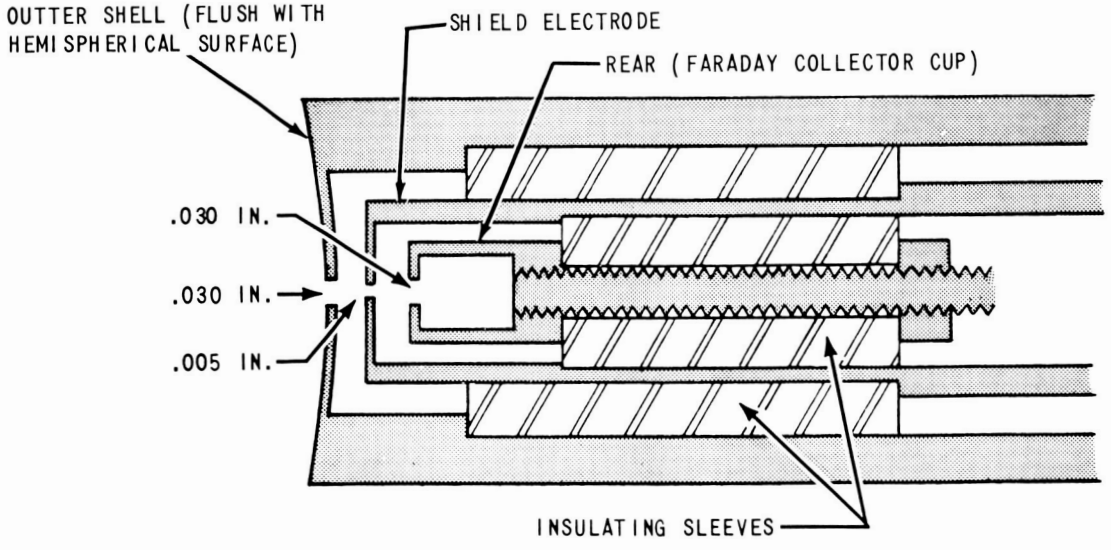

CROSS SECTION SKETCH

Figure 29 COLLECTOR PROBE FOR ION ENERGY MEASUREMENT

current pickup, shielding caps and a shielding tunnel were built for the cables going to the probes. Capacitive coupling among leads was eliminated with individual coaxial shields for each probe lead; these coaxial cables were made using materials and construction procedures to allow bakeout and pumpdown to high vacuum. A small mirror was positioned inside the vacuum chamber to allow illumination and visual observation of the emitter wire. The collector system ready for test is shown in Figure 30. During all the tests the hemispherical collector was grounded directly to the vacuum chamber.

8.2 Tungsten Energy and Density Distribution Measurements

Using the eight-aperture hemispherical collector with a 0.062 inch diameter tungsten wire target as the emitter, measurements were made of the charge and energy distributions of the emitted particles using both available ruby lasers described in Section 3.1.

The charge distribution of the emission as a function of laser input is shown for ruby #2 in Figure 31. The distribution is approximately cosinusoidal with some radially directed charged particles. (The collected charge is finite at 0° elevation angle.) In a symmetric plume of emitted material, the only component of force which provides thrust is that aligned with axis of symmetry. The energy which goes into the emission of radially directed charge is wasted. This is discussed in Appendix A. In an attempt to cause a larger percentage of the emitted charges to travel parallel to the axis of symmetry, experiments were performed with an axial magnetic field. The design of the electromagnet and axial field attained are given in Appendix B.

Distribution of the normalized collected charge is shown in Figures 32 and 33 for rubies #1 and #2 using an 35 mm focal length lens. The variation in the charge distribution is also shown for several values of magnet current. It will be noted that the magnetic field produced significant improvement in the directivity of the emitted material. Since the magnetic force on the charged particle has the form $(\underline{v} \times \underline{B})$, the axial magnetic field

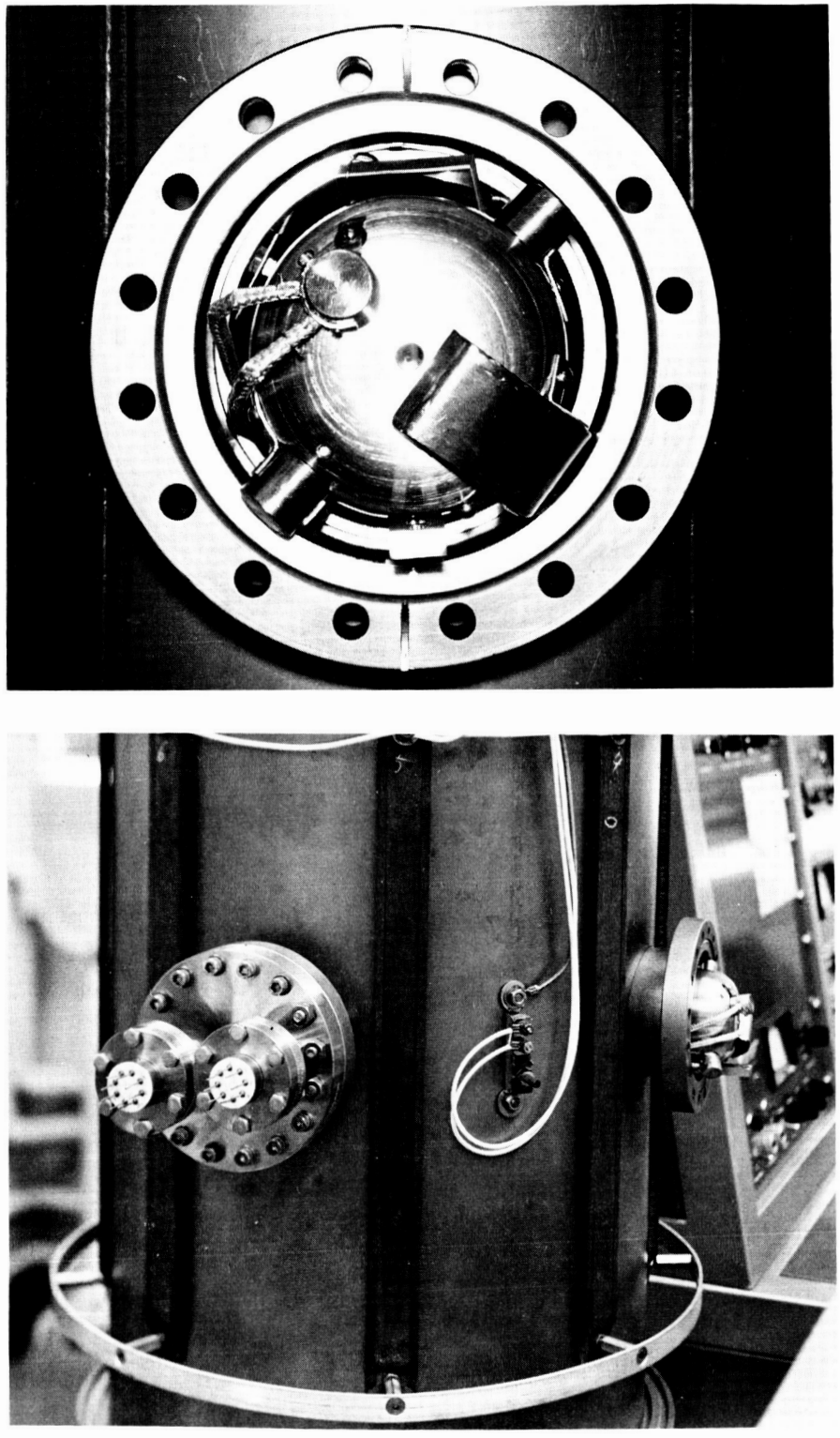

Figure 30 MULTIAPERTURE COLLECTOR SYSTEM INSTALLED IN VACUUM CHAMBER

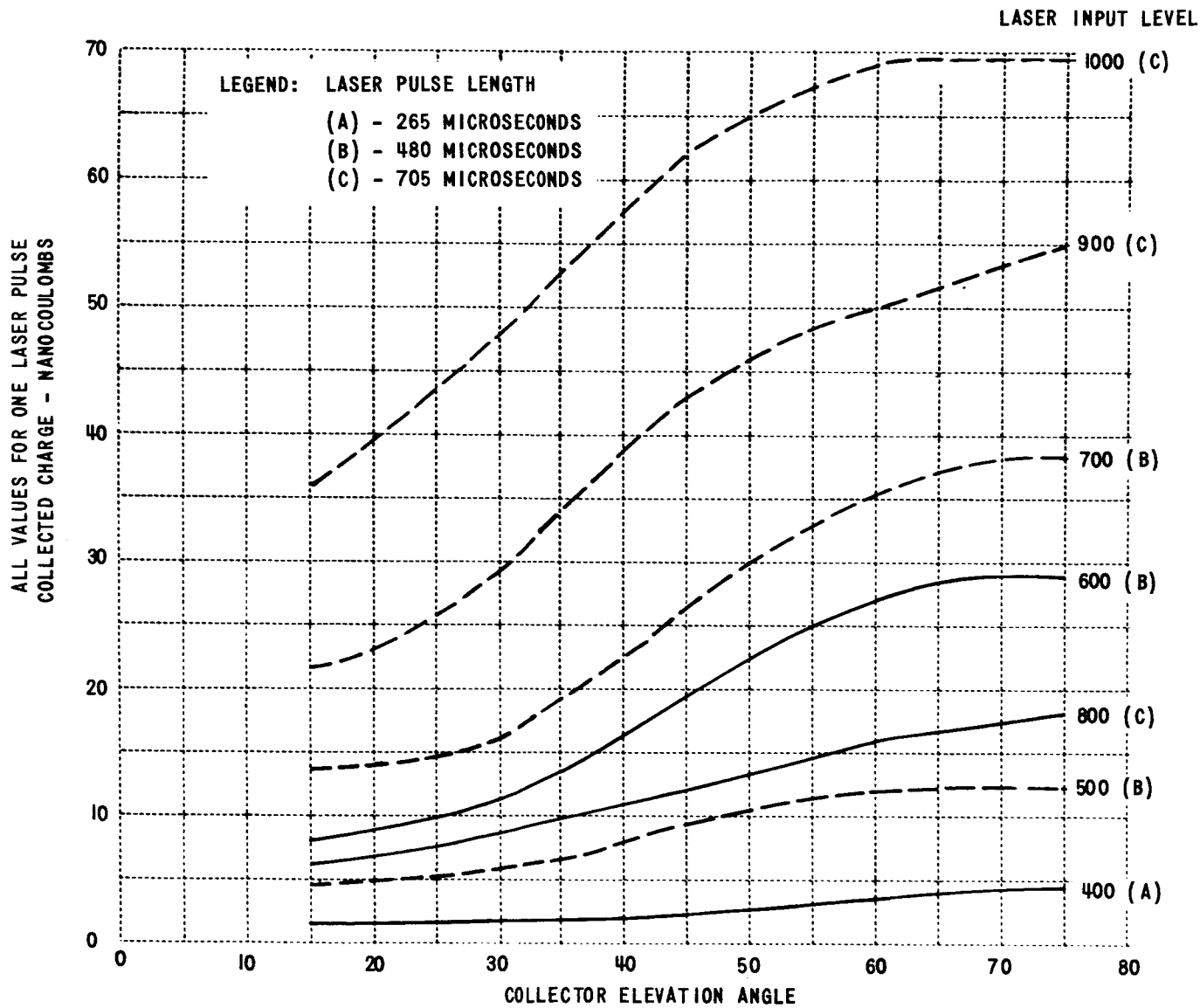

Figure 31 CHARGE DISTRIBUTION

TUNGSTEN EMITTER - RUBY #2

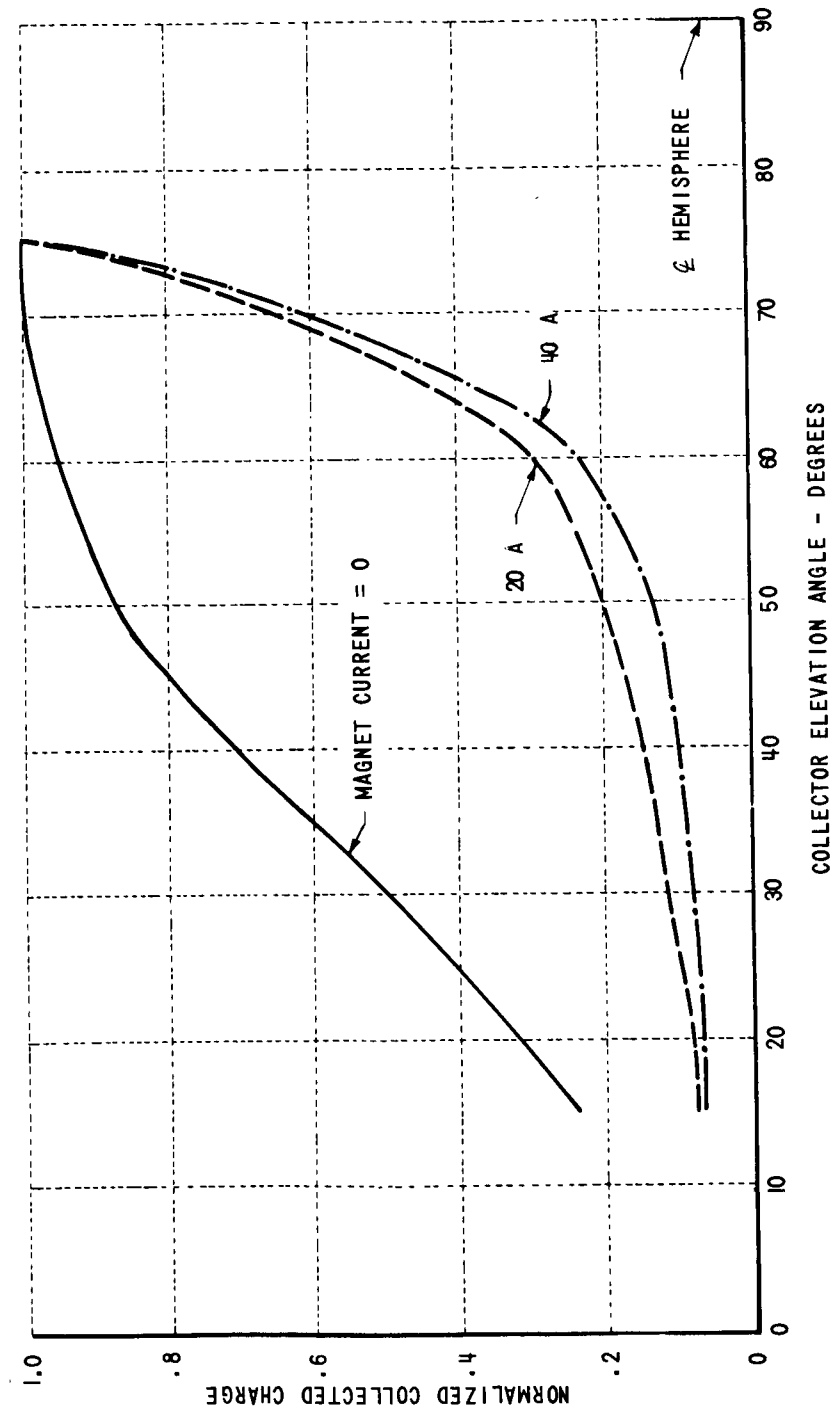

Figure 32 CHARGE DISTRIBUTION

TUNGSTEN EMITTER - RUBY #1

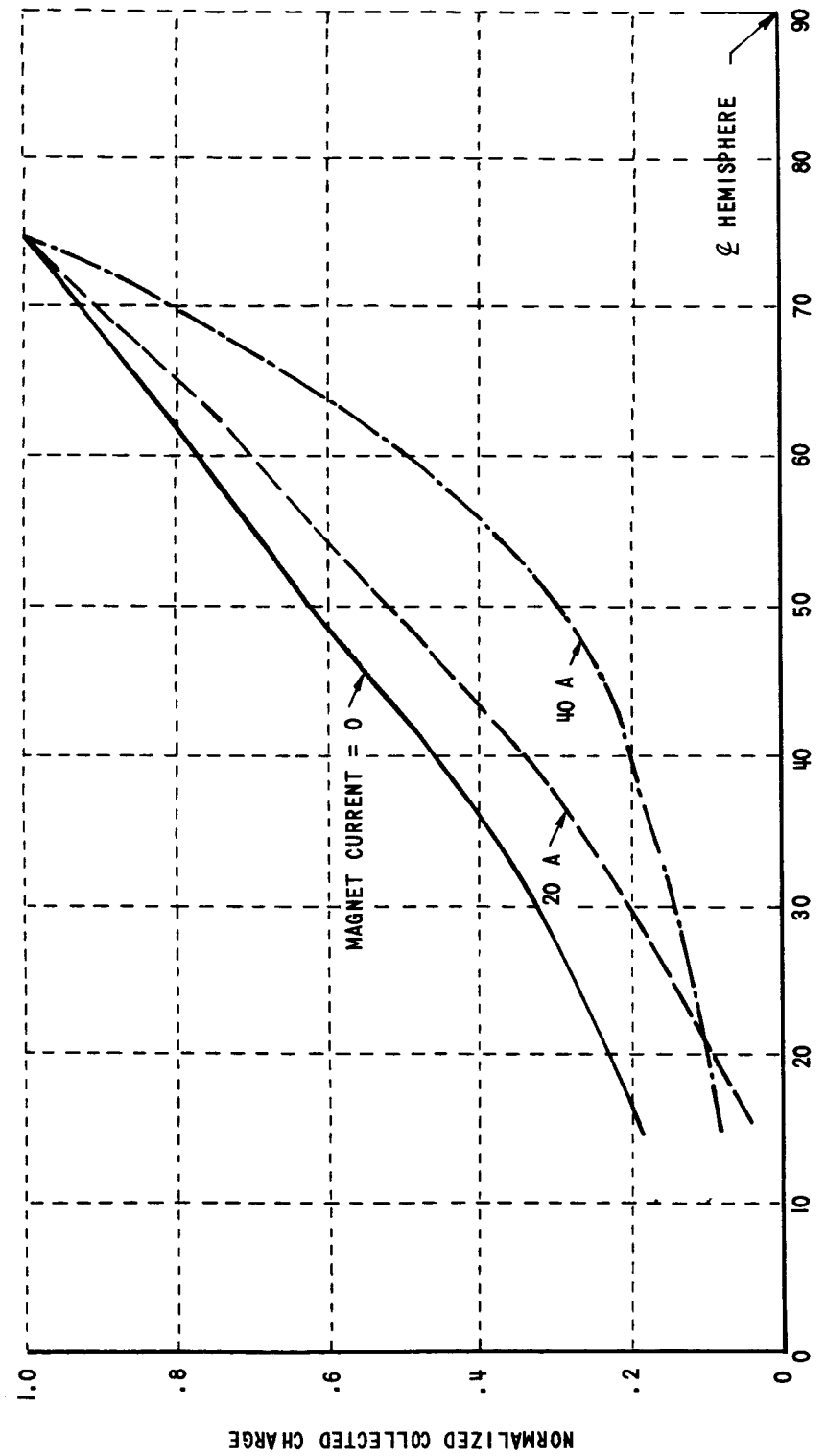

Figure 33 CHARGE DISTRIBUTION

TUNGSTEN EMITTER - RUBY #2

could not decrease the charged particles at 0° elevation but did significantly modify the direction of the other emitted particles. A normalized density distribution of the emitted ions is shown in Figure 34. This representation of the plume density indicates pictorially the improvement that can be realized with an axial magnetic field. As indicated in Appendix A, with ruby # 1, the useful thrust from tungsten was about 67 percent of the total available thrust. By using a 1400 gauss axial magnetic field this value was increased to about 90 percent of the available thrust.

The energy measurements made on the emitted tungsten particles lead to some rather startling conclusions. The shield electrode containing a 0.005 inch diameter hole was varied in potential from -600 to +600 volts. It was possible under these extreme conditions to obtain electron or ion current respectively at the rear collector. This behavior for the three energy-measuring collectors is shown in Figure 35. There are three possible explanations for this behavior. One possibility is that there are actually electrons and ions having sufficient energy, i.e., greater than 600 electron volts, to overcome the retarding potential. The other possibilities were current leakage through the 0.005 inch diameter hole, i.e., the plasma was still dense enough to effectively shield the charges from the applied potential, or capacitive coupling between the multiple plates.

Figure 35 shows the changes in the collected current on the rear collector as the potential on the shield electrode was varied. Since both electrons and ions were present in the discharge, the rear collector was biased to collect predominantly one species of charged particle. The rear collector voltage was set at -72 or +72 volts while the shield electrode voltage was varied from 0 to +600 volts and 0 to -600 volts, respectively. All voltages were with respect to the outer shell which was always electrically connected to the vacuum chamber (at ground potential).

If the bias on the rear collector was +72 volts and the potential in the shield electrode was increased from 0 to -600 volts, the number of electrons collected (at the rear collector) decreased in general. More high

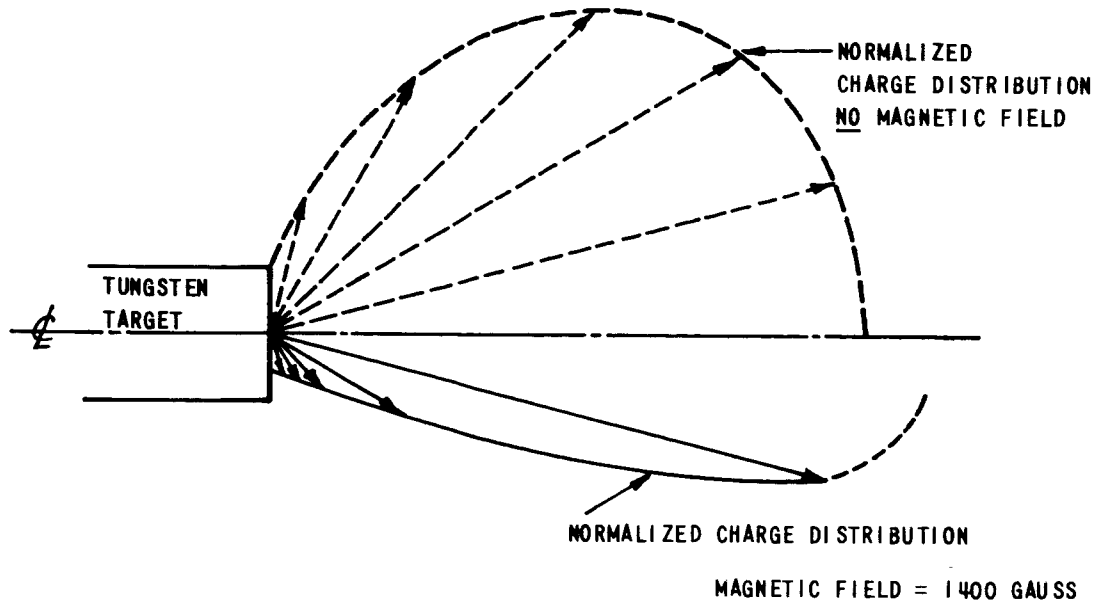

RUBY #1

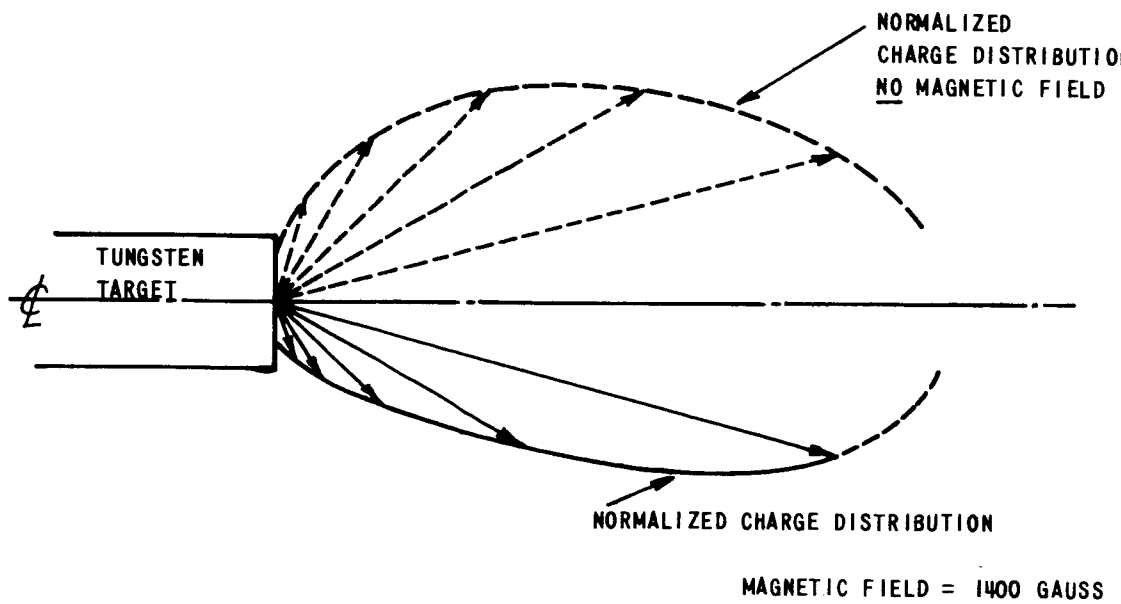

RUBY #2

Figure 34 NORMALIZED DENSITY DISTRIBUTION OF LASER GENERATED IONS

TUNGSTEN EMITTER

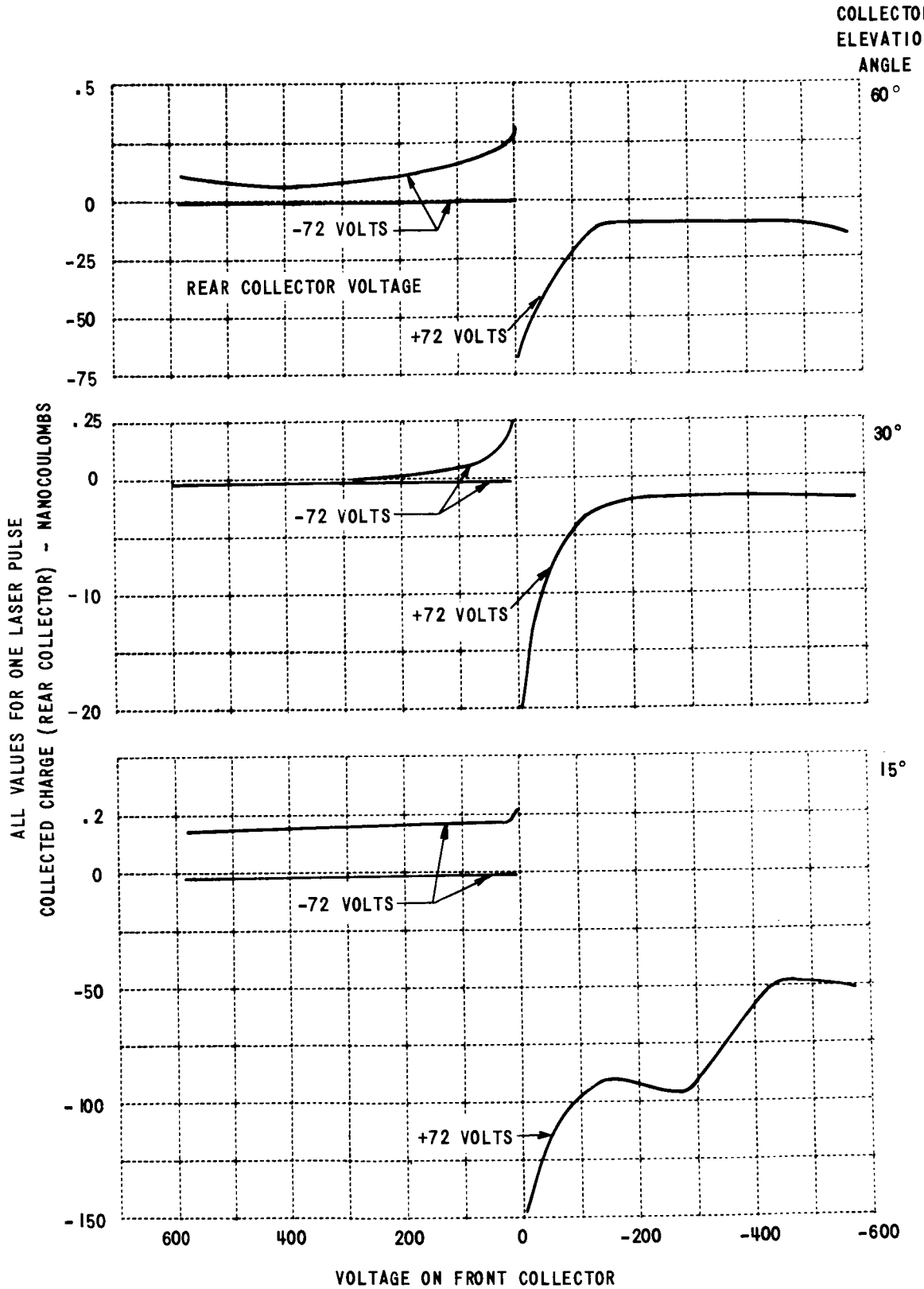

Figure 35 ENERGY DISTRIBUTION

TUNGSTEN EMITTER - RUBY #1

energy electrons were present at the lowest elevation angle (15°) than the other two elevation angles.

When the bias on the rear collector was -72 volts, both electrons and ions were detected (at the rear collector). The instantaneous collected charge was the sum of the two species, with electrons or ions predominating at any particular instant. Thus, the plots with -72 volts on the rear collector show the sum of the integrated electron and ion charge. As the shield electrode voltage was increased from 0 to +600 volts the collected electron current increased while the collected ion current in general decreased. The higher energy ions appear at the highest elevation angle (60°). However, since both electrons and ions were collected the values obtained are of relative value only.

Evidence that there may be very energetic electrons and ions is provided in Figure 36. It has been well established in our measurements that if the collector voltage exceeds about 30 volts, there is no change in collected charge for any further increase in collector voltage except, of course, in the case of breakdown. However, Figure 36 shows that with a fixed rear collector voltage, collected current varied with the shielding voltage. The current collected on the rear collector should not have varied widely for a change in the shield electrode voltage (no change in polarity) when the retarding potential exceeded the particle energy. However, Figure 36 indicates a large change in collected ion current with the front aperture voltage changed from -35 to -400 volts. This increasing ion current collection with the larger negative voltage indicates that fewer electrons were being allowed through the aperture or, conversely, that the electron current passing a negative potential was not just leakage current. Another feature to be noted on the curves is the variation in the rear-collector voltage required to give zero collected current. (The energy of the ions at a 60° elevation angle is greater than at 15°; or the electron energy at a 15° elevation angle is greater than that at 60°; or a combination of both conditions exist). Figure 36 again shows ions and electrons being collected at the rear collector when the combination of negative voltages on the shield electrode and the rear collector was incapable of repelling all the electrons.

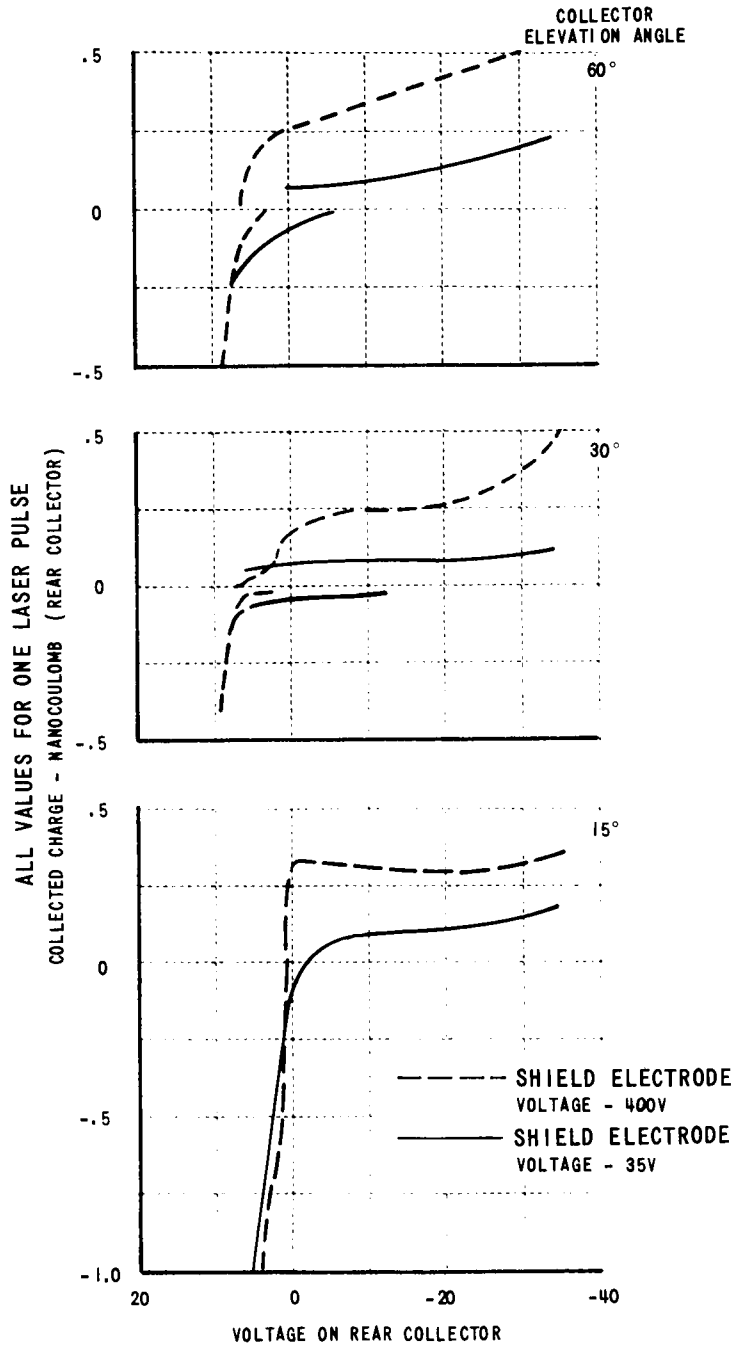

Figure 36 ENERGY DISTRIBUTION

TUNGSTEN EMITTER - RUBY #2

The current being collected on the rear collector can be considered as consisting of ions and electrons at their respective velocities. That is:

$$J_{COLL} = -\rho_e v_e + \rho_i v_i$$

If we consider the situation with -30 volts on the rear collector (V_2 =-30) and -35 volts on the front aperture (V_1=-35) we get

$$J_{COLL}\Big|_{-35,-30} = \sum_{i:\, V_i \geq 0} \rho_i \sqrt{\frac{2q_i}{m_i}} \left(\sqrt{V_i + 30}\right) - \sum_{e:\, 35 \leq V_e \leq 400} \rho_e \sqrt{\frac{2q_e}{m_e}} \left(\sqrt{V_e - 30}\right) - \sum_{e:\, V_e \geq 400} \rho_e \sqrt{\frac{2q_e}{m_e}} \left(\sqrt{V_e - 30}\right)$$

while with the same potential on the rear collector (V_2 =-30) and -400 volts on the front aperture (V_1 =-400) we obtain:

$$J_{COLL}\Big|_{-400,-30} = \sum_{i:\, V_i \geq 0} \rho_i \sqrt{\frac{2q_i}{m_i}} \left(\sqrt{V_i + 30}\right) - \sum_{e:\, V_e \geq 400} \rho_e \sqrt{\frac{2q_e}{m_e}} \left(\sqrt{V_e - 30}\right)$$

Thus, if electrons exist with energies over -35 ev, the collected ion current will increase with a higher negative retarding potential on the shield electrode. In fact, the collected ion current did increase as the negative retarding potential was increased up to 600 volts.

8.3 Thorium Energy and Density Distribution Measurements

A 0.040 inch diameter thorium wire was mounted as the emitter in the eight-aperture hemispherical collector after the tests on tungsten were completed. Tests were run using ruby # 1 with a 35 mm focal length lens. Ruby # 2 was not used with the thorium emitter, since extreme damage was incurred with this combination in earlier experiments. Thorium is an extremely soft, ductile material and extreme care had to be used in aligning the material and the direction of laser impingement. If the material was bombarded by a focused laser beam near its edge and with a slight angle between the axis of the emitter material and the axis of the laser beam, the edge material was moved backward. The material seemed to flow back down the wire out of the region of the impinging laser energy.

The laser generated ion emission for thorium was quite high, although there was an upper limit to allowable laser power density before extreme damage was noted. The same level of output was obtained from thorium as tungsten but at lower laser power density. Figure 37 gives the density distribution for the the thorium using ruby # 1 and the 35 mm lens.

The variation in the ion density with magnetic field was measured on a new piece of thorium wire. This is shown on Figure 38 with no axial magnetic field and with 1400 gauss (40 amperes of magnet current). This ion density plume is shown pictorially in Figure 39. It will be noted that although the magnetic field improved the shape of the ion plume substantially, there was still a reasonable amount of radially directed ion flux which did not effectively contribute to the generated thrust.

The energy measurements again indicated results very similar to those found in the tungsten measurements. Figure 40 shows the charge on the three energy-measuring collectors. The lowest elevation collection indicates that the high-energy electrons are travelling in a more radial than axial direction. The majority of the ions in the case of thorium appear to have energies less than 30 ev except for the group which can overcome a 600 volt retarding potential. The electrons are also capable of overcoming a retarding potential of -600 volts.

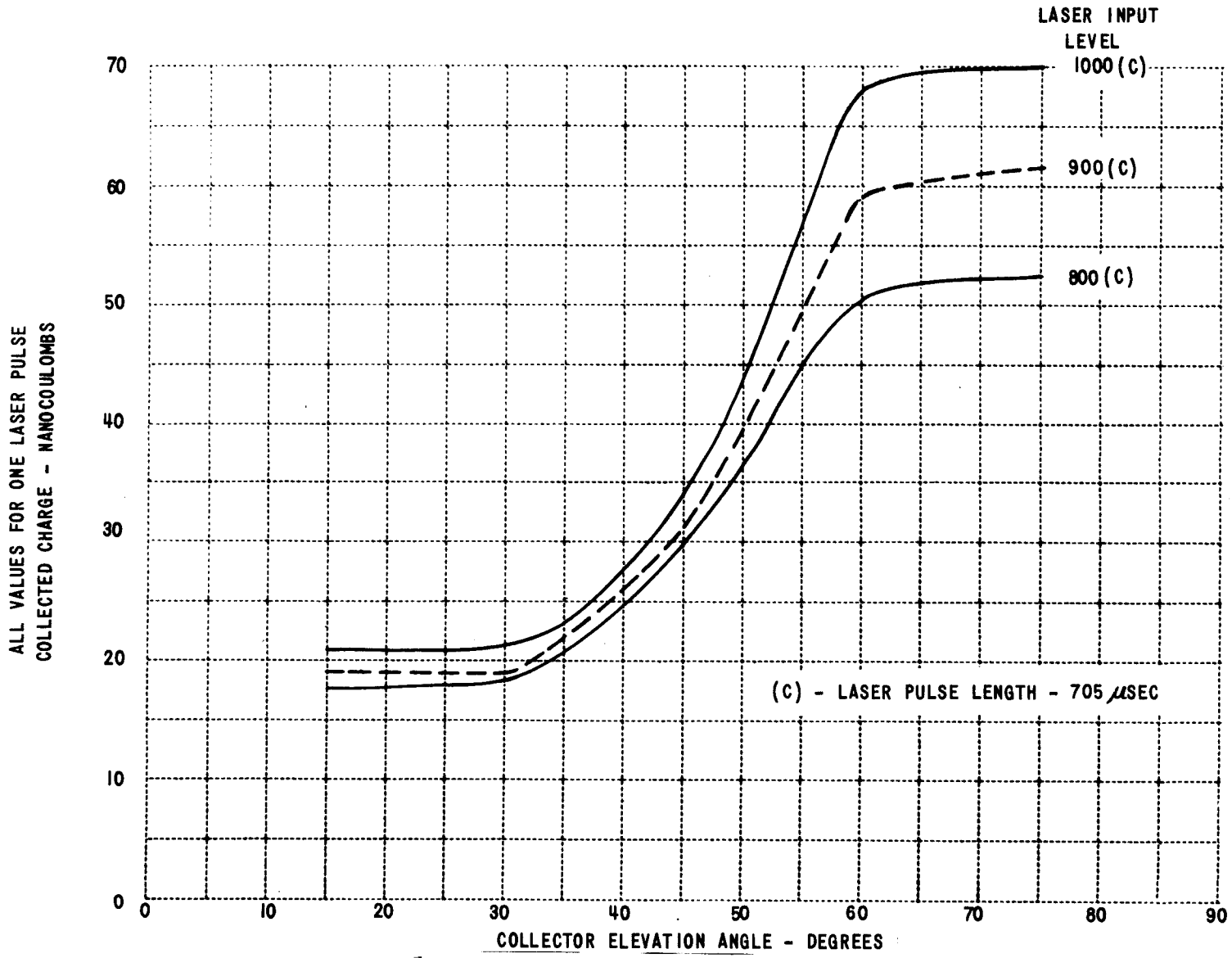

Figure 37 CHARGE DISTRIBUTION

THORIUM EMITTER - RUBY #1

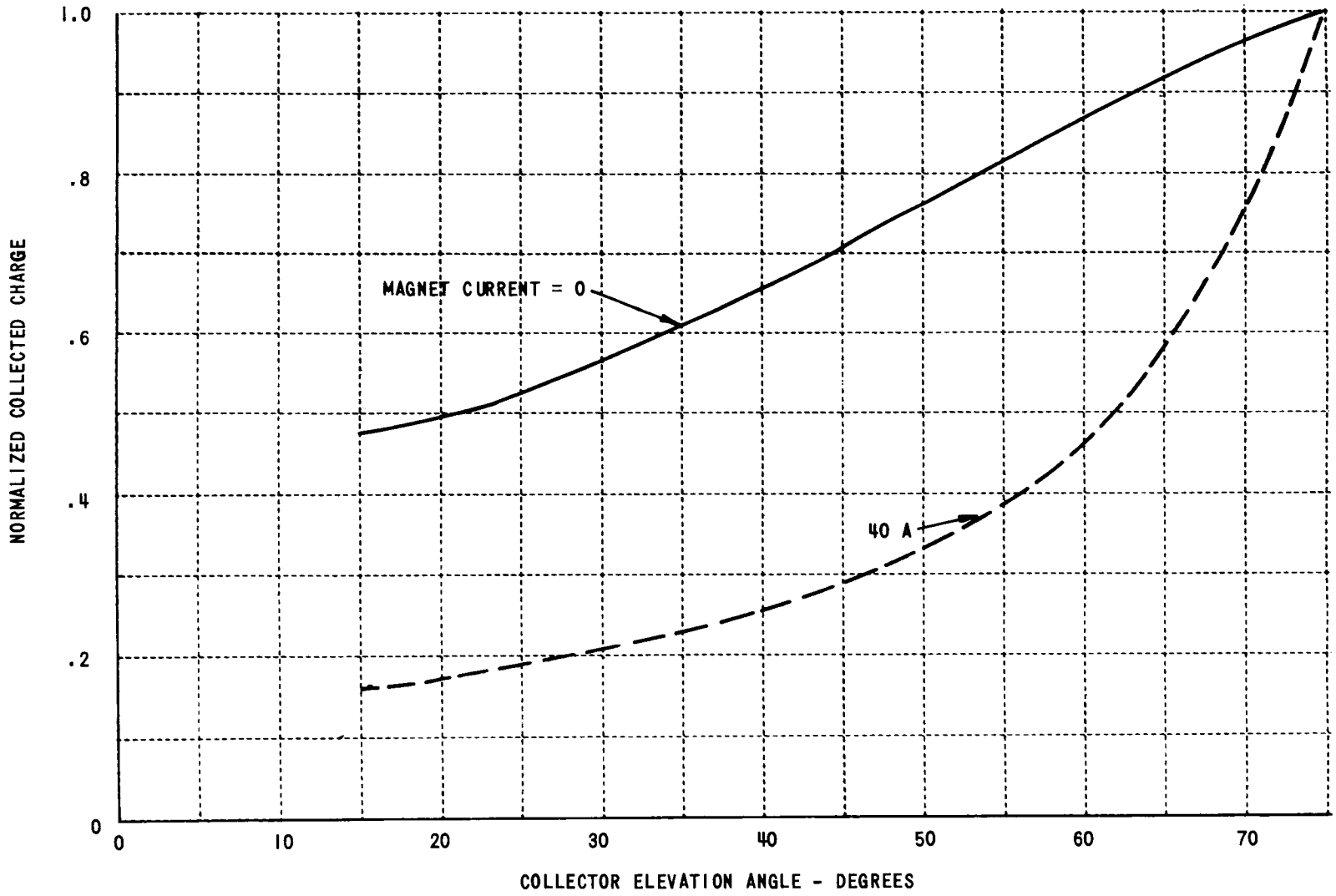

Figure 38 CHARGE DISTRIBUTION

THORIUM EMITTER - RUBY #1

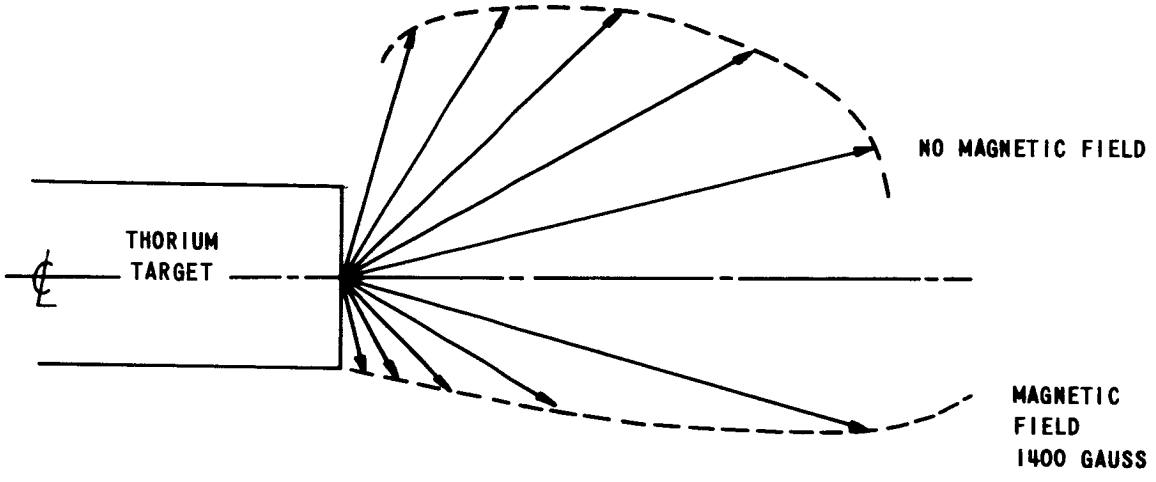

RUBY#1

Figure 39 NORMALIZED CHARGE DISTRIBUTION

THORIUM EMITTER

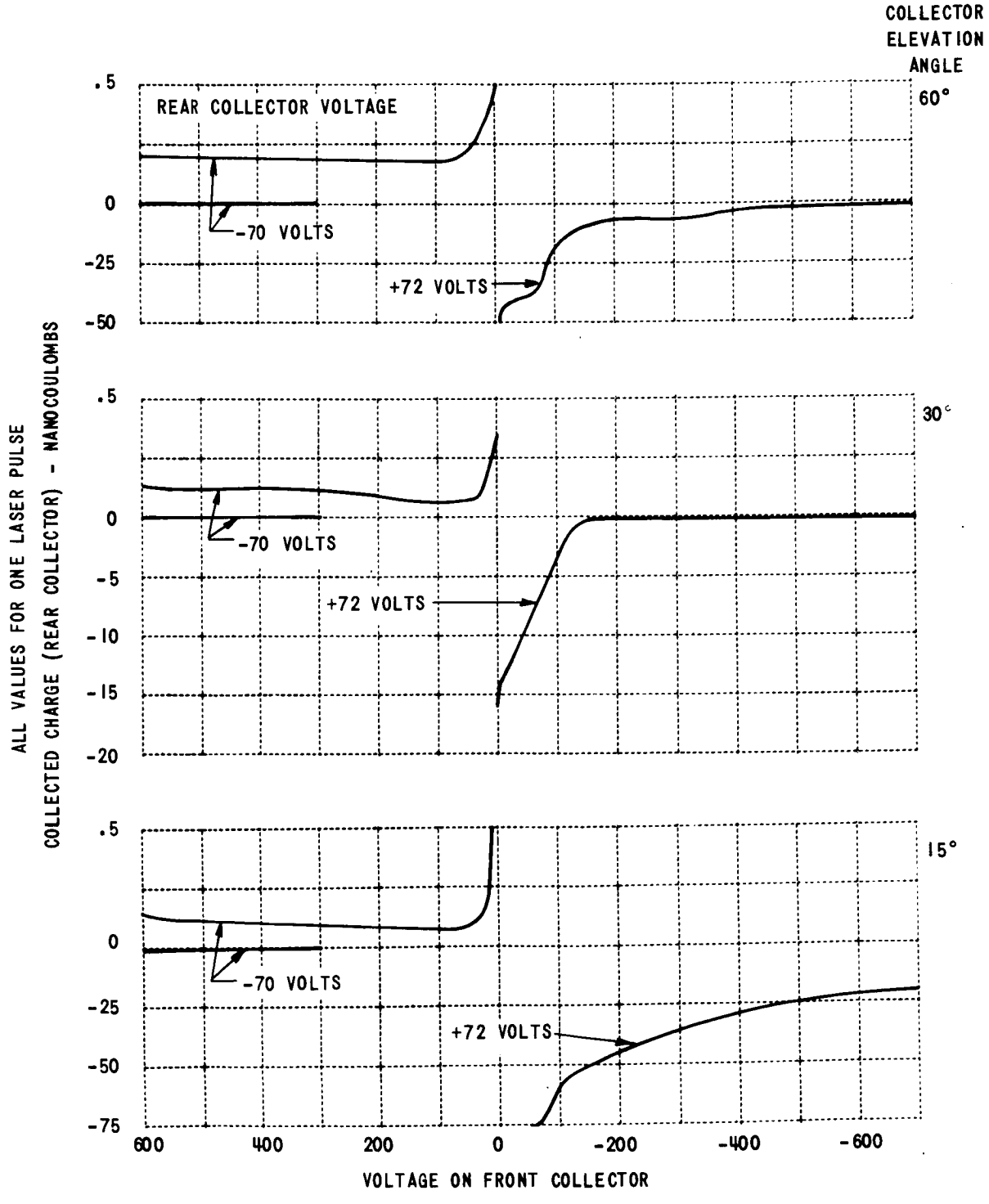

Figure 40 ENERGY DISTRIBUTION

THORIUM EMITTER - RUBY #1

8.4 Tantalum Energy and Density Distribution Measurements

A 0.062 inch diameter tantalum wire was used as a target in the eight-aperture hemispherical collector. The energy and density distribution measurements were made using ruby # 1 with the 35 mm lens.

The density distribution of the tantalum ion emission is shown in Figure 41. The emitted ion current at 1000 joules laser input was 200 micro-coulombs. This is about half the value obtained with tungsten under the same conditions. The collected currents on the various portions of the collector have approximately the ratio of one half. The effect of the magnetic field on the density distribution of the tantalum ion emission is shown on Figures 42 and 43. The initial emission configuration was very similar to that found with a tungsten emitter but the effect of the magnetic field on the ion density distribution was not as great, especially in the region of the 45 degree collector elevation angle.

The energy distribution of the tantalum emission can be surmised from Figure No. 44. When the retarding potential on the shield electrode with a 0.005 inch aperture was increased in the positive direction the positive charge on the rear collector increased. This anomaly occurred because the electron current being collected on the shield electrode was increasing, thus the apparent increase in ion current was, instead, a decrease in electron current. This inability to cut off electron current is shown even more effectively in Figure 45. With a -600 volt retarding potential on the shield electrode of the energy measuring assemblies of the hemispherical assembly, the voltage on the rear collector was varied. The electron current completely dominated the collected ion current and the true value of ion energy could not be obtained. It will be noticed from Figure 45, however, that the high energy ions were more prevalent at the higher elevation angles.

Figure 44 shows that, as in the other materials tested, the high energy electrons were present at the lower elevation angles. A positive retarding voltage of 600 volts was insufficient to stop all ions from passing thru the aperture and - 600 volts did not eliminate the electrons.

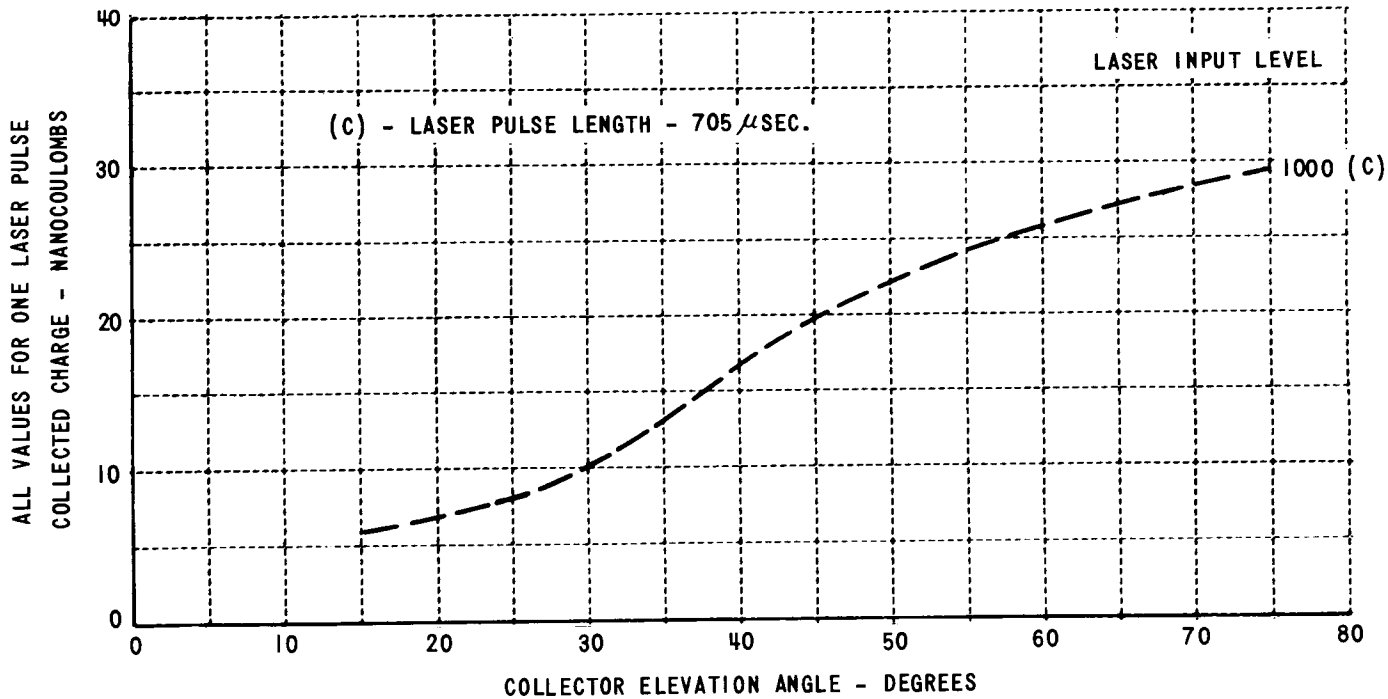

Figure 41 DENSITY DISTRIBUTION

TANTALUM EMITTER - RUBY #1

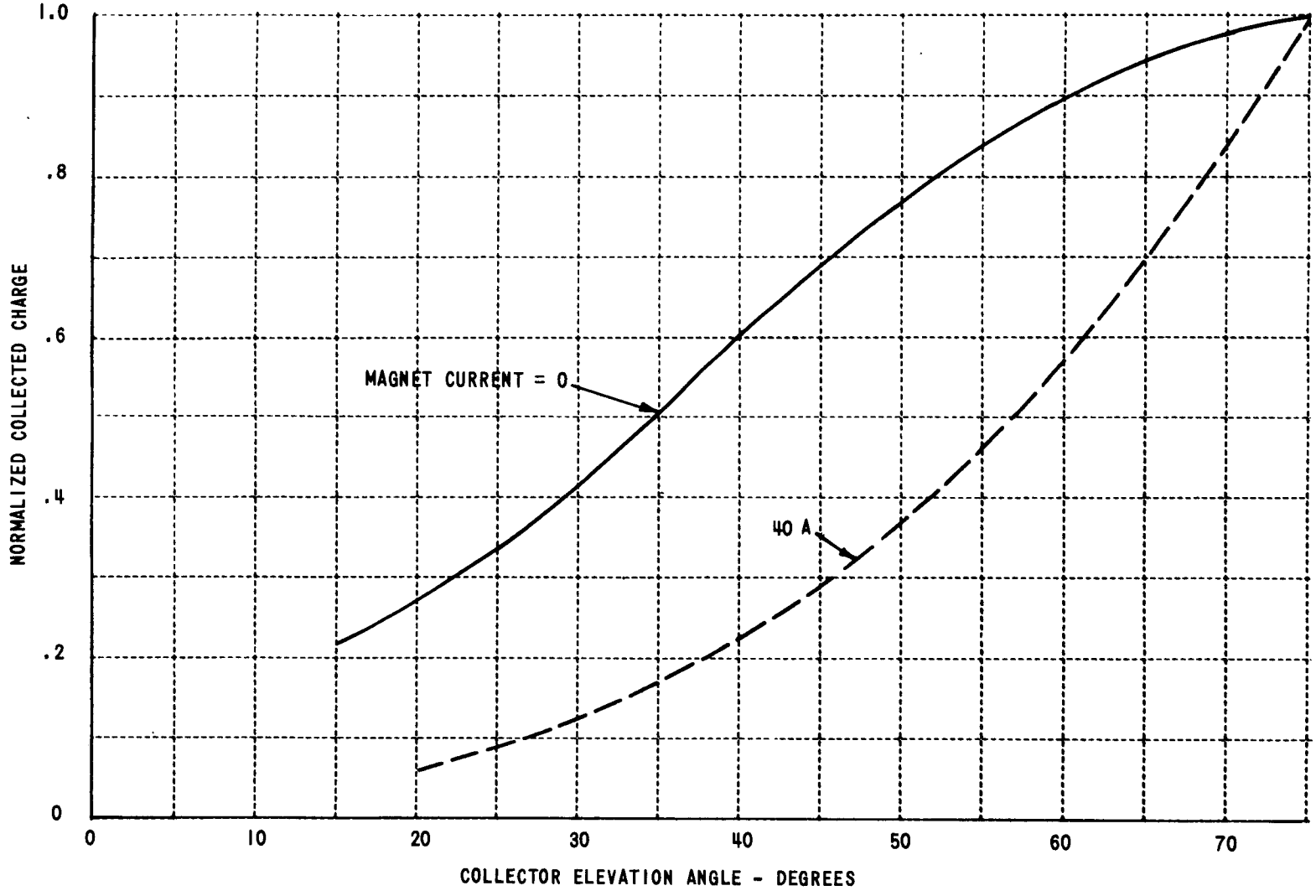

Figure 42 CHARGE DISTRIBUTION

TANTALUM EMITTER - RUBY #1

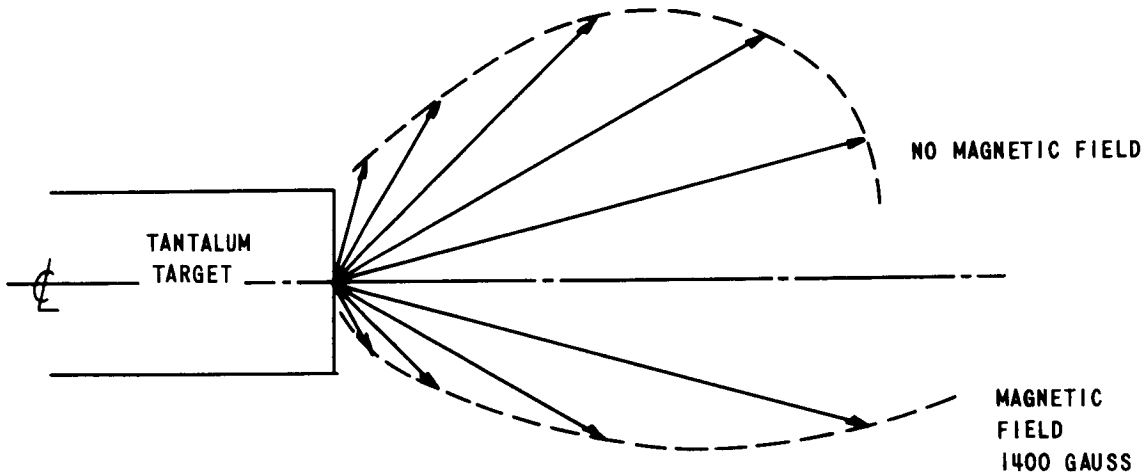

RUBY#1

Figure 43 NORMALIZED CHARGE DISTRIBUTION

TANTALUM EMITTER

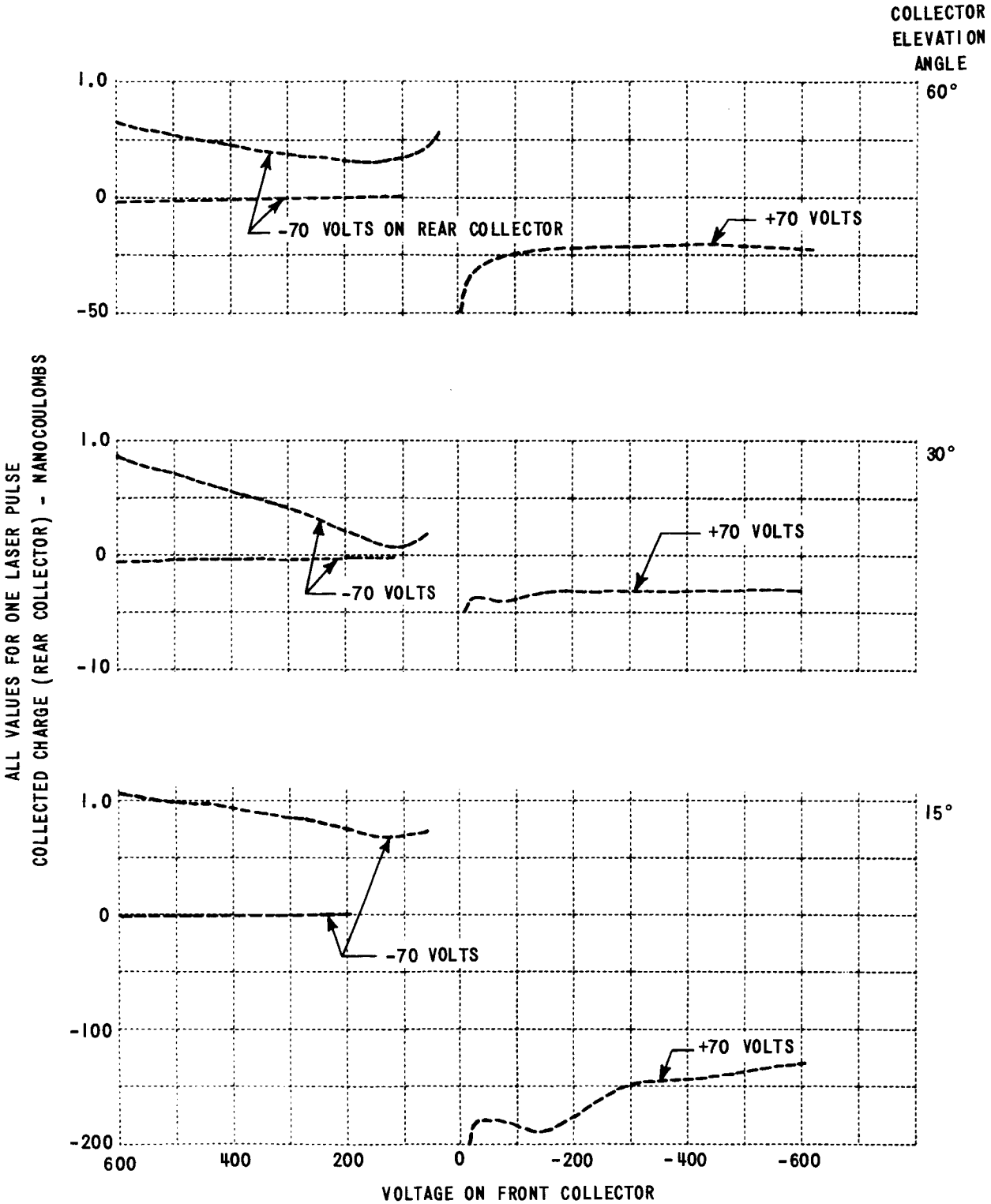

Figure 44 ENERGY DISTRIBUTION

TANTALUM EMITTER - RUBY #1

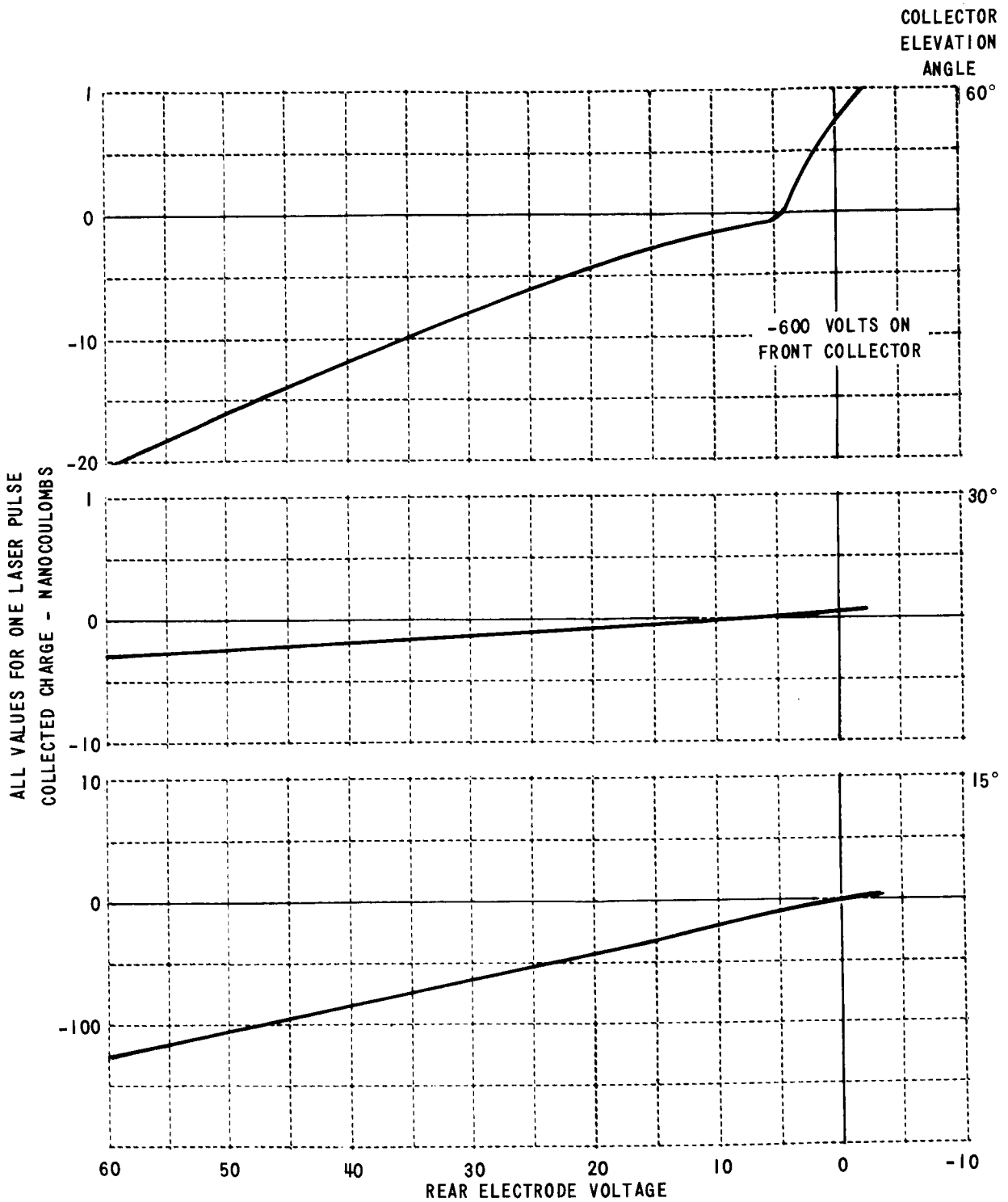

Figure 45 ENERGY DISTRIBUTION

TANTALUM EMITTER - RUBY #1

8.5 Rhenium Energy and Density Distribution Measurements

Rhenium is a material which remains undamaged by laser illumination but showing no significant ion emission with the exception of the pendulum experiment (see Section 7.0) where it did have a relatively high ion yield and thrust. During the emitter evaluation experiments, although the ion yield and the weight loss were low, a reasonably heavy plating was formed on the vacuum window directly in front of the emitter. This behavior is partially explained by the density distribution of the material. Figure 46, which shows the density distribution with ruby #1, indicates from the shape of the curve that a good part of the emission even without a magnetic field was contained within a 20 degree semiangle around the axis normal to the emitter. Figure 47 shows this even more distinctly with the 1400 gauss axial magnetic field and ruby # 1. The emission caused by ruby # 2 did not possess, to as great a degree, this preferred emission orientation.

The energy distribution of the electrons and ions emitted from rhenium as a result of laser illumination are shown on Figures 48 and 49. The electrons and ions again possessed energies greater than 600 volts.

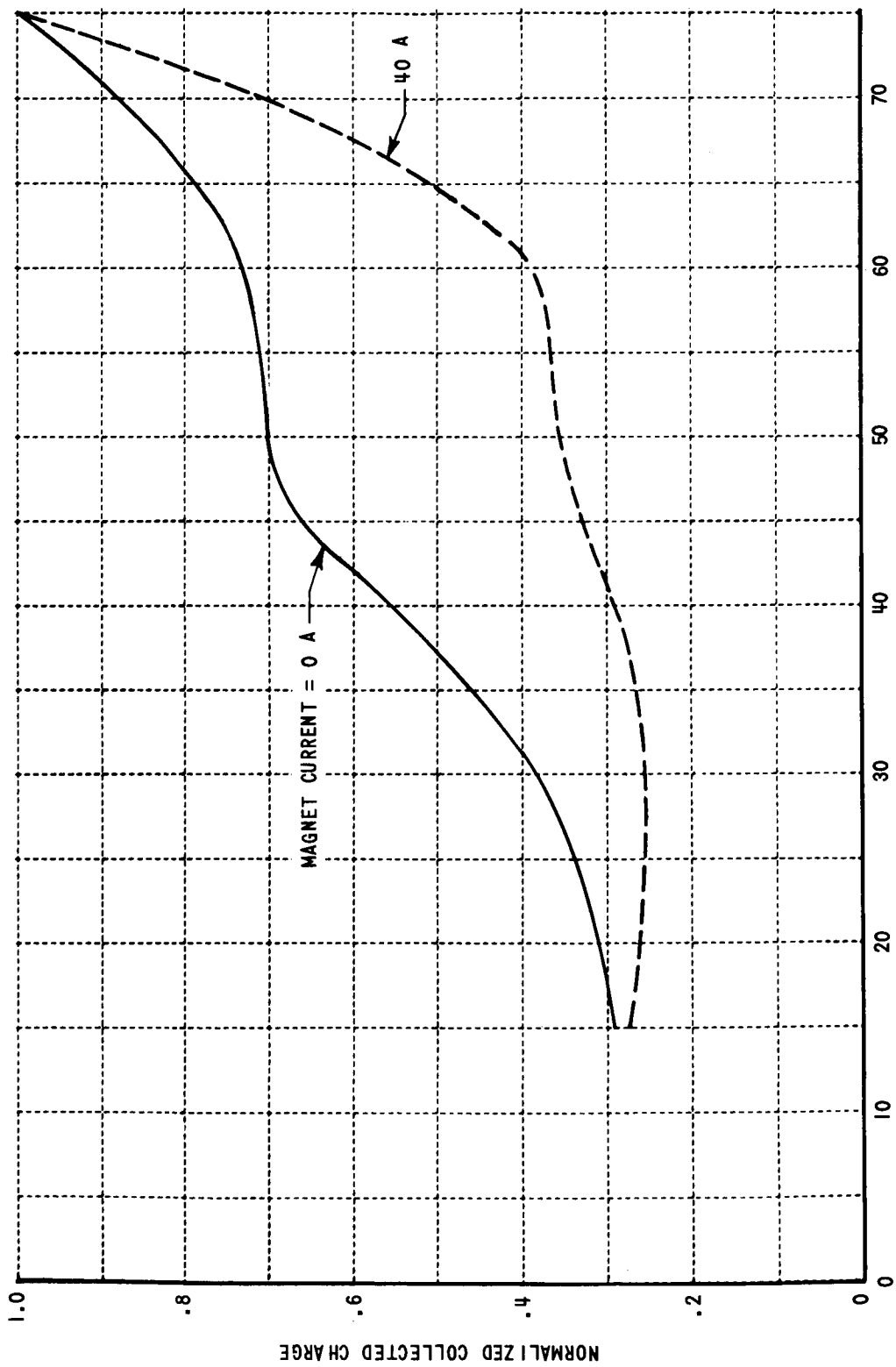

Figure 46 CHARGE DISTRIBUTION

RHENIUM EMITTER - RUBY #1

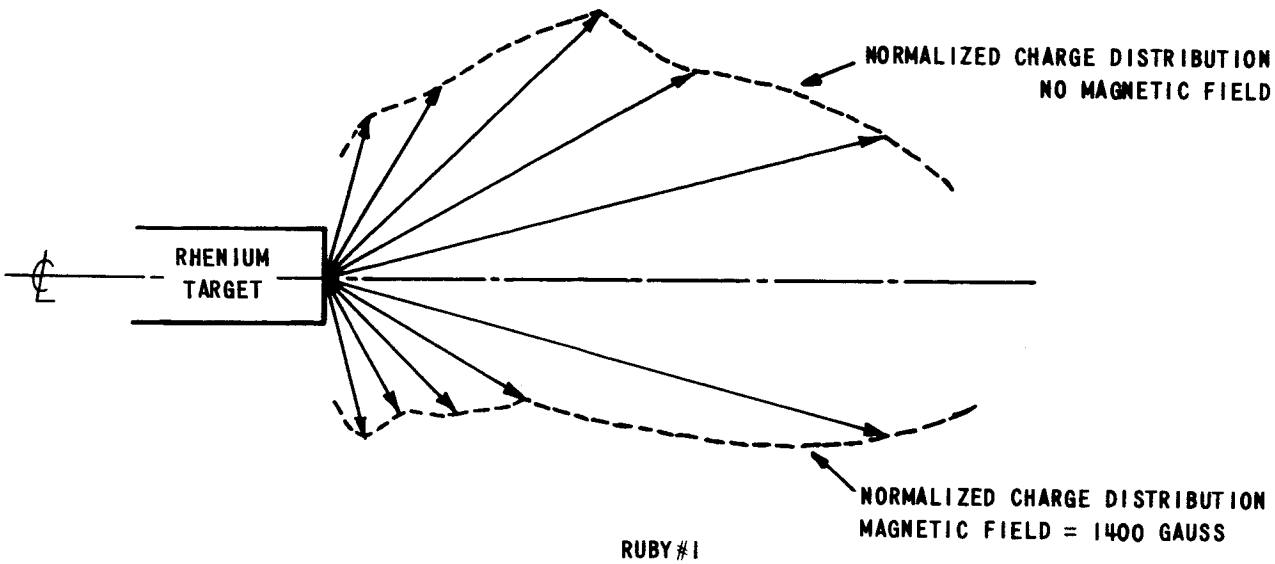

RUBY#1

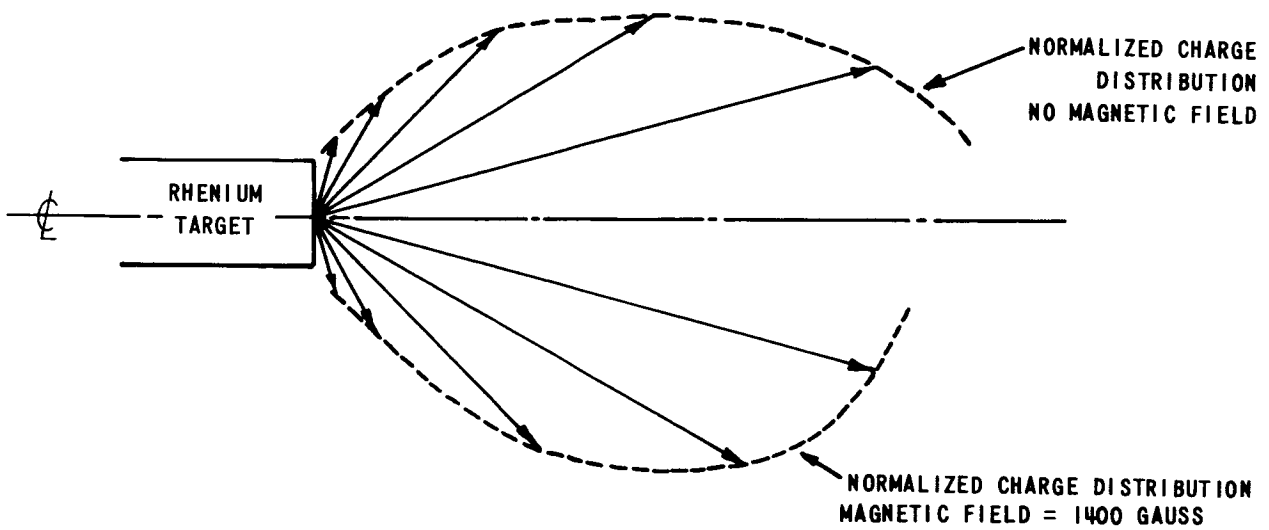

RUBY#2

Figure 47 DENSITY DISTRIBUTION OF LASER GENERATED IONS

RHENIUM EMITTER

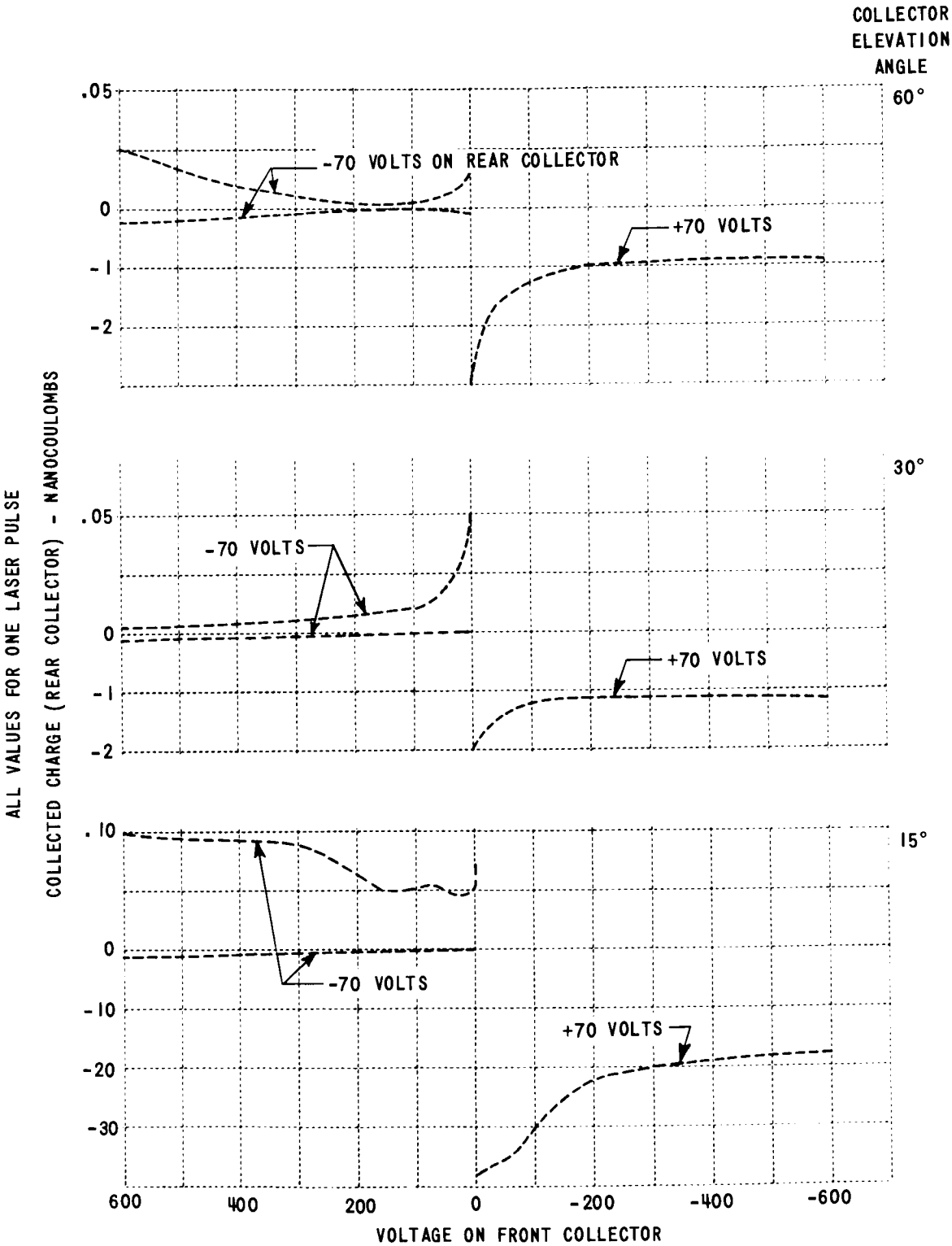

Figure 48 ENERGY DISTRIBUTION

RHENIUM EMITTER - RUBY #1

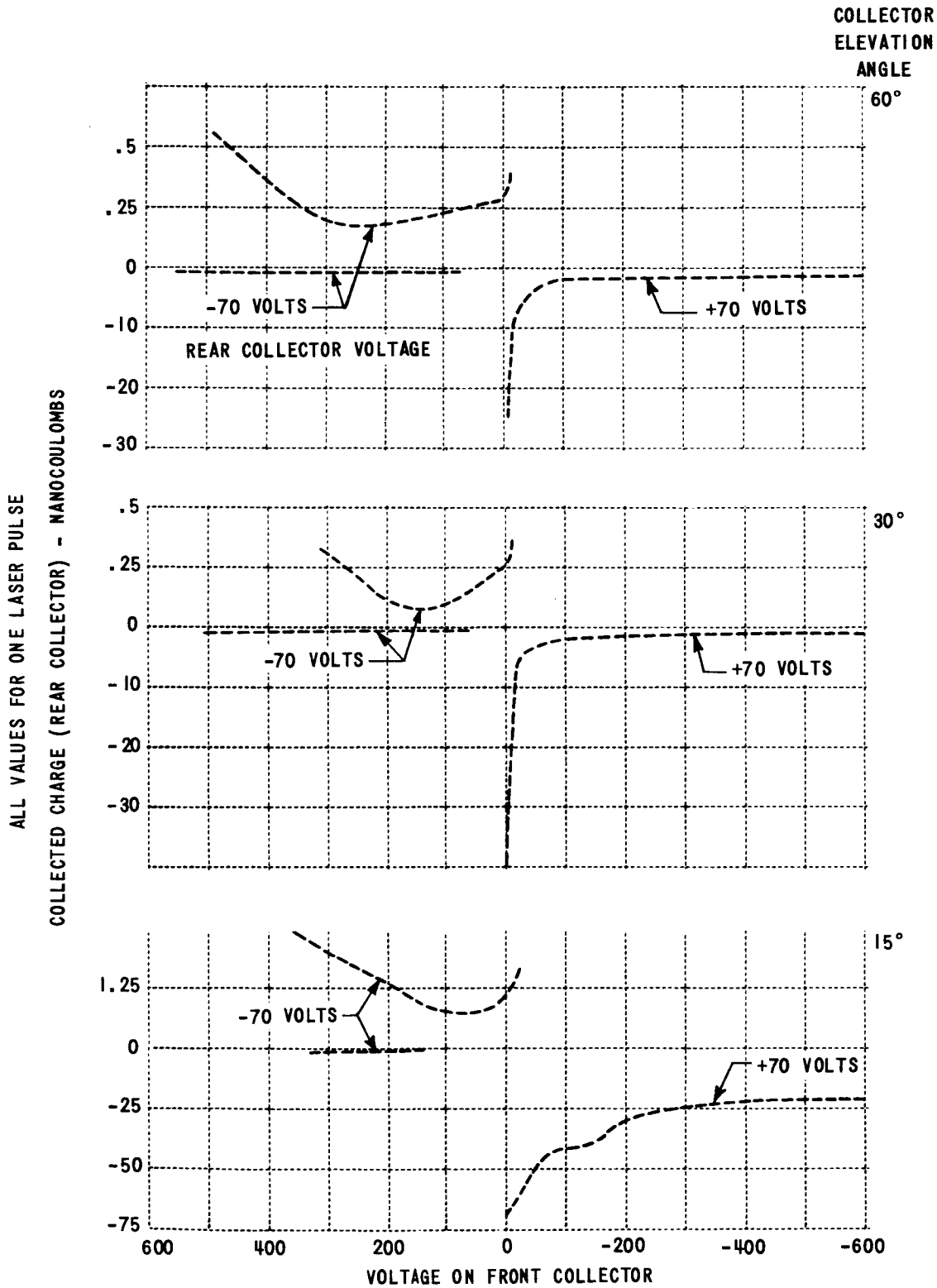

Figure 49 ENERGY DISTRIBUTION

RHENIUM EMITTER - RUBY #2

9.0 QUADRUPOLE MASS SPECTROMETER EXPERIMENTS

The properties of positive ionized particles emitted as a result of laser surface illumination were investigated using a quadrupole mass spectrometer. This type of spectrometer contains a mass filter which permits the transmission of only those ions whose charge-to-mass ratio lies within a range of values of externally variable width. The four symmetrically located mass filter rods were biased to reject incident electrons.

The mass spectrometer mounted in its own vacuum envelope with associated grids, apertures, ionizers and Faraday cup collector was bolted to an assembly containing the emitter and surrounding grid and shield. The surface of the emitter was placed normal to the axis of the laser beam, and the spectrometer axis at 30° to the emitter surface. A photograph of the assembly is shown in Figure 50 and in the schematic drawing of Figure 51. Although a larger angle would have been desirable, the 30° angle was made necessary by the dimensions of the spectrometer and the vacuum port through which laser light passed.

A shield, i.e., a cylinder with a gridded aperture, was present around the emitter to eliminate any possible dependence, particularly angular dependence, of emission on focusing voltages. In addition, there was a helix and a thermionic emitter between the shield and quadrupole structure to permit testing for neutral particles. The helix, which had a gridded entrance aperture in line with the laser induced emission, could be biased to reject ionized particles. The grid, regardless of its potential, has no effect on any neutral particles emitted in the direction of the quadrupole structure except to intercept any which might strike it.

When testing for neutral particles, the helix is biased to repel the laser generated ions from the quadrupole structure. Thermionically emitted electrons (accelerated through 160 volts) then bombard any neutral particles inside the helix, ionization should occur and a Faraday cup at the far end of the quadrupole structure should collect ion current. It must be remembered

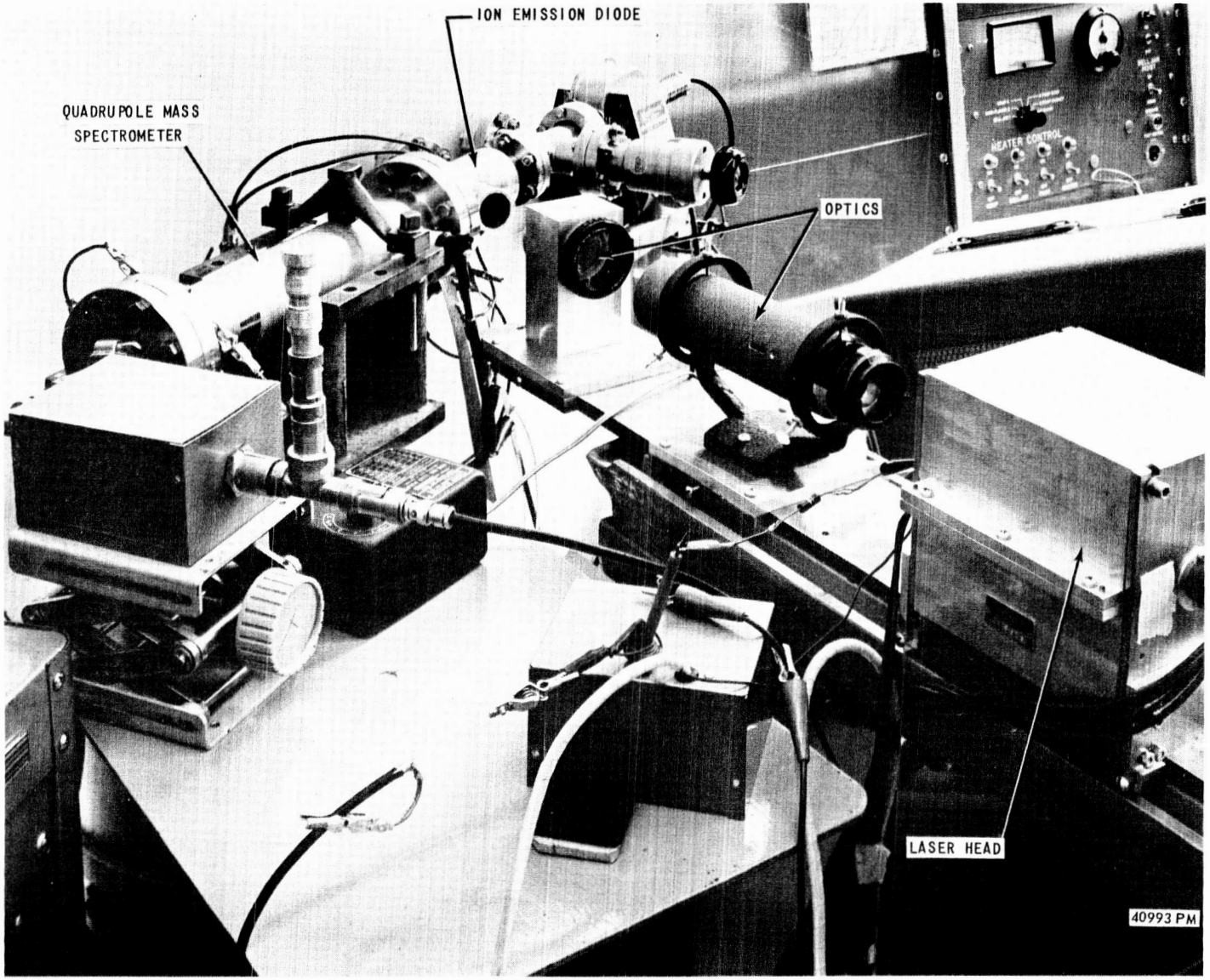

Figure 50 QUADRUPOLE MASS SPECTROMETER EXPERIMENTAL CONFIGURATION

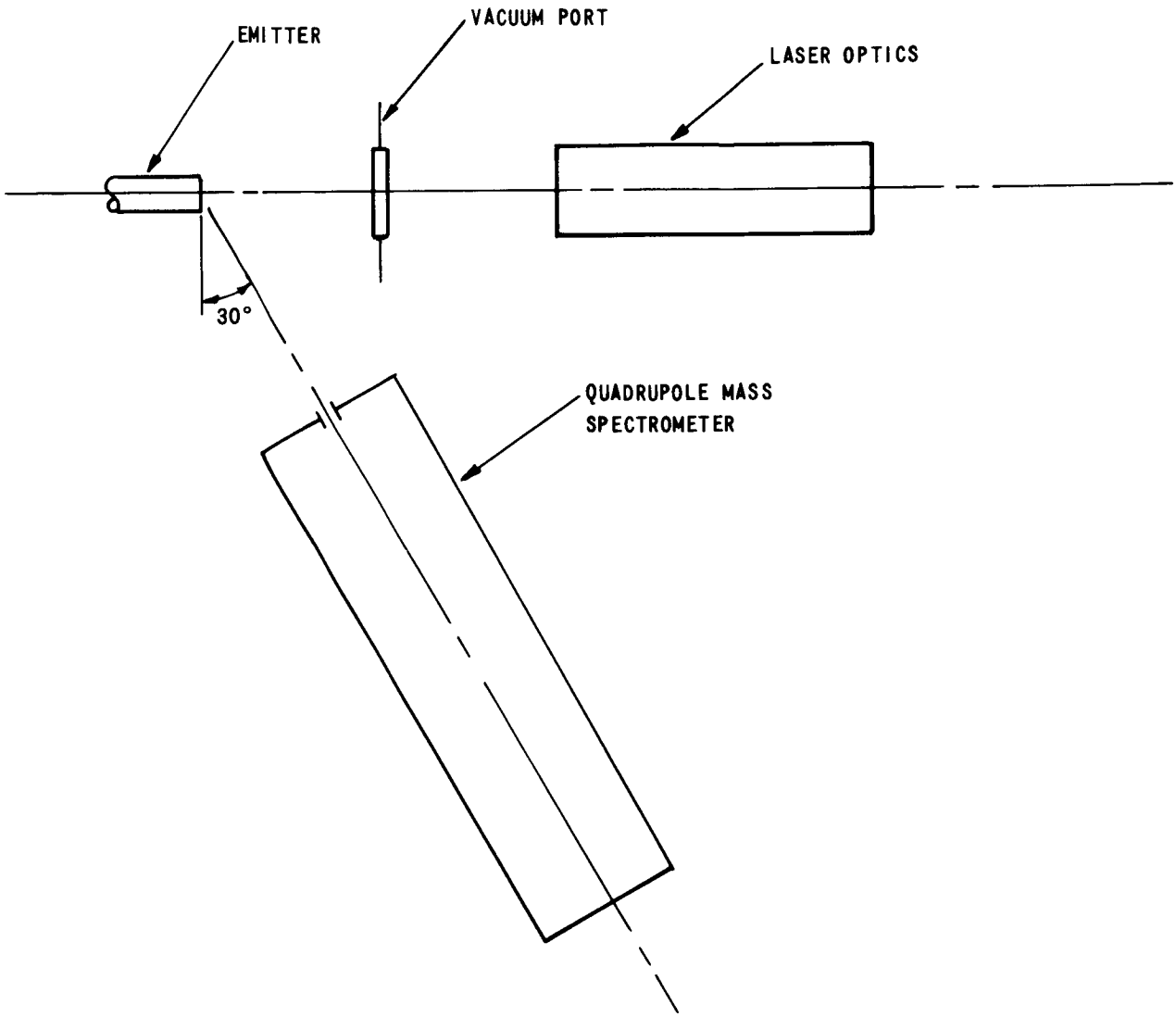

Figure 51 SCHEMATIC DRAWING OF APPARATUS USED FOR SPECTROMETER EXPERIMENTS

that the neutral particles which have been ionized must have a velocity component predominantly in the axial direction of the quadrupole structure and be nearly on-axis in order to enter the sorting and focusing region and be collected on the Faraday cup collector.

Tests were made for four classes of particles in the experiments with the spectrometer. These classes were: (1) singly charged atomic ions, (2) doubly charged atomic ions, (3) singly charged molecular ions, and (4) neutral particles. Figure 52, which is a stability diagram for the various ions monitored, serves to show the manner in which searches were made for the three classes of ions. The singly charged and doubly charged atomic ions were examined by computing the RF and DC voltages at which they should have been selected, and then applying those voltages to the spectrometer and looking for the ions. Because the RF power source used would not supply voltages larger than 3000 volts, the search for singly charged molecular ions was made by reducing the DC voltage to zero and using the spectrometer in the high-mass-pass mode. The RF and DC voltages required for the selection of various charged particles can be calculated quite accurately based on the physical dimensions of the mass spectrometer assembly. The calculated and measured voltages were within a few percent for all the materials tested and species found.

9.1 Quadrupole Mass Spectrometer Results

Six materials were tested in the mass spectrometer assembly. Two were subsequently eliminated from further tests. Both chromium and lead exhibited a high yield of neutral material and no further tests were performed on these materials. The results of the experimental search for various classes of particles is summarized in Table III. The results of the tests with both ruby #1 and #2 and with a 35 mm lens are shown.

While investigating the presence of singly charged atomic ions the voltages on various electrodes or apertures were changed and the effect of these retarding potentials on the various ions was noted. The relative ion energy distribution of the various materials tested are shown in Figures 53, 54, 55, and 56. This experimental data indicates that these materials (rhenium, tantalum, thorium and tungsten) have ions with energies exceeding 150 ev.

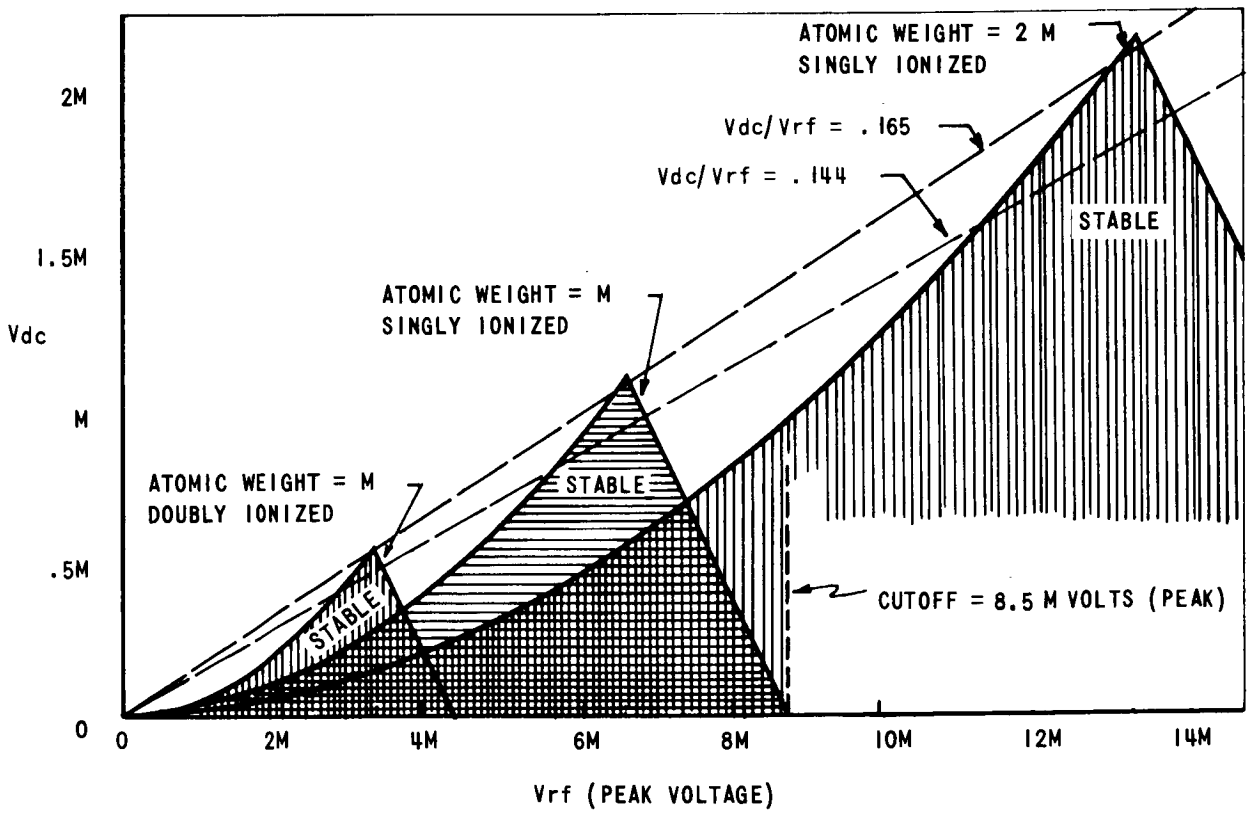

Figure 52 STABILITY DIAGRAM (ATOMIC WEIGHT = M)

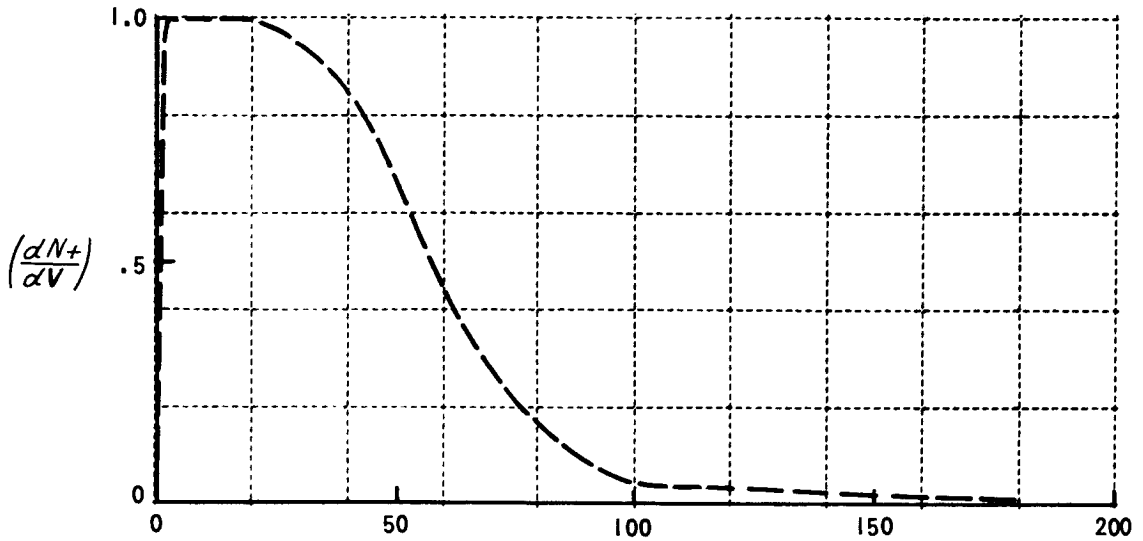

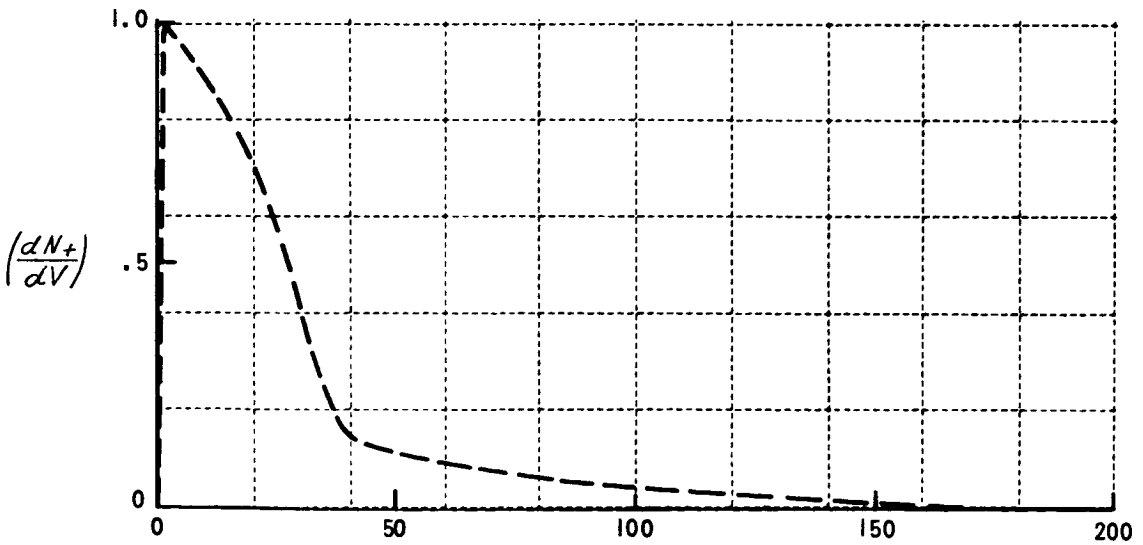

Figure 53 NORMALIZED ION ENERGY DISTRIBUTION

INCIDENT LASER POWER - 1.5 KW

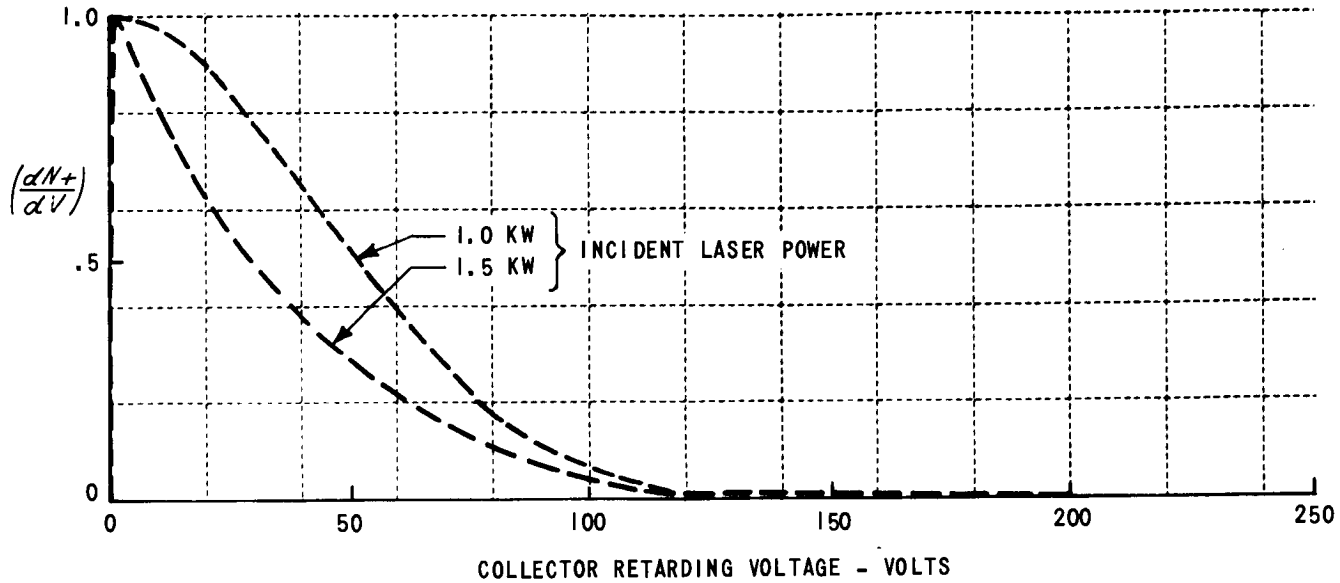

Figure 54 NORMALIZED ION ENERGY DISTRIBUTION

TANTALUM EMITTER - RUBY #1

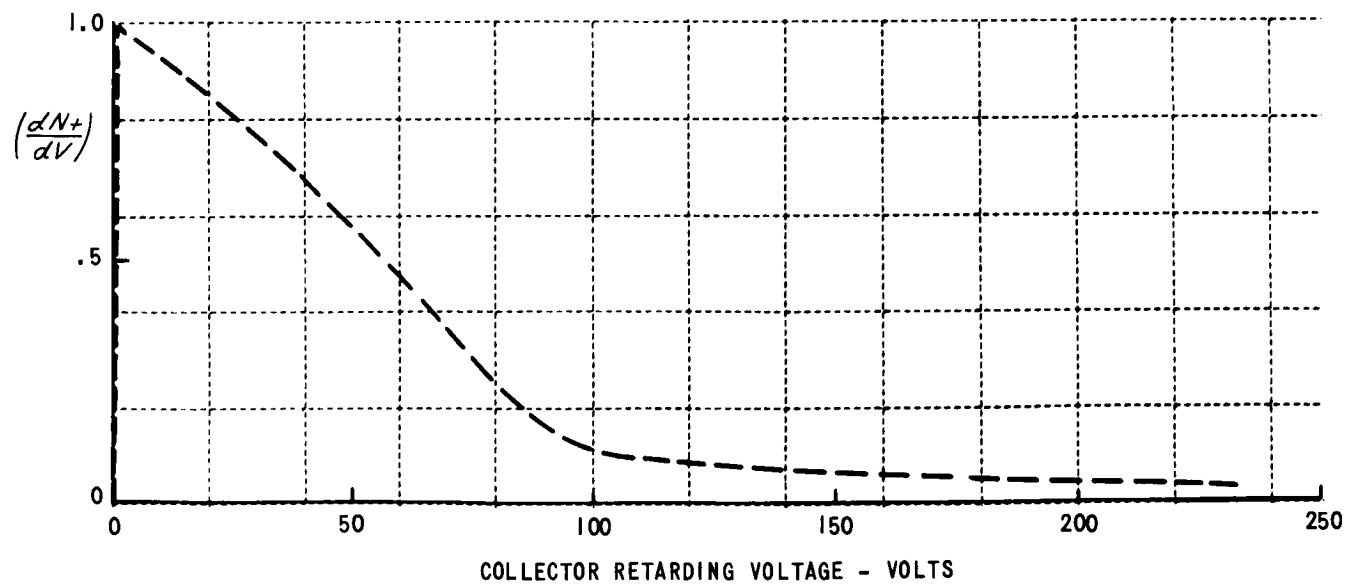

Figure 55 NORMALIZED ION ENERGY DISTRIBUTION

THORIUM EMITTER - RUBY #1

INCIDENT LASER POWER - 5.5 KW

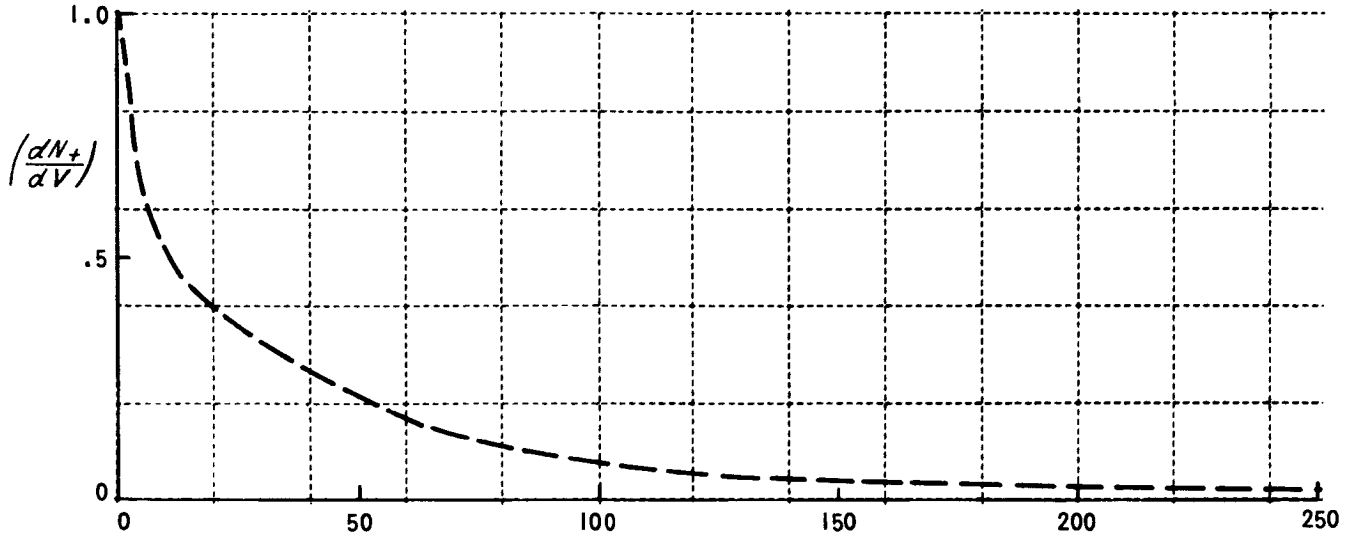

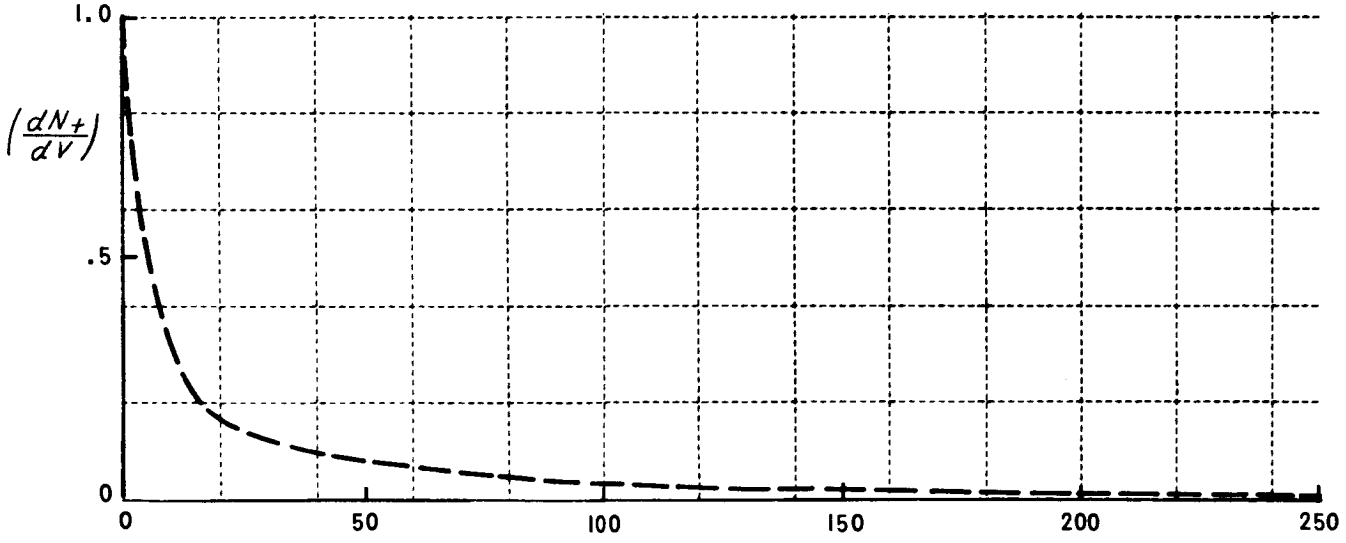

Figure 56 NORMALIZED ION ENERGY DISTRIBUTION

INCIDENT LASER POWER - 5.0 KW

Table III

Material	Ruby No. 1				Ruby No. 2			
	Singly Charged Atomic Ions	Doubly Charged Atomic Ions	Singly Charged Molecular Ions	Neutral Particles	Singly Charged Atomic Ions	Doubly Charged Atomic Ions	Singly Charged Molecular Ions	Neutral Particles
Chromium	Yes	--	--	Yes	--	--	--	--
Lead	Yes	--	--	Yes	--	--	--	--
Rhenium	Yes	Yes (20%)	No	No	Yes	Yes (3%)	No	No
Tantalum	Yes	Yes (20%)	No	No	Yes	Yes (3%)	No	No
Tungsten	Yes	No	No	No	Yes	No	No	Yes
Thorium	Yes	No	No	No	--	--	--	--

The average energy of the emitted ions is greater using ruby #1 than when using ruby #2, e.g., measurements on tungsten and rhenium. This information in conjunction with the data on tantalum, Figure 54, for two different levels of incident laser power indicates that the higher incident laser power densities (ruby #2 has regions of high power density - see Section 3.1), gave a lower ion energy distribution. The number of emitted ions increased rapidly with increasing laser power density but the ion energy decreased. Therefore, there will be some limiting level of power density for maximum thrust generation.

Using the mass spectrometer, a measurement of the transit time of a half-millisecond long ion burst has been obtained and this gave an average

ion velocity of 6 to 7 km/sec for tungsten and thorium which agrees with earlier velocity measurements. An attempt to measure the velocity of individual groups of ions was unsuccessful. The emitted current could not be used for comparison since only a small percentage of this current was admitted into the quadrupole assembly. An attempt to use the intercepted current on the aperture at the beginning of the quadrupole structure as a comparison also proved to be impossible. This aperture electrode was capacitively coupled to the mass spectrometer structure and a large fraction of the applied RF voltage was coupled out, masking the intercepted ion current.

The various targets were weighed before and after use. Over 80% of the weight loss could be accounted for from the measured emitted charge. The other 20% could easily have been collected on the glass port in front of the target and thus not measured in the viewing circuits. The two materials which were eliminated from further consideration, lead and chromium, showed significantly higher weight loss than was accounted for by the measured emitted charge.

10.0 THRUST MEASUREMENTS

The characteristic of primary interest in laser-surface interaction when applied to thrustor performance is the thrust developed as a result of the laser induced emission. Section 7 describes the thrust measurements taken on all the thirteen original emitter materials. This configuration did not permit absolute calibration and only relative values were obtained in these initial experiments.

One of the specialized tests performed on the four materials (tungsten, thorium, tantalum, and rhenium) selected for further study was an accurate thrust measurement. A simple pendulum arrangement utilizing a linear variable differential transformer was constructed. The original expectation of using a seismic pendulum mounted on flex-free pivots was abandoned since the thrust which would be developed required an inordinately long lever arm for mounting of the target, in order to attain a reasonable motion of the pendulum. This long lever arm made the experimental mounting of the seismic pendulum in either of the two vacuum systems available virtually impossible.

The experimental arrangement used in the thrust measurements is shown schematically in Figure 57. This arrangement, with the recording instruments used, had a readability of 0.02 mils (2×10^{-5} inches). In general the residual motion of the pendulum after electromagnetic damping was 0.1 mils and the minimum deflection measured due to the laser ion generation was 0.8 mils. Since the period of the pendulum was in the order of 1 second, the laser beam could be timed to strike the pendulum at a known position and the error incurred from this residual motion could be eliminated.

The pendulum arrangement and motion (less than 0.025 inches) were such that the relative weight and flexing of the supporting wires and any friction at the pivot points were extremely small. Since the pendulum bob was supported by two separate wires, an

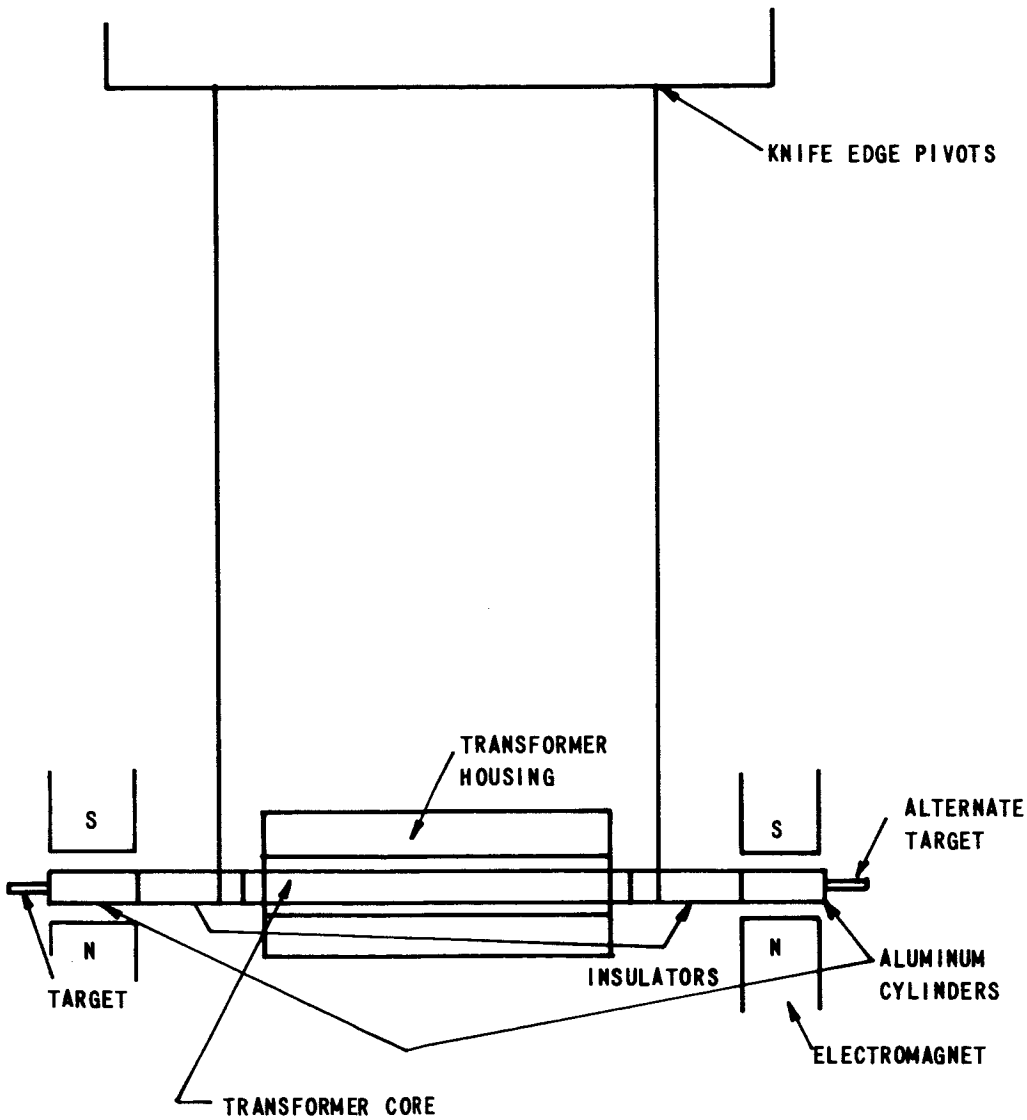

Figure 57 EXPERIMENTAL CONFIGURATION FOR THRUST MEASUREMENTS

effective pendulum length was calculated from the measured period of the pendulum using

$$L_{eff} = \frac{g}{4\pi^2} \tau^2 \tag{12}$$

This effective length was found to be 4 percent smaller than the measured length. The effective length of the pendulum was calculated whenever a new material was mounted in the thrust-measuring assembly. The thrust was calculated using

$$F\tau = M \sqrt{\frac{g}{L_{eff}}} \; x \tag{13}$$

or

$$F\tau = \frac{2\pi M}{\tau} x \tag{14}$$

In Section 7.1 the above expressions were derived for a pendulum whose weight of supporting wires was comparable to the weight of the pendulum bob. In the present case, the weight of the support wires was less than 0.5 percent of the bob weight and can be neglected.

The motion of the pendulum bob as evidenced by the variation in voltage output of the linear transformer was monitored on a strip line recorder. The maximum sensitivity of the recorder was 370 millimeters of pen deflection per mil of core displacement. Both a dynamic and static calibration of core displacement was performed with good correlation between the two measurements.

In order to damp the twisting and longitudinal motions of the core between measurements, two electromagnets wound on horseshoe forms, were used. The magnet pole pieces were placed around the aluminum cylinders on each end of the pendulum bob. As noted previously, the core displacement could be damped out to a maximum of 0.1 mils.

10.1 Results of Thrust Measurements

The laser generated thrust was measured for four materials--rhenium, tantalum, thorium and tungsten. Both rhenium and tungsten were tested with ruby #1 and #2, while tantalum and thorium were only tested with ruby #1. (These two latter materials showed significant damage with ruby #2 indicating a high neutral yield which is undesirable in an electric thrustor application.)

The measured thrust is shown on Figure 58. Note that the level of incident laser power was quite low as compared to that used for data taken earlier in the contract. The difference in laser powers resulted from a decrease in laser efficiency from 0.6 percent to 0.2 percent. The decrease in efficiency could be due to a change in the flash tube efficiency, a change in the spectral output of the flash tube, poorer absorption by the laser due to surface pitting, lower quantum efficiency in the ruby due to internal discontinuities, or loss of light output through the surface discontinuities of the rod.

As a result of the low laser output power, a condition present over the last month of testing during this contract, the measured thrust was far lower than projected from the initial level of ion generation. It will be noted from Figure 58 that the projected thrust for an incident laser power of 5 KW, (the output power level obtained earlier in the program at a laser input energy of 1000 joules), should be greater than 6 millipounds and in the case of thorium perhaps even double that level. In fact, using Figure 7 to project the expected thrust at an incident power level of 5 KW, tantalum would have a 3 to 1 increase in thrust and tungsten would have an 8 to 1 increase, which again would indicate a thrust of slightly over 6 millipounds for these two materials.

Using ruby #2 to illuminate rhenium and tungsten yielded results which showed an increase of 3 to 1 in measured thrust over that obtained with ruby #1. There was still the problem of material damage which resulted in the presence of neutrals and variations in thrust level due to changes in neutral yield on a shot to shot basis.

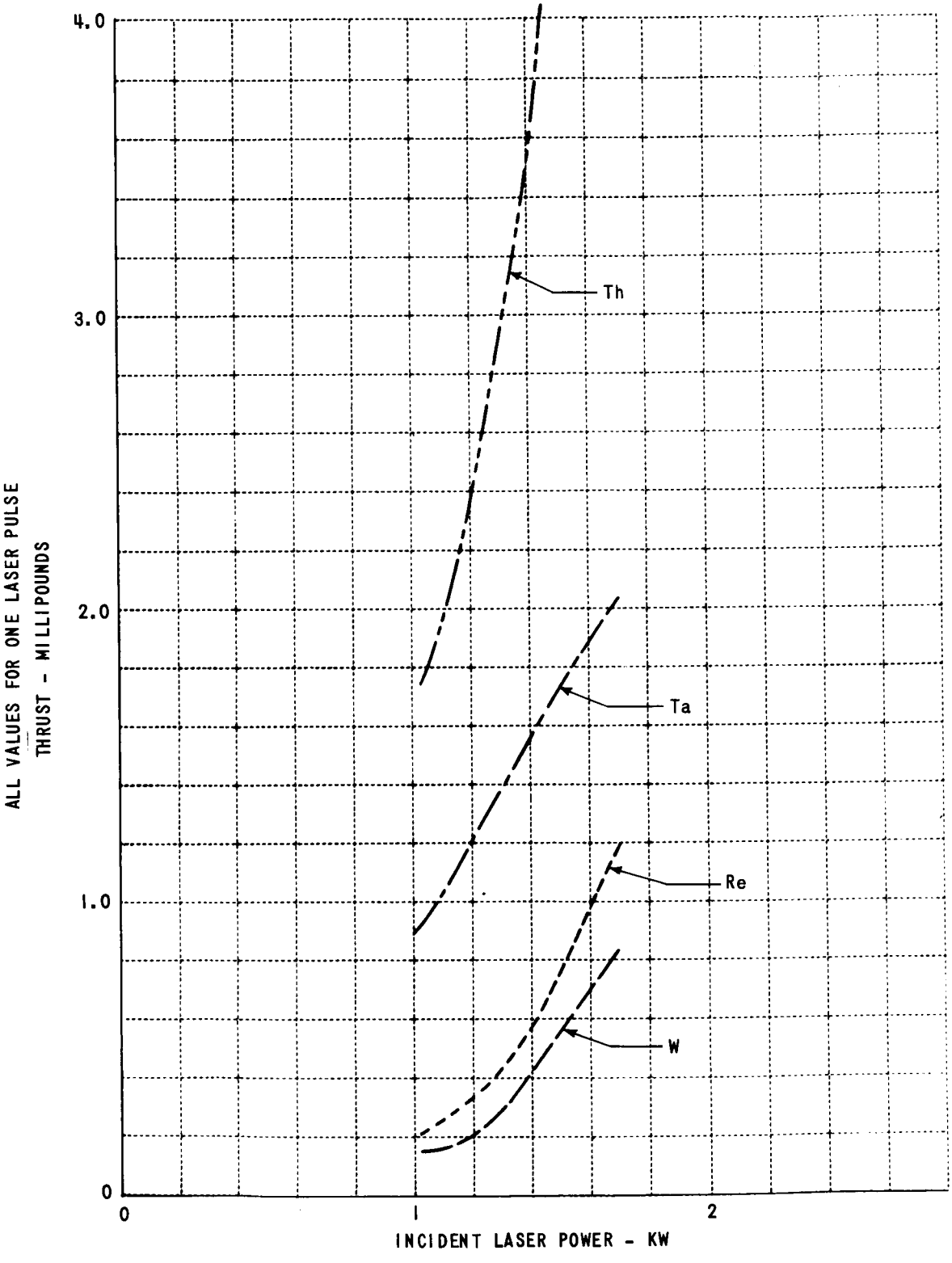

Figure 58 THRUST OUTPUT AS A FUNCTION OF LASER POWER

RUBY #1

In order to attain higher levels of thrust it appears desirable to use higher power density lasers. However, extremely high power densities in extremely small areas must be avoided, (as evidenced in our results with ruby #2). A ruby similar to #1 in our tests, i.e., one with no dominant modes, with uniform power density across the entire laser beam, when operated at higher power levels will give larger thrusts without excessive material loss. In the tests performed with ruby #1 the material surface indicated melting and reforming without any large material displacements. The operating power density limit (start of excessive material loss) was not reached during the contract for most materials with this ruby.

11.0 EMISSION MECHANISMS

In the preceding sections, experiments and experimental results have been discussed which show that extremely high emission densities (10^5 to 10^6 amperes per cm^2 for electrons and 10^3 to 10^4 amperes per cm^2 for ions) as well as high emission energies (15 ev for ions) can be obtained from laser-surface interactions. The purpose of sections 11.1 through 11.4 is to identify and explain some of the possible mechanisms responsible for the electron and ion emission. For convenience, the mechanisms discussed are summarized in Figure 59.

11.1 Similarities to Vacuum Arc Phenomena

There are many similarities between the electrical properties of laser-surface interaction and those of vacuum arcs. Frequent reference is made in this section to experiments with vacuum arcs and theories which have been established to explain their behavior.[16]

The vacuum arc is an electrical discharge established in vacuum between a cathode and an anode when the material of the cathode is evaporated and ionized to the extent that it provides a high conductivity path between the two electrodes. Apparently, continuous arcs can be established with almost any conductor acting as a cathode. For example, in his paper on the vacuum switch, Reece [17] lists data from 19 cathode materials including mercury, copper, cadmium, steel, and tungsten. Of course, the most common use of the vacuum arc is in the ignitron where mercury is the cathode material.

The voltage at which a vacuum arc is sustained is found to be a characteristic of the cathode material and varies from 8 volts for mercury to 33 volts for cold steel. The electron current required for stable arc formation is also a function of material and varies from 2 amperes for bismuth to over 60 amperes for tungsten.

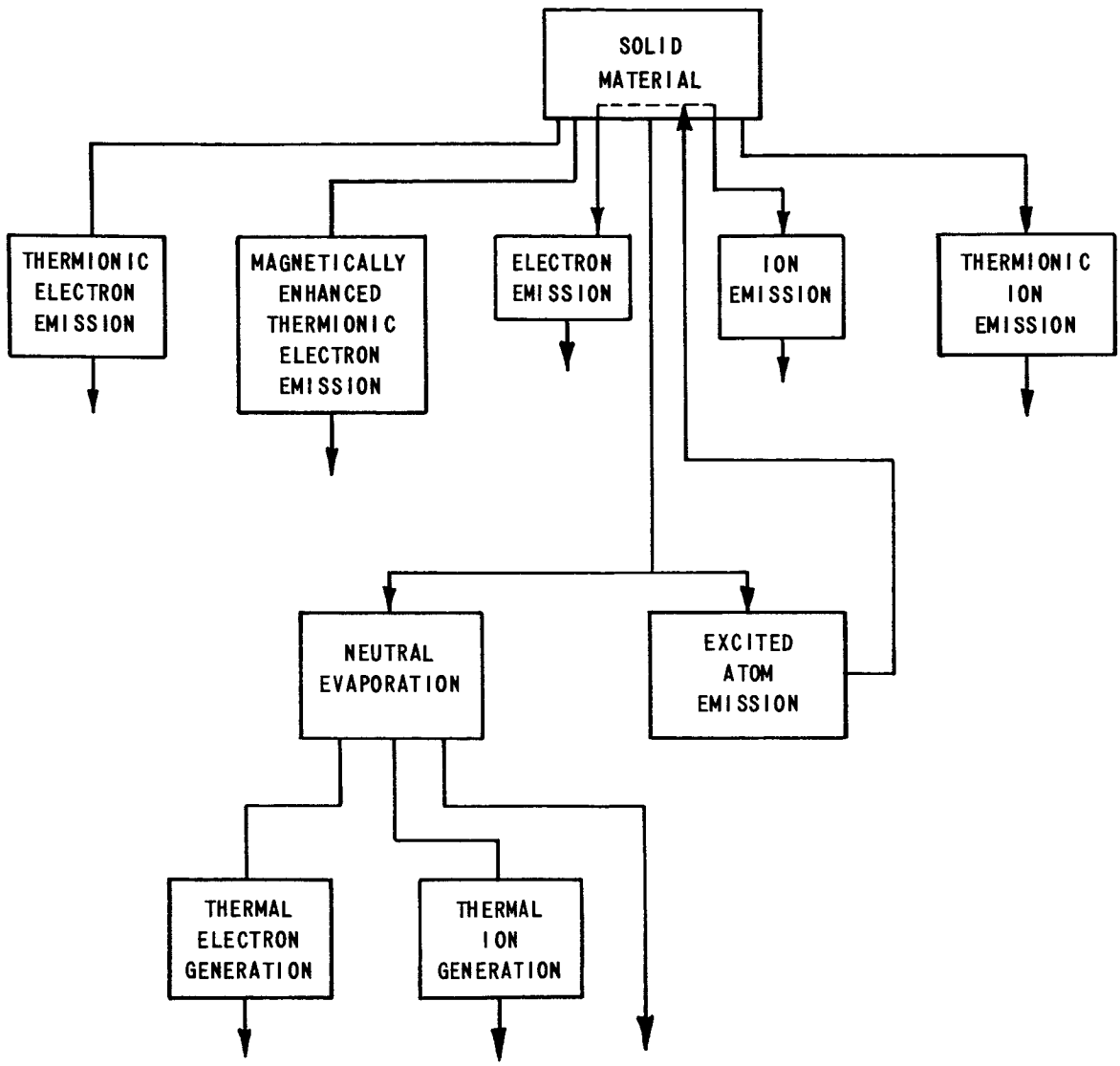

Figure 59 LASER ILLUMINATED-SURFACE EMISSION MECHANISMS

The plasma cloud leaving the cathode in the vacuum arc has been found to have the shape of a conical plume with a semiangle that may vary from material to material and which is typically about 30°. It is thought that the plasma is confined to this plume by magnetic pinching which results from the extremely high emission current density at the cathode. As is the case for the laser surface interaction the plasma plumes are found to have velocities far exceeding thermal emission velocities. The velocities depend, to some extent, on the cathode material with a typical value for copper of 2×10^4 m/sec.This means that the average ion energy is about 130 ev which is several hundred times the thermal energy of the surface.

11.2 Electron Emission Mechanisms:

In materials which have high melting and boiling points and/or low work functions like tungsten, the primary electron emission mechanism for either a vacuum arc or laser surface interaction is probably thermionic emission. The thermionic emission electron current density is computed to be [18]

$$J_{THERM} = \left(\frac{4\pi me}{h^3}\right)(kT)^2 \exp\left(-\frac{e\varphi}{kT}\right) \quad AMPS/m^2 \tag{15}$$

Equation (15) is derived assuming that the only electrons emitted from the material are those that have sufficient momentum normal to the surface to overcome the surface potential barrier.

The value of the electron current density resulting from normal thermionic emission for the various materials at their respective boiling points is shown in Figure 60. Because of the low boiling points of chromium and lead, calculations indicate that no thermionic electron emission should be expected. Both of these materials, however, has reasonable laser generated ion and electron emissions and thus the thermionic mechanism does not account for their performance. Materials such as iron, copper, and aluminum also have extremely low yields of electron emission which might be accounted for by thermionic emission.

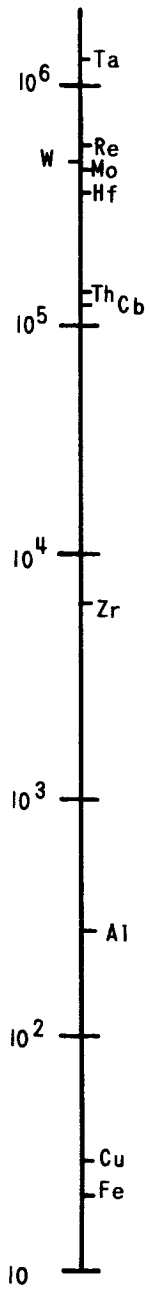

Figure 60 MAGNITUDE OF THERMIONIC EMISSION CURRENT

When a large current is drawn from a small spot in the emitting surface, as is the case with laser surface interaction or the vacuum arc, an extremely large toroidal magnet field ($B > 10,000$ gauss) is established. This magnetic field, which exists inside and outside the metal surface at the cathode spot, combined with the acceleration due to the electric field produced by a slight potential depression resulting from space-charge effects enhances the rate of thermionic emission. (The electrons which return to the emitter from the space-charge well will be accelerated.) The effect of the crossed electric and magnetic fields in the metal will be a redirection of the electron momentum vectors and the enhancement of thermionic emission.[19] This enhanced thermionic emission, if all the electron momentun vectors are redirected normal to the emitter surface will be given by

$$J_{enhanced} = \left(\frac{16\,m\pi e}{h^3}\right)\left[\left(E_o + e\varphi\right) kT + \left(kT\right)^2\right] exp\left(-\frac{e\varphi}{kT}\right) \tag{16}$$

The relative value of enhanced (as a result of magnetic and electric forces) to normal thermionic emission is given by

$$\frac{J_{enhanced}}{J_{thermionic}} = 4\left(\frac{E_o + e\varphi}{kT} + 1\right) \tag{17}$$

Figure 61 gives a plot of Equation (17) as a function of kT for the typical case when $E_o + e\varphi = 10\ ev$. An enhancement of over 100 can be expected for normal values of kT .

In materials with low boiling points, where surface temperatures high enough for appreciable thermionic emission cannot be attained, it is probable that intense electron emission results from the bombardment of the emitting surface by excited atoms. It has been estimated by Oliphant (1929) and Dorrestein (1942) from experiments and Massey (1930) and Cobas and Lamb (1944) from theoretical calculations, that the yield probably lies between 0.1 and 1 electron per incident atom, provided the excitation energy of the atom exceeds the work function of the metal. This is in contrast to the relatively low yields that result from the bombardment of a surface by ions or by photons.

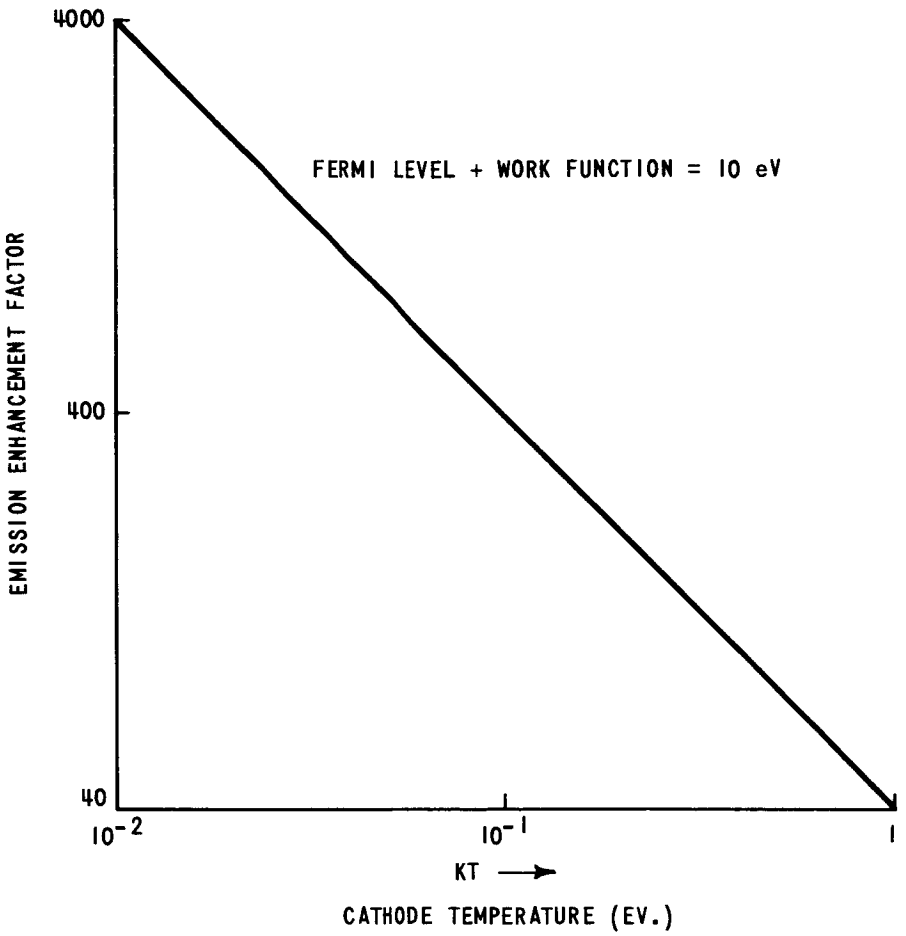

Figure 61 EMISSION ENHANCEMENT RESULTING FROM MAGNETIC FIELD

Vacuum arc experiments were performed at CAL with high-purity copper and gold in an effort to obtain data in support of this excited atom theory. These two metals were chosen because, although most of the electrical and thermal characteristics of these two metals are similar, there is an important difference in the energies of the doublet P levels in the copper and gold atoms. As is shown in Figure 62, in the case of gold, the doublet P levels of the atoms have energies above the work function of the gold, whereas with copper, the doublet P levels of the atoms have energies below the work function of copper. Bombardment of the metallic surface of the copper by excited copper atoms would lead to much less efficient electron emission than would bombardment of the metallic surface of the gold by excited gold atoms. The experiments showed that, whereas the copper arc was stable with a minimum current of 30 amperes and a potential drop of 21 volts, the gold arc was stable with only 8 amperes at 18 volts. The lower power required for sustaining the gold arc is attributed to the more efficient electron emission mechanism. Similar copper and gold experiments could not be performed with laser illumination because of the high reflectivities of these metals. This excited-atom theory is probably also of importance in laser-surface interactions which has many similarities with the vacuum arc. It is probable that excited atoms which can contribute to electron emission are produced primarily by collision processes with occasional photon absorptions in the high-density vapor from the cathode surface.

11.3 Ion Emission Mechanisms

When the low melting point, low boiling point, low thermal conductivity materials are illuminated with focused laser energy, the percentage ionization of the vapor plumes generated is relatively small. In these cases the ionization can probably be accounted for by thermal processes.

In the case of high-melting point, high-boiling point materials which have reasonable thermal conductivities, however, the explanation is not as simple since over 99 percent ionization has been observed. It is highly unlikely that a thermal process can account for this high ionization percentage.

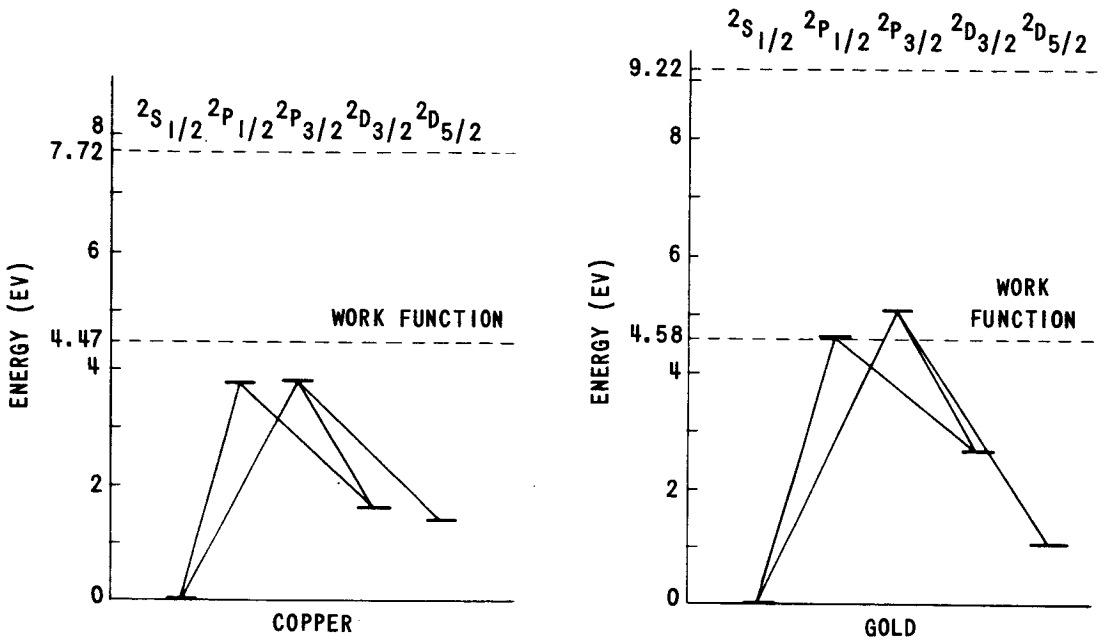

Figure 62 ENERGY LEVELS IN COPPER AND GOLD

The temperature of the gas is not thought to have been high enough to produce more than a few percent ionization and if the temperature was high enough to produce complete ionization, a high percentage of multiply charged ions should have been observed. No significant amount of multiply charged ions were observed except in tests on rhenium and tantalum where a significant number of doubly charged ions were measured. The materials included in this high-ionization-percentage group are columbium, molybdenum, tantalum, thorium, and tungsten. Materials such as hafnium and zirconium are eliminated because of their low thermal conductivities and chromium because of its low boiling point which lead to a high level of neutral emission.

Thermionic ion emission [20, 21, 22] has been experimentally investigated for several materials. The literature shows large discrepancies in the data which have been obtained, and the ion emission levels are quite low. In addition the thermionic ion emission mechanism assumes evaporation of neutral material with a small percentage of the evaporated particles being ionized. This does not fit with the experimental results found on the highly ionized materials.

A mechanism being investigated at CAL which might account for the intense ionization is one in which the thermionic emission rate of positive ions from the laser-heated metal is enhanced when atoms near the metallic surface are excited by electrons or photons. This phenomenon would be similar to that of contact ionization of a low-ionization-potential material, such as cesium on a hot high-work-function material.

11.4 Energy Required for Laser-Generated-Emission

Regardless of the ionization mechanism associated with laser generated emission, the material must acquire sufficient energy to raise the surface temperature and to vaporize material. Consider the energy required for each atom to be raised to the boiling point, vaporized and then ionized.

$$E_H = m C_{p1} \left|\Delta t_1\right| + H_F + m C_{p2} \left|\Delta t_2\right| + H_V + V_1 \qquad (18)$$

The total source energy required includes both the incident and reflected energy. Thus

$$E_T = \frac{E_H}{(1-R)} \tag{19}$$

This value for most of the materials is shown in Figure 63. Neither thorium nor lead is plotted due to the lack of information on the first ionization potential of thorium and the spectral reflectance of lead. However, from the known quantities, both of these materials will have a reasonably low value of $\left(\frac{E_H}{1-R}\right)$.

It would be expected that the lower the energy required for heating and ionizing the material the more rapidly it will be ionized. However, several materials which satisfy this criteria give poor ion generation results. Hafnium is one example which requires a relatively low level of energy for heating and ionization yet gives a poor performance as an ion generator. The thermal conductivity of hafnium is very low and apparently energy is dissipated by molten material being splattered from the target.

11.5 Acceleration Process

Along with postulating that the primary ionization mechanism is a thermal one occurring at a temperature near the boiling point of a metal, it is necessary to postulate that ions can be accelerated from thermal energies less than 1 ev to very high energies (15 ev or higher). It is thought, at present, that energy is transferred from the thermionically emitted electrons to the ions. The following consideration of the conversion of energy shows that this could be the case.

It is assumed that electrons and ions are emitted from a one dimensional hot metallic surface(Figure 64) with average velocities corresponding to the surface temperature. (Actually it is expected that ions do not leave the surface but instead are formed immediately in front of it. The ions and electrons have velocity distributions which may or may not be Maxwellian; but only average velocities will be used in the following

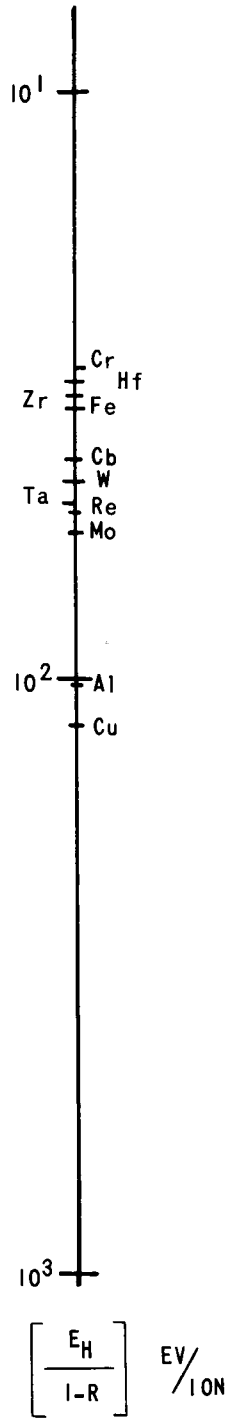

Figure 63 ENERGY REQUIREMENTS TO VAPORIZE VARIOUS MATERIALS

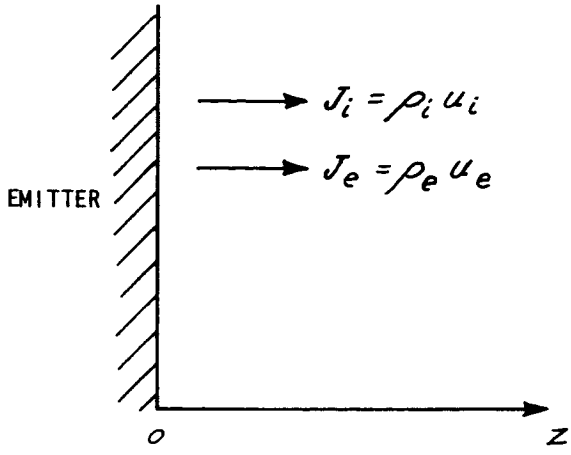

Figure 64 ONE-DIMENSIONAL MODEL ASSUMED FOR CONSERVATION OF ENERGY CONSIDERATIONS

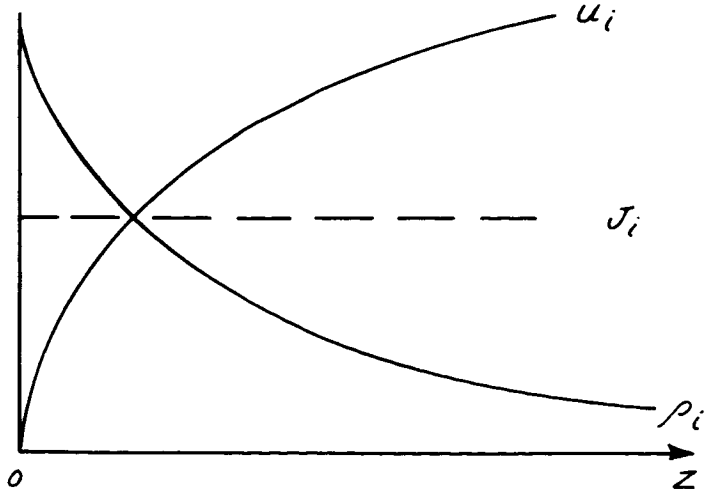

Figure 65 VARIATIONS IN ρ_i , u_i , AND J_i WITH DISTANCE ASSUMING ACCELERATION OF THE IONS BY THE ELECTRONS

computations). The ion current density, J_i, is the product of the ion charge density and the velocity of the ions. Before making any statements concerning the total electron current density moving away from the surface, it is necessary to consider qualitatively how the various quantities, J_i, ρ_i, u_i, etc., vary with distance. If, in some manner not specified at this point, the electrons accelerate the ions, then the quantities ρ_i, u_i, and $\mathcal{J}_i$ will vary as is shown in Figure 65. That is, the velocity u_i, will increase and, because $\mathcal{J}_i$ remains constant (no recombination or wall losses of any kind are considered), then ρ_i will decrease as shown.

Because the plasma formed by ρ_i and the electrons emitted or freed from the ions must remain essentially neutral, then ρ_e very nearly equals ρ_i. This means, of course, that ρ_e decreases with distance as is shown in Figure 66. Because it has been assumed that the electrons give up energy to the ions as they move away from the emitter, it is necessary that the velocity of the emitted electrons decrease with distance. This leads directly to the conclusion that the current carried by the emitted electrons (designated $J_{e_{forward}}$ in Figure 67) must decrease with distance.

Since electron current is conserved (still assuming no recombination or wall losses) we must conclude that a large portion of the electron current is returned to the emitter as is shown in Figure 67. The difference between J_{e_f} and $J_{e_{reverse}}$ (J_{e_r}) depends on how much electron current is drawn by a collector placed at some position along Z. If no collector is present and the plasma is allowed to drift to infinity, or to an insulated collector, then, because no net current flows, the electron current must equal the ion current and the difference between J_{e_f} and J_{e_r} is J_i.

Next, consider analytically the transfer of energy from the electrons to the ions. As shown in Figure 68 there are nine quantities that must be considered. These are the forward and reverse electron currents, J_{e_f} and J_{e_r}, the forward and reverse electron charge densities, ρ_{e_f} and ρ_{e_r}, and the velocities at which they are moving, u_{e_f} and u_{e_r}, and the forward ion current J_i, with its associated charge density ρ_i and velocity u_i. The relations among these quantities are as follows:

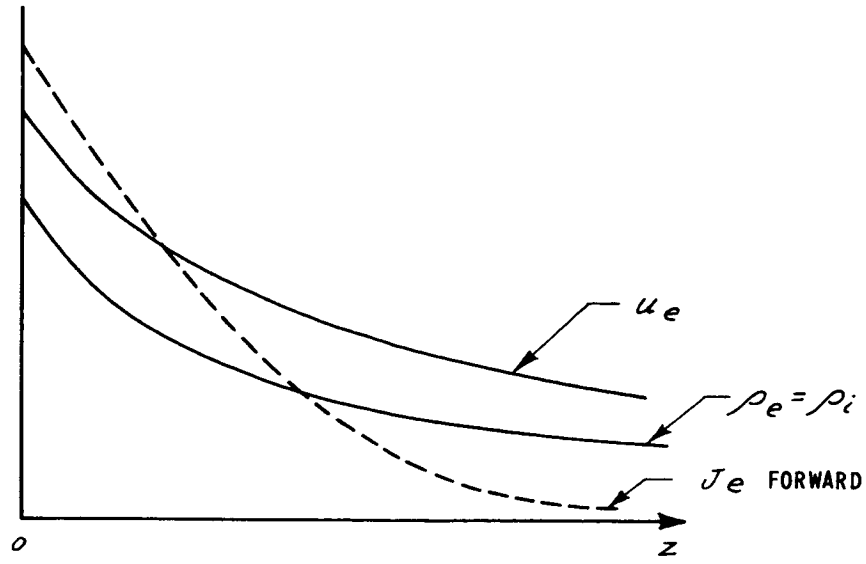

Figure 66 VARIATIONS IN ρ_e, u_e AND J_e FORWARD WITH DISTANCE ASSUMING ACCELERATION q OF THE IONS BY THE ELECTRONS.

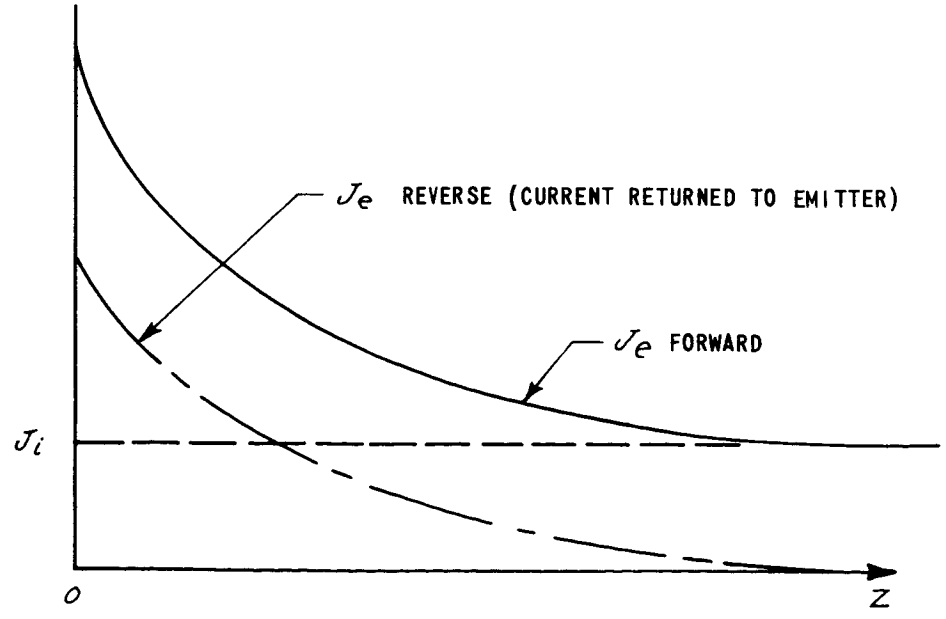

Figure 67 COMPARISON OF FORWARD AND REVERSE ELECTRON CURRENT WITH ION CURRENT AS A FUNCTION OF DISTANCE

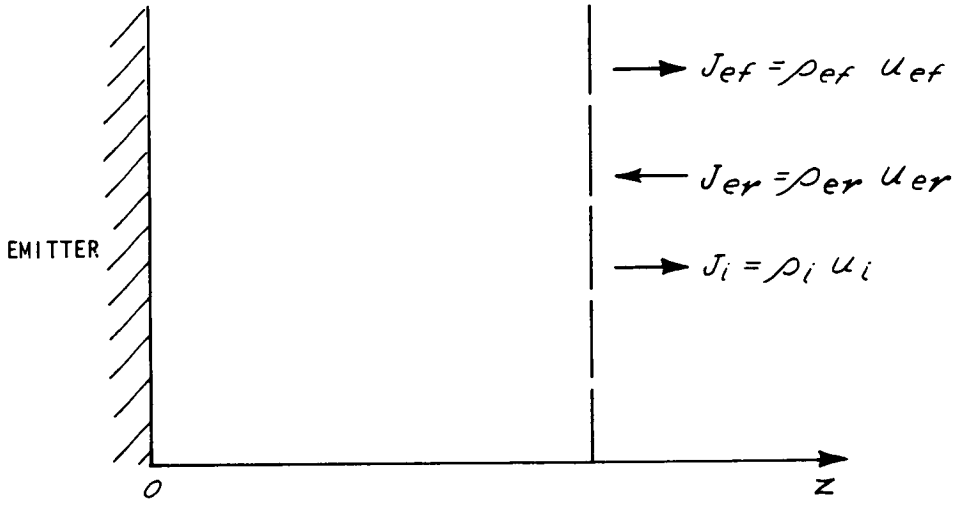

Figure 68 QUANTITIES THAT MUST BE CONSIDERED IN COMPUTING TRANSFER OF ENERGY FROM ELECTRONS TO IONS

From the requirement for charge neutrality in the plasma, it must be true that the total electron charge density equals the ion charge density:

$$\rho_{ef} + \rho_{er} = \rho_i \tag{20}$$

When it is assumed that no recombination occurs and that no current is intercepted by walls or collectors, then current is conserved and it is required that

$$J_{ef} - J_{er} = J_i = \text{constant} \tag{21}$$

Finally, assuming that the plasma is near the potential of the emitter, all of the energy appears as kinetic energy of the electrons and ions, and we can write

$$\omega = J_{ef}\left(\frac{1}{2}\ \frac{m_e}{e}\ u_{ef}^2\right) - J_{er}\left(\frac{1}{2}\ \frac{m_e}{e}\ u_{er}^2\right) + J_i\left(\frac{1}{2}\ \frac{m_i}{e}\ u_i^2\right) \tag{22}$$

where ω is the total power density in the stream at any plane Z

As $Z \to \infty$, $J_{er} \to 0$ and we get:

$$\omega = J_i\left(\frac{1}{2}\ \frac{m_i}{e}\ u_{i\infty}^2\right) + J_{ef\infty}\left(\frac{1}{2}\ \frac{m_e}{e}\ u_{ef\infty}^2\right)$$

$$= J_i\left(\frac{1}{2}\ \frac{m_i}{e}\ u_{i\infty}^2\right) + J_i\left(\frac{1}{2}\ \frac{m_e}{e}\ u_{i\infty}^2\right)$$

where the subscript ∞ indicates the limit of a function as $Z \longrightarrow \infty$.

Because $m_e << m_i$,

$$\omega = J_i\left(\frac{1}{2}\ \frac{m_i}{e}\ u_{i\infty}^2\right) \tag{23}$$

By combining equations (22) and (23), we see that

$$m_e\left(J_{ef}\ u_{ef}^2 - J_{er}\ u_{er}^2\right) + J_i\ m_i\left(u_i^2 - u_{i\infty}^2\right) = 0$$

or

$$J_{ef}\, V_{ef} - J_{er}\, V_{er} + J_i \left(V_i - V_{i\infty} \right) = 0 \tag{24}$$

where the V's are the voltage equivalents of the velocities:

$$u_{ef} = \sqrt{\frac{2e\, V_{ef}}{m_e}} \tag{25}$$

By using the conservation of current condition to eliminate J_{e_r}, equation (24) can be written as

$$\frac{J_{ef}}{J_i} \quad \frac{V_{ef}}{V_i} - \frac{J_{ef}}{J_i} \quad \frac{V_{er}}{V_i} + \frac{V_{er}}{V_i} \quad + 1 - \frac{V_{i\infty}}{V_i} \quad = 0 \tag{26}$$

By combining equations (20) and (21), the following expression for V_{e_r} is obtained:

$$\frac{V_{er}}{V_i} = \frac{m_e}{m_i} \left[\frac{\frac{J_{ef}}{J_i} - 1}{1 - \frac{J_{ef}\, u_i}{J_i\, u_{ef}}} \right]^2 \tag{27}$$

It should be pointed out here that, because $\frac{m_e}{m_i}$ is an extremely small quantity, V_{e_r} / V_i is much less than unity (even when all the possible magnitudes of the ratio in the square brackets of equation (27) are considered). Thus, the energies of the electrons traveling in the reverse direction are very small compared to the ion energies.

By using equation (27) to eliminate V_{e_r} from equation (26) we obtain

$$\frac{J_{ef}}{J_i}\;\frac{V_{ef}}{V_i} - \frac{m_e}{m_i}\;\frac{\left(\frac{J_{ef}}{J_i} - 1\right)^3}{\left(1 - \frac{J_{ef}}{J_i}\,\frac{u_i}{u_{ef}}\right)^2} + 1 - \frac{V_{i\infty}}{V_i} = 0 \qquad (28)$$

Although this equation is true for any position in the Z direction, it yields little information for positions other than Z=0 because the variations of the quantities with Z are unknown. These will have to be determined from a study of the acceleration mechanisms that exist in the plasma. At Z=0 and for $J_{ef}/J_i >> 1$, equation (28) reduces to

$$\frac{J_{ef}}{J_i} - \frac{m_e}{m_i}\;\frac{\left(\frac{J_{ef}}{J_i}\right)^3}{\left(1 - \frac{J_{ef}}{J_i}\sqrt{\frac{m_e}{M_i}}\right)^2} + 1 - \frac{V_{i\infty}}{V_i} = 0 \qquad (29)$$

because

$$\left.\frac{V_{ef}}{V_i}\right|_{z=0} = 1 \qquad \text{and} \qquad \left.\frac{u_i}{u_{ef}}\right|_{z=0} = \frac{m_e}{m_i}$$

The term multiplied by m_e/m_i is small compared to J_{ef}/J_i and, in fact, J_{ef}/J_i has been assumed to be large compared to unity so equation (29) reduces to

$$\frac{J_{ef}}{J_i} = \frac{V_{i\infty}}{V_i} \qquad \text{at } z = 0 \qquad (30)$$

This expression, although extremely simple, yields valuable information. If, for example, the ratio of electron to ion emission currents is about 100, i.e., $J_{ef}/J_i = 100$, (the case for tungsten if thermionic emission is the only significant source of electrons) then $V_{i\infty}/V_i$ is 100. Since V_i at Z=0 for tungsten is about .5 volts, then $V_{i\infty}$ should be about 50 volts. The results shown in Section 10.1 indicate that the average value of V_i is 35 to 40 volts.

The next question to be answered is that of exactly what energy exchange mechanism or mechanisms are contributing to the high velocities obtained by the ions. At the present time we are not prepared to identify all of the mechanisms that may exist but expect that ambipolar diffusion** plays a very important role.

** The electrons have higher velocities than the ions and tend to move ahead of the ions. The electric field set up by the resulting charge separation accelerates the ions and decelerates the electrons.

12.0 LASER-ION-GENERATOR ELECTRIC PROPULSION CHARACTERISTICS

The emission of electrons and ions as a result of laser illumination of a metal target must possess several characteristics to be useful in an ion-thrustor application. The velocity of ion emission should be reasonably high, neutral emission should be a minimum, the energy required to form each ion should be as low as possible and the emitted ions should be capable of being accelerated by external electrodes.

As discussed in Section 10.1, the average ion energy lies between 10 and 40 ev. This corresponds to ion velocities in the order of 3 to 6 kilometers per second and specific impulses of 300 to 600 seconds. During this program no experiments were performed on accelerating the ions after emission, however, there is no theoretical reason why external accelerating voltages can not be applied to raise the specific impulse to a value of several thousand seconds.

12.1 Energy Required per Ionization

The energy required to form each laser-generated ion has been found to be a function of laser power density, emitter material and length of the laser pulse. Another variable which did not change the energy required per ionization but radically affected the measured ionization was the shape of the collector. In the CAL experiments all of the collector systems contained apertures to permit the laser beam to strike the target and, as a result, some ionized particles were lost from the measuring circuit.

In the CAL sponsored internal research program, LASIG I, the emitter-collector assembly was a moderately open circuit, placed reasonably far back from the vacuum window. The vacuum window must have had a thin plating across its entire surface after a period of operation since the

measured emitter current was 40 percent larger than the measured collector current. The current not intercepted by the collector returned to the emitter through the window plating and the grounded outer wall of the vacuum chamber. This plating was never noticed because it was uniform across the entire window surface. Subsequent platings have always been visible because of the contrast between the edge of the plating and the clear portions of the glass.

In the program LASIG II, being discussed, the collector assemblies were all designed to have apertures no larger than required for the admittance of the laser beam. This was done to try and collect as great a percentage of emitted charge as possible. However, ions were still lost from the measuring circuit and only a relative rather than absolute values of energy required per ionized particle can be calculated.

Another means of checking the level of laser-generated-ion emission is the measurement of total weight loss of the emitter. Due to the large number of different tests made during the program, the maximum number of laser shots on any one target was about 200. The average weight loss per shot was 20 micrograms so that the total maximum weight loss was 4 milligrams. The uncertainty in weight loss due to measurement accuracy, weight loss due to tweezer handling of the materials, and weight loss in removing from the various emitter fixtures was estimated to be $\pm$ 0.05 milligrams or $\pm$ 1.2 %. Thus each shot had a minimum uncertainty of $\pm$ 0.25 micrograms, or an average ion charge uncertainty for the materials tested of $\pm$ 130 microcoulombs. In the testing of many materials, where at least 100 to 200 laser shots were taken under one set of conditions, the weight loss was only 20 percent higher than the weight loss accounted for by the emitter charge measurements. Thus, there was fairly good correlations between the two measurements.

12.2 Thrust per Unit Area

Using the data obtained during the hemispherical collector tests, the thrust generated by the ions can be calculated from $T = \dot{m} u$. This information and the estimate of laser spot size given in Section 6 can then be used to obtain the thrust per unit area of the various materials. Table IV gives a summary of this data.

Table IV
CALCULATED ION THRUST

MATERIAL	AVERAGE THRUST	THRUST PER UNIT AREA	AVERAGE INCIDENT LASER POWER	EMISSION PULSE LENGTH	ENERGY INCIDENT PER ION GENERATED	INCIDENT POWER PER AVERAGE THRUST	NEUTRALS PRESENT	DOUBLY IONIZED IONS
	LBS	LBS/CM^2	KW	μSEC	ev/ION	WATTS/MLB		%
RUBY NO. 1								
RHENIUM	5.6×10^{-6}	5.2×10^{-3}	2.3	450	1.6×10^{6}	4.2×10^{5}	NONE	20
TANTALUM	1.1×10^{-3}	1.0	2.3	500	8.1×10^{3}	2.1×10^{3}	NONE	20
THORIUM	1.5×10^{-3}	1.4	2.7	400	8.3×10^{3}	1.8×10^{3}	NONE	NONE
TUNGSTEN	$5.3 \times .0^{-4}$	0.5	4.7	300	4.9×10^{4}	9.0×10^{3}	NONE	NONE
RUBY NO. 2								
RHENIUM	1.1×10^{-4}	0.41	2.6	450	5.4×10^{4}	2.4×10^{4}	NONE	3
TUNGSTEN	6.9×10^{-4}	2.6	4.7	500	1.4×10^{4}	6.7×10^{3}	YES	NONE

The calculated ion thrust based on emitted ion current and velocity was significantly smaller than that measured as shown in Figure 58. There are several possible explanations: 1) there is a large percentage of high velocity neutrals, 2) a large percentage of high velocity ions are being lost from the measuring circuit, and 3) the average velocity estimate is low by an order of magnitude.

Ions directed normal to the emitter face, as evidenced from the plating obtained in both LASIG I and II (this program), as well as values obtained in a parallel program* presently being conducted at CAL, do in fact constitute a large percentage of the ionized particles generated by laser illumination. Thus the second possibility (that many high velocity ions were lost from the measuring circuit) appears to be the most logical explanation to the low measured ion yield. In some of the original CAL sponsored laser ion generation experiments, the face of the target was at an angle to the laser beam and material preferentially plated a small area just in front of the emitter face. These particles would be lost to the measuring circuit in all the experiments performed during the contract. In addition, this unrecorded emission probably contained the highest energy ions (based on the ion energy distribution obtained on the hemispherical collector experiments).

The third possibility, that the measured ion velocity estimate was too low by an order of magnitude, does not appear reasonable. The average ion velocity estimate was accurate to within $\pm$ 10% and this cannot provide the additional required thrust. The results of the experiments performed during this contract cannot resolve this discrepancy. Additional experiments are required before a firm explanation can be given.

Tantalum gives the best correlation between measured and calculated thrust. Reference to Figure 43 shows this material has, what appears to be, a far less axially directed emission plume than either rhenium or thorium. This material may lose relatively less current through the incident laser beam aperture.

---

* Project DEFT, CAL Internal Research Project, Final Report No. UD-2037-E-1.

The laser energy required per ionization as measured during the hemispherical collector tests, was quite high. On the average, several thousand electron volts were required per ion generated. During the geometry experiments however, the value went as low as 460 electron volts per ion. The effect of the ionization energy on the maximum attainable efficiency is shown on Figure 69. For a useful engine the ionization energy will have to be minimized.

12.3 Propellant Weight Loss

In any propulsion system an extremely important parameter is the propellant weight requirement. In this report the charge collected as a function of incident laser energy has been found. This collected charge can be transformed into weight loss per unit incident laser energy, Figure 70 shows this information. As discussed in Section 12.2, this weight loss should be increased to account for the unmeasured charge generated. This weight loss (in order to acquire greater accuracy) should be checked for at least 200 shots under each specific condition of operation, i.e., at each power density level and each focal point position. When the weight loss was checked for several materials after a large number of shots, the correlation between the weight loss and the collected charge was within 20%.

The generated thrust as a function of weight loss is shown on Figure 71. These data are again calculated from the collected charge measured on the various materials. The data obtained from the emitter material experiment and the hemispherical collector experiment are within 10% of each other.

All the data plotted are for ruby #1 since ruby #2 never provided a good weight to charge correlation. The high power density present due to the selective moding of the laser, while providing higher ion yields and thrust, is also wasteful of material.

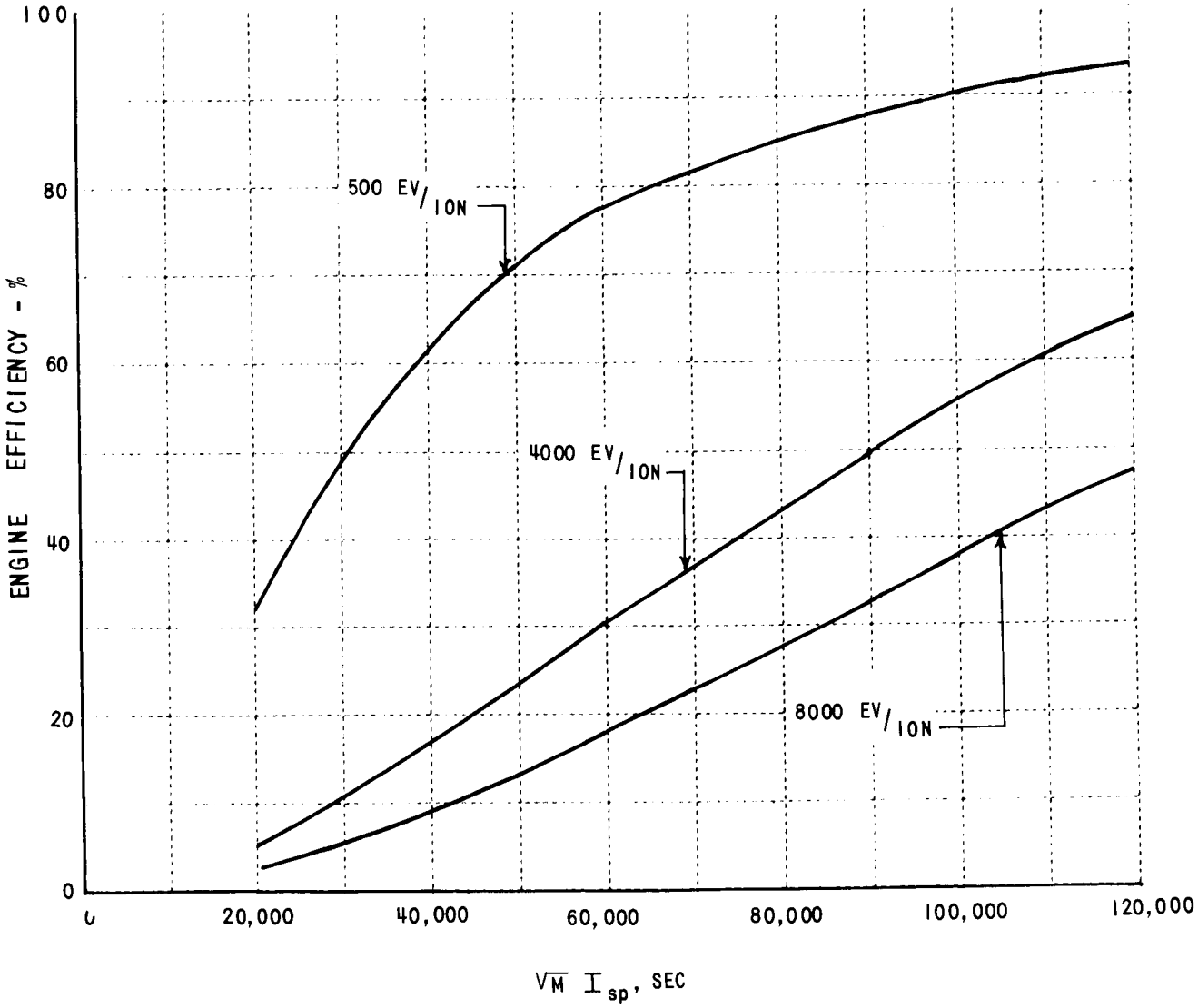

Figure 69 MAXIMUM ATTAINABLE EFFICIENCY AS A FUNCTION OF MASS, SPECIFIC IMPULSE AND IONIZATION ENGERGY

RHENIUM M = 186.31
TANTALUM M = 180.95
THORIUM M = 232.05
TUNGSTEN M = 183.92

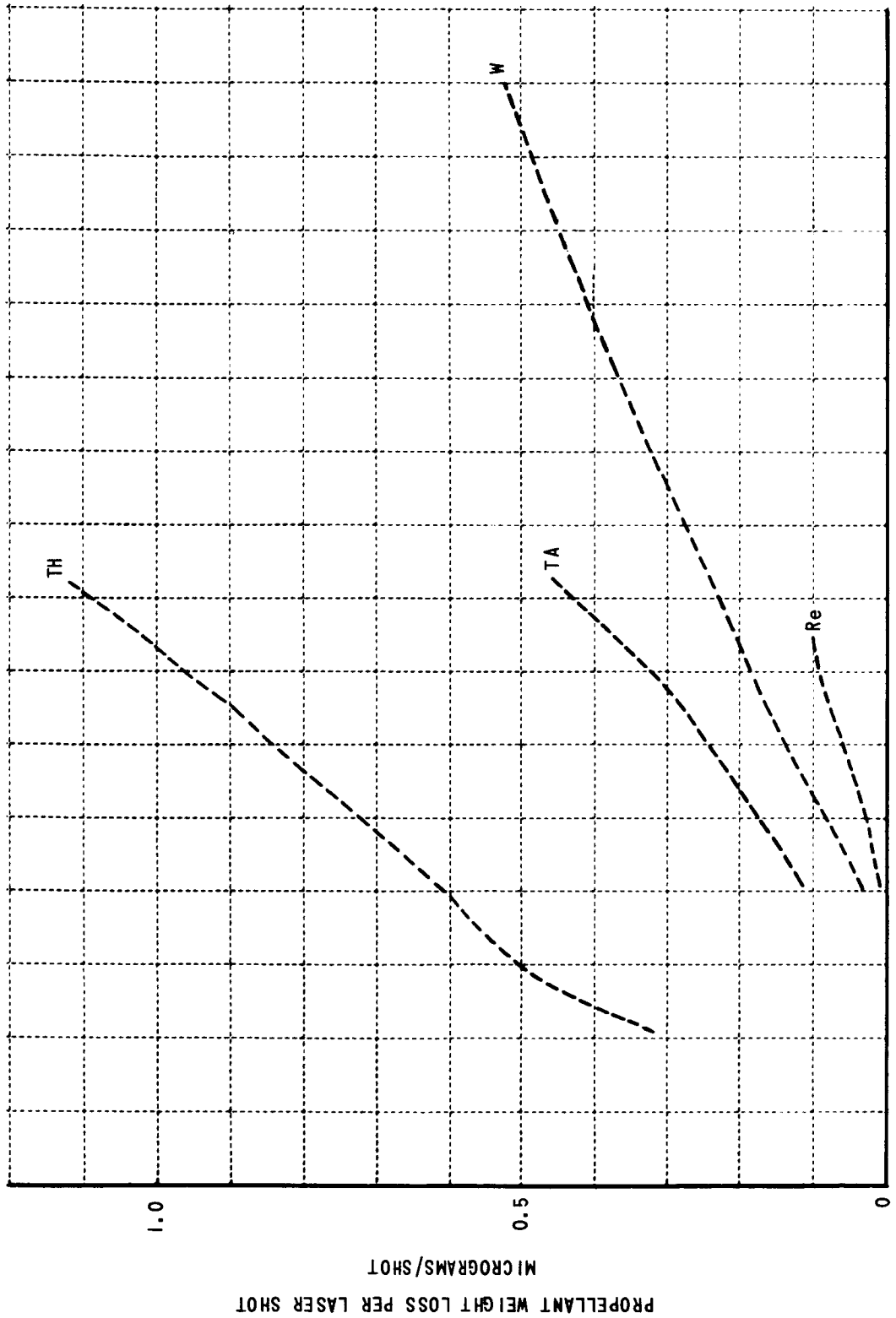

Figure 70 PROPELLANT WEIGHT LOSS AS A FUNCTION OF INCIDENT LASER ENERGY RUBY #1

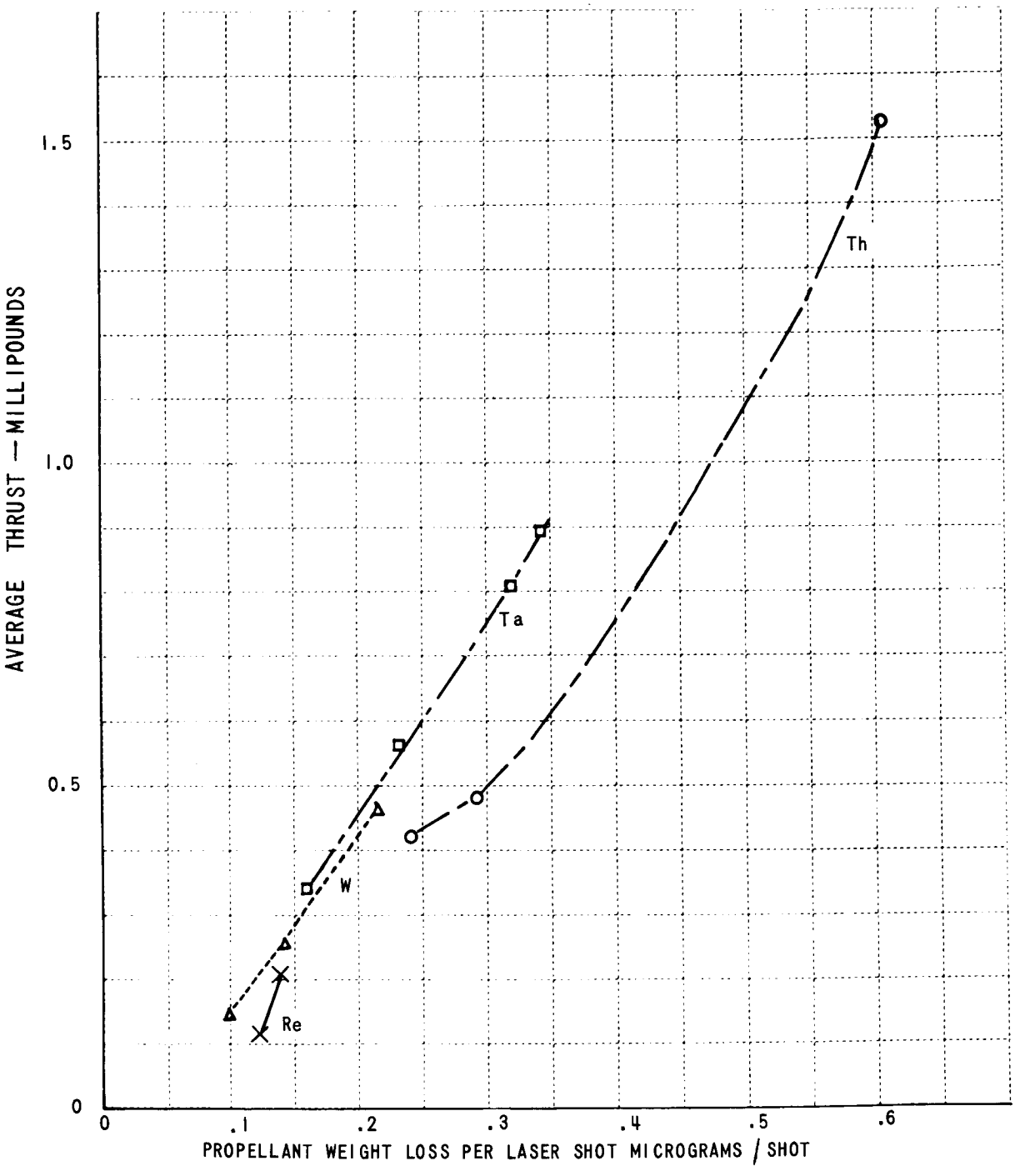

Figure 71 AVERAGE THRUST AS A FUNCTION OF PROPELLANT WEIGHT LOSS
RUBY #1 LASER PULSE DURATION 705μ SEC

12.4 Application of Laser-Ion-Generation As An Electric Thrustor

Two possible applications for a Laser Excited Thrustor are shown in Table V.

TABLE V

Attitude Stabilization of a 1500 Lb. Synchronous Satellite

Design Assumptions

Design max. disturbing torque	10^{-4} ft-lbs. (any axis)
Average disturbing torque (3 year average)	5×10^{-5} ft-lbs. (per axis)
Moment arm	20 ft. for laser thrustor* 5 ft. for ion engine
Max. tolerable error angle	0.5 degrees = 8.7×10^{-3} radians

Operating Conditions, Laser Excited Thrustor

Max. thrust	2.5×10^{-6} lbs. continuous
Average thrust (3 year average)	1.25×10^{-6} lbs.
Pulse repetition rate (0.60 micro-lb-sec. impulse bits)	1 pulse/.24 sec. max. 1 pulse/.48 sec. average
Error angle accumulated between firings	4×10^{-6} radians
Average power from batteries or solar cells (assume 50% efficiency diode laser)	4.5 watts/thrustor 54 watts total (12 thrustors)
Propellant consumption	.24 lbs/3 year/thrustor = 2.9 lbs/3 years total (12 thrustors)

* Because of the simplicity and low mass of the laser emitter and because no tubing or electrical connections are needed to the thrustor itself, a 20 ft. torque arm is considered to be reasonable; published reports suggest a 5 ft. torque arm for the heavier more complicated ion engine.

TABLE V (continued)

Operating Conditions, Ion Engine	
Operating thrust	0.5 mlb. for 5% duty cycle
Pulse rep. rate	1 actuation/424 secs.
Error angle accumulated between firings (404 seconds)	$0.5° = 8.7 \times 10^{-3}$ radians
Average joules/cycle/axis	10,413
Average power/axis	24 watts
Power from batteries or solar cells	103 watts average
Propellant and tankage weight	2.5 lbs/3 years
Station Keeping of a 1500 Lb. Synchronous Satellite	
Total impulse required	26,500 lb-sec. (3 years)
Operating Conditions Laser Excited Thrustor	
Avg. force	$.280 \times 10^{-3}$ lbs.
Avg. force/thrustor (assuming 12 thrustor array)	$.07 \times 10^{-3}$ lbs.
Pulsing frequency	116 p.p.s.
Average power	250 watts/thrustor
Total power from satellite supply (4 thrustors active)	1000 watts
Propellant consumption (I_{sp} = 615 sec.)	54.4 lbs. total
Operating Conditions, Ion Engine	
Specific Impulse	4500 sec.
Specific power	200 lbs/mlb.
Duty cycle	20%
Thrust interval	approx. 12 minutes each hour
Operating power	375 watts
Avg. power from satellite supply	140 watts
Propellant consumption	5.9 lbs.

The thrust and propellant values used in calculating the above parameters are those shown in Table IV, Section 12.2 for thorium using ruby #1. The thrust values calculated on this table using collected charge and velocity measurements are an order of magnitude lower than the measured thrust values, Section 10.1, Figure 58. Thus the power requirements using a Laser Excited Thrustor may be significantly lower than those noted on Table V.

13.0 CONCLUSIONS AND RECOMMENDATIONS

Laser-surface illumination is capable of providing a source of high velocity, axially directed and magnetically focusable ions. The thrust levels attained (about ten millipounds) make it comparable in thrust level to many electric propulsion systems now under development. The measured specific impulse was as high as 660 seconds. While no attempt was made to increase this value through the use of external fields, it is expected that a specific impulse value in the thousands can be achieved through the use of conventional accelerating-field configurations.

There are several features of this laser-surface interaction which are still unexplained. While operating parameters of laser induced emission were measured under various experimental conditions, the fundamental phenomena remain unresolved. These are the mechanisms by which ions are accelerated, the extremely high level of ionization of the emitted particles and the presence or absence of neutral or recombined particles.

The main difficulty in this laser-ion generation is the low efficiency of existing high power, low divergence, high coherence lasers. The type of optical pumping system used on the contract, i.e., a flash lamp, which emits a wide frequency spectrum of light, is inherently a low efficiency system. The solid state laser, ruby in these experiments, can only use discrete energy levels to excite electrons into higher order states. Thus, a large percentage of the flash lamp energy is wasted and in fact decreases the system efficiency by heating the ruby rod. By tailoring the frequency output of the flash lamp and shielding the ruby from unwanted radiation system efficiencies of 5% have been attained.

There is another method of pumping[23] the solid state lasers which is inherently more efficient. This entails the use of small diode semiconductor or injection lasers to pump the solid state laser. Injection lasers emit coherent light when biased with a dc voltage. Efficiencies up to about 50% have been attained. At the present time most injection lasers

operate at extremely low temperatures (77°K). It is expected however that cw[24] operation of uncooled diode lasers will be achieved in the near future. With a hybrid (injection and solid state) laser assembly[23] it is expected that system efficiencies of about 40% should be realized.

The current and power requirements of injection lasers can be provided with solar cells. The operating voltage and current for each laser will be in the range of 1.5 to 2.5 volts and 10 to 40 amperes. Several injection lasers will be needed to pump the solid state high power laser.

Another type of low power, high efficiency laser (a tunnel laser)[25] is presently being studied at Cornell University. The projected efficiencies for tunnel lasers are over 80%. Again, dc power will be converted into coherent light output.

The other difficulty in the use of laser generated ions in a thrustor application is the optical system requirements. A focusing scheme is required which will permit the laser to be located behind the emitter. One possible scheme is that shown in Figure 72.

There are many problems associated with the application of laser generated ions to an electric thrustor. However, the projected power and fuel requirements are comparable to values required by present ion engines. If high-efficiency, high-power, low-divergence, high-coherence lasers become a reality, the ion-generation method described in this report might become an attractive means of attaining an electric thrustor utilizing high mass charged particles.

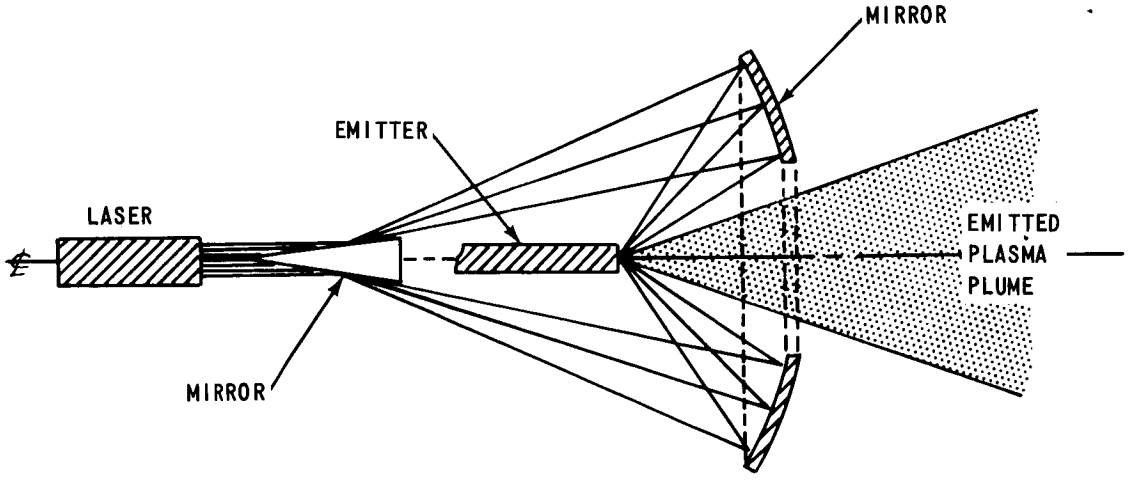

Figure 72 TYPICAL EMITTER—OPTICS CONFIGURATION SUITABLE FOR THRUSTOR APPLICATIONS

APPENDIX A

Thrust

When particles are being emitted from a target or an engine with cylindrical symmetry, the only useful force is axial.

The emitted positive charge distribution shown in Figure 11 for Ruby No. 1 without a magnetic field is essentially cosinusoidal. The useful portion of a cosinusoidal charge distribution (Figure A-1) can be estimated by determining the component in the axial direction.

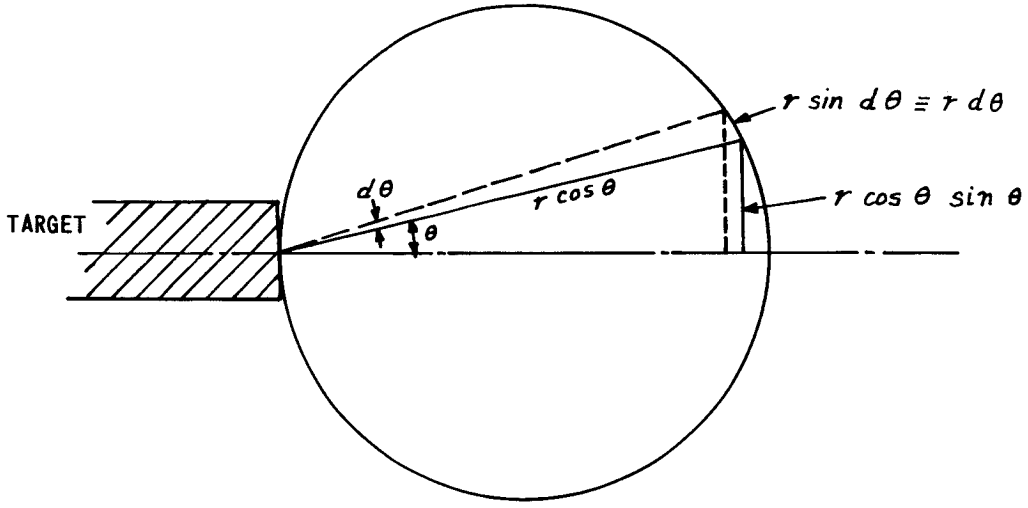

Figure A-1 COSINUSOIDAL VARIATION IN ION DENSITY

The total charge or ionized mass emanating from the sphere can be calculated from geometric considerations.

$$\dot{m} = \int_0^{\pi/2} v \rho_0 \left(2\pi r \cos\theta \sin\theta\right)\left(r \sin d\theta\right)$$

For small increments of d θ

$$\dot{m} = 2\pi \rho_0 r^2 v \int_0^{\pi/2} \cos\theta \sin\theta \, d\theta$$

or

$$\dot{m} = \pi \rho_0 r^2 v \qquad [A-1]$$

The axially directed charge or ionized mass emanating from the sphere can be expressed as

$$\dot{m}_{ax} = \int_0^{\pi/2} v(\rho_0 \cos\theta)(2\pi r \cos\theta \sin\theta)(r \sin d\theta)$$

For small increments of $d\theta$

$$\dot{m}_{ax} = 2\pi \rho_0 r^2 v \int_0^{\pi/2} \cos^2\theta \sin\theta \, d\theta$$

or

$$\dot{m}_{ax} = \frac{2}{3} \pi \rho_0 r^2 v$$

Thus, the total thrust is only two thirds the thrust that would be produced if all emitted particles were axially directed.

Using an axial magnetic field, however, minimizes the radial component of the emitted particles. The useful portion of the emitted ionized material can be increased from 67 to over 85 or 90 per cent.

APPENDIX B

Electromagnet

An electromagnet was constructed with physical dimensions to fit around the vacuum port where the density distribution and energy measurements were being made with the eight-aperture hemisphere. The coil was wound of Formalac coated No. 10 gauge copper wire. The magnet had 759 turns and was 4-1/8 inches long.

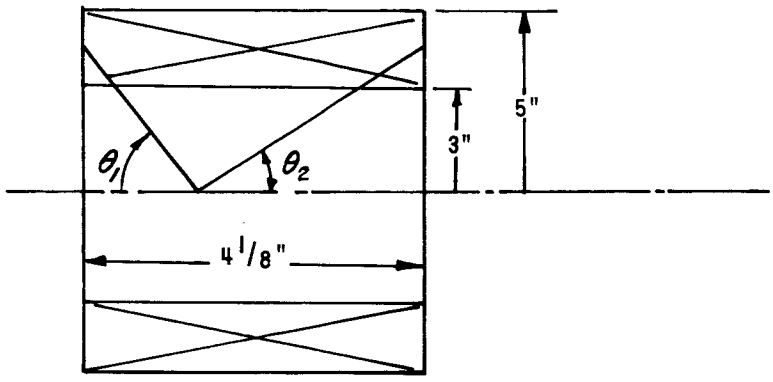

Figure B- 1

The axial field of the electromagnet can be calculated using

$$B = \frac{2\pi NI}{10} (\cos\theta_1 + \cos\theta_2) \quad \text{gauss}$$

where

NI - ampere-turns per cm.

The measured values shown in Figure B-2 are within 5 percent of the calculated values.

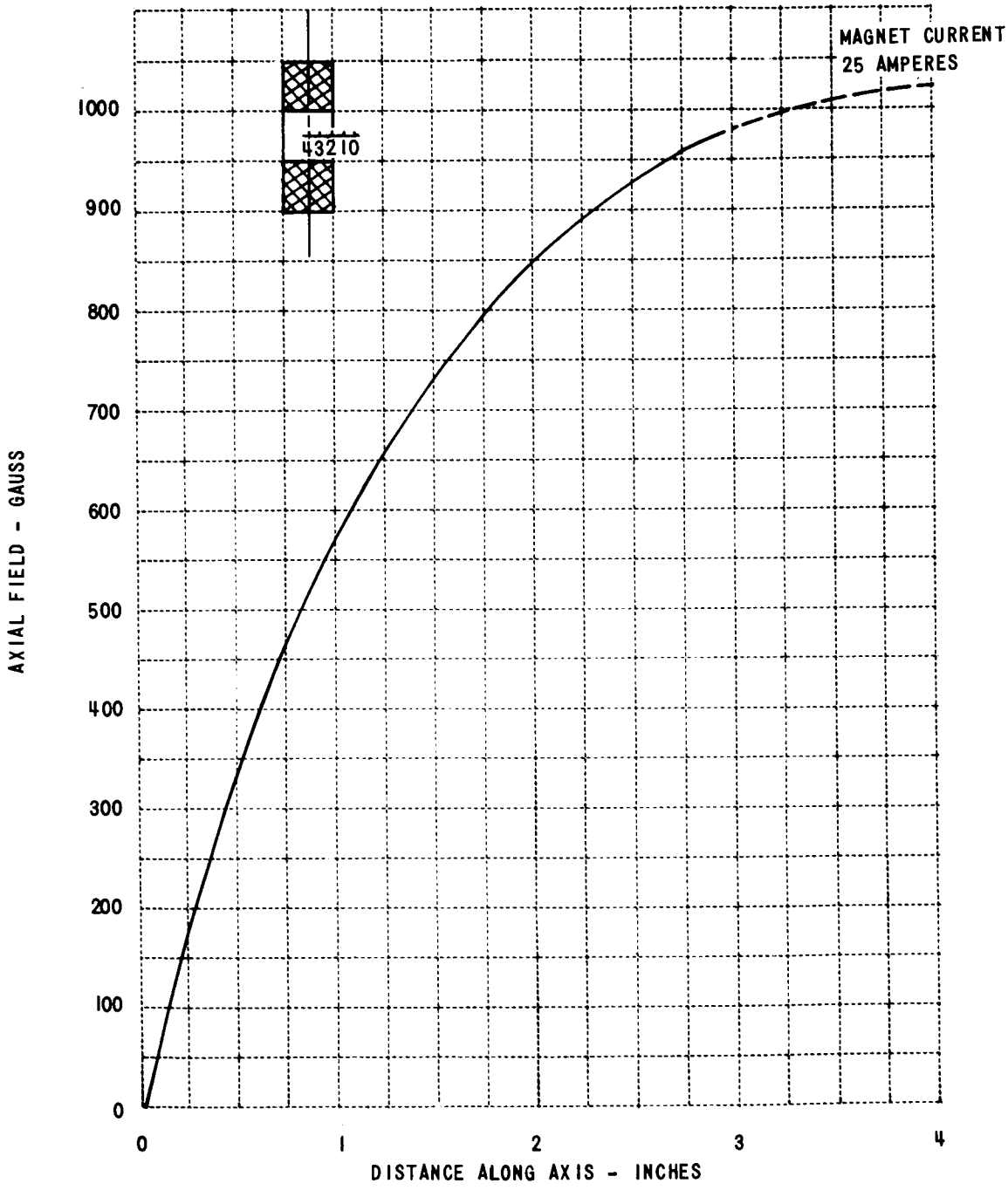

Figure B-2 AXIAL MAGNETIC FIELD

BIBLIOGRAPHY

1. "Investigation of New Concepts for Microwave Power Generation (Laser Studies)," Technical Documentary Report No. RADC-TDR-63-465 December 1963 Prepared under Contract No. AF 30(602) - 2833 by School of Electrical Engineering Cornell University, Ithaca, New York.

2. Giori, F. A., MacKenzie, L. A., and McKinney, E. J. "Laser-Induced Thermionic Emission" Applied Physics Letters, Vol. 3, No. 2 15 July 1963.

3. Giori, F. A., and Gilmour, A. S. Jr. Final Report "Ion Generation by Laser-Surface Interaction" Cornell Aeronautical Laboratory, Inc. Report No. RM-1863-E-1 May 1964.

4. Myers, J. D. "Power Density Effects in Laser Produced Craters" Paper presented at the Sixth Electron Beam Symposium, Boston, Massachusetts April 27-28, 1964.

5. Rae, W. J. and Hertzberg, A. "On the Possibility of Stimulating Meteoroid Impact by the Use of Lasers" Cornell Aeronautical Laboratory, Inc. Report No. AI-1821-A-1 March 1964.

6. Williams, D. L. "Laser Machining Techniques" 18th Annual Spring Technical Conference on the Applications of Lasers and Masers to Science, Medicine, and Industry April 7-8, 1964 Cincinnati, Ohio.

7. Ready, J. F. "Effects Due to Absorption of Laser Radiation" Paper presented at the 1963 Spring Meeting of the Optical Society of America Jacksonville, Florida March 25-27, 1963.

8. Honig, R. E. and Woolston, J. R. "Laser-Induced Emission of Electrons, Ions and Neutral Atoms from Solid Surfaces" Applied Physics Letters, Vol. 2 pp. 138-139 April 1963.

9. Honig, R. E. "Laser-Induced Emission of Electrons and Positive Ions from Metals and Semiconductors" Applied Physics Letters, Vol. 3 pp. 8-9 July 1963.

10. Chang, T. Y. and Birdsall, C. K. "Laser Induced Emission of Electrons, Ions and Neutrals from Ti and TiD Surfaces" Applied Physics Letters, Vol. 5, No.9 pp. 171-172 1 November 1964.

11. Iannuzzi, M. and Williamson, R. "Effects of Absorption of Laser Radiation on Metals" Il Nuovo Cimento Vol. XXXVI, No. 4 pp. 1130-1134 16 April 1965.

12. Verber, C. M. and Adelman, A. H. "The Interaction of Laser Beams with Metals" Battelle Technical Review Vol. 14, No. 7 pp. 3 - 8 July 1965.

13. Verber, C. M. and Adelman, A. H. "Laser-Induced Thermionic Emission from Tantalum" Journal of Applied Physics Vol. 36, No. 5 May 1965.

14. Gilmour, A. S. Jr. and Giori, F. A. "The Use of the Quadrupole Mass Spectrometer for Laser-Surface Studies" Presented at the Thirteenth Annual Conference on Mass Spectrometry and Allied Topics St. Louis, Missouri May 16-21, 1965.

15. Giori, F. A. and Gilmour, A. S. Jr. "Application of the Laser to Electric Propulsion" Presented at the Second Space Congress April 5-7, 1965 Cocoa Beach, Florida.

16. Germer, L. H. and Boyle, W. S. "Anode and Cathode Arcs" Nature, 176, 4491, p. 1019: Boyle, W. S. and Germer, L. H. "Arcing at Electrical Contacts on Closure. Part 6, The Anode Mechanism of Extremely Short Arcs" Journal of Applied Physics Vol. 26, No. 5 pp. 571 - 574

17. Reece, M. P. "The Vacuum Switch" Proc. IEEE, 110, 4 pp. 797 1963.

18. Sproull, R. L. "Modern Physics" John Wiley and Sons, Inc. New York 1956.

19. Lecture Notes EE 4090 Professor A. S. Gilmour, Jr. Cornell University Course given at Cornell Aeronautical Laboratory, Inc. Spring Term 1965.

20. Smith, L. P. "The Emission of Positive Ions From Tungsten and Molybdenum" Physical Review Vol. 35 pp. 381-395 February 15, 1930.

21. Mueller, G. J. "The Distribution of Initial Velocities of Positive Ions from Tungsten" Physical Review Vol. 43 March 1, 1934.

22. Barnes, L. L. "The Temperature Variations of the Positive Ion Emission from Molybdenum" Physical Review Vol. 42 November 15, 1932.

23. Keyes, R. J. and Quist, T. M. "Injection Luminescent Pumping of $CaF_2:U^{3+}$ with GaAs Diode Lasers" Applied Physics Letters, Vol. 4, No. 3 1 February 1964 pp. 51-53

24. Lamorte, M. F. "Continuous Operation Is Near For Uncooled Diode Lasers" Electronics, January 10, 1966 pp. 95-99.

25. Wade, G., Wheeler, C. A., Hunsterger, R. G. and Tarroll, T. O. "A Tunnel Injection Laser" Presented at the Fifth International Congress on Microwave Tubes, Paris, France September 14-18 1964 pp. 485-488.

LIST OF MAJOR SYMBOLS

e	charge of a singly charged atom
e	electron charge
$\hbar$	Plank's constant $\div 2\pi$
k	Boltzmann's constant
m	electron mass
m_i	emitted ion mass
m_t	weight of pendulum target
m_w	weight of pendulum wire
$\dot{m}$	mass flow rate
n_i	emitted ion charge
Δt_1	temperature difference between the melting point and 25°C of the material
Δt_2	temperature difference between the boiling point and the melting point of the material
t	time duration of laser pulse
u_i	emitted ion velocity
v_t	velocity of pendulum target
v_w	velocity of pendulum wire
x	horizontal pendulum displacement
A	constant in Richardson - Dushman thermionic emission equation
C_{P1}, C_{P2}	specific heat
E	energy of emitted ions

E_H energy to heat, vaporize and ionize material

E_0 Fermi level of material

E_T total energy including reflection to heat, vaporize and ionize material

F force due to ion emission

H_F heat of fusion

H_V heat of vaporization

I_t total impulse due to ion emission

J_e electron current density

J_i ion current density

$J_{enhanced}$ - magnetically enhanced thermionic electron emission

$J_{thermionic}$ - thermionic electron emission

L length of pendulum wire

L_{eff} effective pendulum length

M atomic weight of material

N Avogadro's number

R reflectivity at 6943Å

T temperature of material surface

T laser-generated-ion thrust

V_I first ionization potential

V_e electron energy (ev)

V_i ion energy (ev)

θ angular deflection of pendulum

φ electron work function

φ_i	ion work function
ρ_e	electron charge density
ρ_i	ion charge density
τ	period of pendulum

DISTRIBUTION LIST FOR CONTRACT NAS3-5919

	No. of copies
NASA-Lewis Research Center Spacecraft Technology Procurement Section 21000 Brookpark Road Cleveland, Ohio 44135	
Attention: John H. DeFord	1
NASA -Lewis Research Center Electromagnetic Propulsion Division 21000 Brookpark Road Cleveland, Ohio 44135	
Attention: H. R. Kaufman	1
W. E. Moeckel	1
W. D. Rayle	1
NASA-Lewis Research Center Spacecraft Technology Division 21000 Brookpark Road Cleveland, Ohio 44135	
Attention: Frank Kavanagh	1
D. L. Lockwood	1
J. H. Childs	2
R. R. Nicholls	9
NASA-Lewis Research Center Technology Utilization Office 21000 Brookpark Road Cleveland, Ohio 44135	
Attention: John Weber	1
NASA Headquarters FOB-10B 600 Independence Avenue, S.W. Washington, D. C. 20546	
Attention: RNT/James Lazar	2
NASA Marshall Space Flight Center Huntsville, Alabama 35812	
Attention: M-RP-DIR/Dr. E. Stuhlinger	1
NASA Scientific and Technical Information Facility Box 5700 Bethesda, Maryland	
Attention: NASA Representative /RQT-2448	6

No. of copies

Commander
Aeronautical Systems Division
Wright-Patterson Air Force Base,
Ohio 45433

Attention: AFAPL (APIE)/Robert Supp 1

NASA-Lewis Research Center
21000 Brookpark Road
Cleveland, Ohio 44135

Attention: Library 2

NASA-Lewis Research Center
21000 Brookpark Road
Cleveland, Ohio 44135

Attention: Reports Control Office 1

AFWL
Kirtland AFB, New Mexico

Attention: WLPC/Capt. C. F. Ellis 1

Jet Propulsion Laboratory
Pasadena, California

Attention: J. J. Paulson 1

Aerospace Corporation
P. O. Box 95085
Los Angeles, California 90045

Attention: Library Technical Documents Group 1

North American Aviation, Inc.
12214 Lakewood Avenue
Downey, California

Attention: Technical Information Center 1

Colorado State University
Fort Collins, Colorado

Attention: L. Baldwin 1

Hughes Research Laboratories
3011 Malibu Canyon Road
Malibu, California 90265

Attention: Dr. G. R. Brewer 1
Mr. R. C. Knechtli 1

No. of copies

Ion Physics Corporation
Burlington, Massachusetts

Attention: Dr. S. V. Nablo 1

United Aircraft Corporation
Research Department
East Hartford, Connecticut

Attention: Dr. R. G. Meyerand, Jr. 1

Space Technology Laboratories
8433 Fallbrook Avenue
Canoga Park, California

Attention: Dr. D. B. Langmuir 1

General Electric Company
Flight Propulsion Lab.
Cincinnati, Ohio 45215

Attention: M. L. Bromberg 1

Westinghouse Astronuclear Laboratories
Pittsburgh, Pennsylvania 15234

Attention: H. W. Szymanowski, Manager 1
Electrical Propulsion Laboratory

Aerojet General
San Ramon, California

Attention: Dr. J. S. Luce 1

Electro-Optical Systems, Inc.
125 North Vinedo Avenue
Pasadena, California

Attention: R. C. Speiser 1

TRW Electromechanical Division
TRW Inc.
23555 Euclid Avenue
Cleveland, Ohio 44117

Attention: R. T. Craig 1

Rocketdyne
6633 Canoga Avenue
Canoga Park, California

Attention: J. F. Hon 1

No. of copies

Department of Physics
Hiram College
Hiram, Ohio

Attention: Prof. Laurence Shaffer 1

Cornell University
Ithaca, New York

Attention: Library 1

Princeton University
Plasma Physics Laboratory
James Forrestal Research Center
P. O. Box 451
Princeton, New Jersey 1

United Aircraft Corporation
400 Main Street
E. Hartford, Connecticut 06108

Attention: Library 1

Department of Nuclear Engineering
College of Engineering
University of California, Berkeley
Berkeley, California 94720

Attention: Mr. Harold P. Smith 1

Air Force Weapons Laboratory
Attn (WLIL)
Kirtland AFB
New Mexico 87117 1